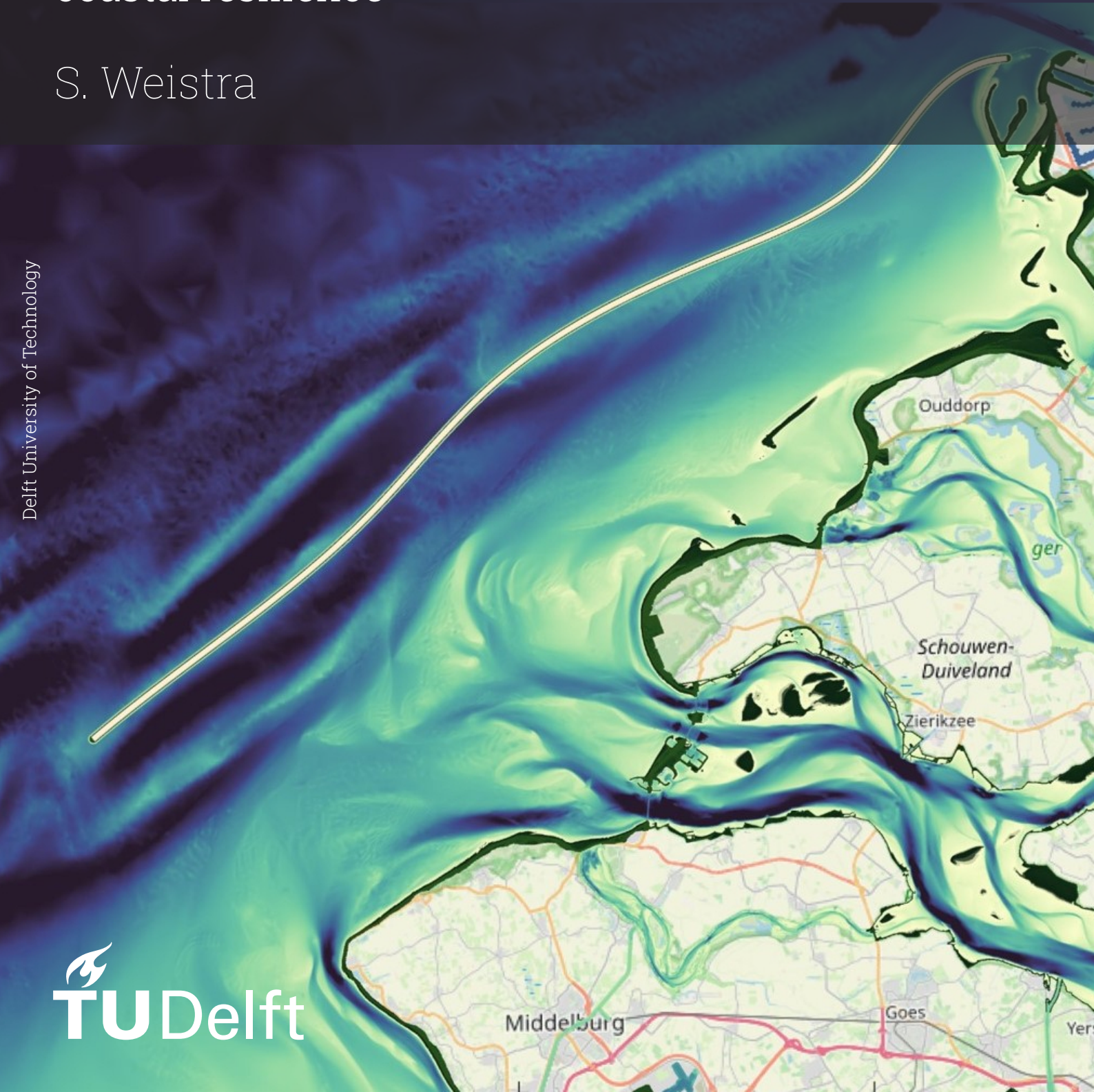


Dynamic Tidal Power in the Voordelta

Assessing the potential of a southwest-oriented DTP dam in the Netherlands for renewable energy and coastal resilience

S. Weistra



Dynamic Tidal Power in the Voordelta

Assessing the potential of a southwest-oriented
DTP dam in the Netherlands for renewable
energy and coastal resilience

by

S. Weistra

to obtain the degree of Master of Science

at the Delft University of Technology,

to be defended publicly on Friday July 14, 2023 at 15:00.

Student number: 4658930
Project duration: October 31, 2022 – July 14, 2023
Thesis committee: Prof. dr. ir. S. G. J. Aarninkhof TU Delft, Chair
Ir. Y. H. Attema Svašek Hydraulics, Daily supervisor
Dr. ir. R. J. Labeur TU Delft
Dr. J. A. Arriaga García TU Delft

An electronic version of this thesis is available at <https://repository.tudelft.nl/>.

Preface

In front of you lies my master's thesis 'Dynamic Tidal Power in the Voordelta: Assessing the potential of a southwest-oriented DTP dam in the Netherlands for renewable energy and coastal resilience'. This thesis concludes my Master of Science studies in Hydraulic Engineering at the Delft University of Technology. This also marks the end of my time as a student in Delft, which has been a great six years.

The subject of this thesis is the potential for applying Dynamic Tidal Power in The Netherlands through construction of an oblique dam. With the use of numerical models, an assessment has been carried out focusing on energy generation, coastal safety and morphological development.

I would like to express my thanks to my supervisor Ype Attema, with whom I spent many hours debating the direction of the thesis and who spent many more hours educating me on the modelling software and correcting and proofreading my work. Besides that I want to thank my supervisors at the TU Delft. Stefan Aarninkhof, for his enthusiasm and interest in the subject, Robert Jan Labeur for the many hours spent helping to add structure to my thesis and Jaime Arriaga García for the clear and specific feedback. I would also like to thank everyone else at Svašek Hydraulics, as every single one of you has helped or advised me at one point during the past months.

Finally, a large thank you to my family and friends, who have helped me tremendously in the past months.

*Sietse Weistra
Rotterdam, July 2023*

Summary

A possible way of generating a stable and predictable base load of renewable energy, supplementing the unpredictable wind and solar energy, is dynamic tidal power (DTP). DTP is generated with the use of large dam, which is built in the sea, under an angle with the propagating tidal wave. A dam of sufficient length can create a phase difference between the propagating tidal waves on either side of the dam, creating head differences over the dam, which can be used to generate renewable energy using large turbines in the dam. Previous studies considered a DTP dam built perpendicular to the coast and the direction of the propagating tidal wave. However, a structure of this size extending into the North Sea interferes with other functions of the area such as shipping. Instead of a perpendicular dam, an oblique dam off the Dutch delta coast has been proposed to reduce this interference. This design has the additional benefits that it could increase the coastal safety of the surrounding area and potentially increase the sediment budget of the Voordelta area in front of the coast.

In this study, a first-order assessment of an oblique DTP dam has been carried out. This assessment focuses on three aspects: the expected energy yield and how this compares to the expected energy yield of a perpendicular dam under the same conditions; the impact this dam has on the coastal safety of the surrounding area. To this end, an analysis of the change in hydrodynamic and morphological processes in the Voordelta as a result of the construction of such a dam has been carried out.

The propagation of the tidal wave around an oblique DTP dam in the North Sea has been modelled using the FINEL modeling software, applied as a two-dimensional flow model. The reference layout of the DTP dam has been determined beforehand based on several requirements concerning the location and length. Using a turbine module integrated into FINEL, the discharge through each turbine has been determined, based on which the energy output of the DTP dam has been calculated. A comparison was made of the energy output of the oblique dam and that of a perpendicular dam, as used in previous studies. To do this, the same model has been run with a dam positioned perpendicular to the Dutch coast.

A DTP dam with a length of 62.5 km and a southwest orientation starting at the Maasvlakte 2 was found to have a maximum power output in the order of $8 \cdot 10^2$ MW and a yearly generated energy yield in the order of 2 TWh. Both of these values were approximately a factor five lower than the power output of the perpendicular dam with the same length also starting at Maasvlakte 2. This is because, in the case of the perpendicular dam, a phase difference in the tidal wave over the dam was created, creating a large head difference over the dam. In the case of the oblique dam, the phase difference was lower, significantly reducing the water head over the dam. As opposed to the perpendicular dam, the head difference was created as a result of amplification of the tidal wave within the estuary.

Subsequently, a SWAN wave model has been coupled to the FINEL flow model. In this coupled model, a design storm with a return period of 10000 years has been simulated. Of this storm, the wave characteristics and water level in the area were compared between the scenarios with and without oblique dam. A large decrease in both significant wave height and peak period behind the dam was found across nearly the whole Voordelta area, with the largest decrease offshore immediately behind the dam. However, the significant wave height increased on the outside of the dam and near Westkapelle. The same result was found for scenarios where 25 cm and 80 cm mean sea level rise has been applied. This is because the incoming waves from a northwestern direction are blocked by the dam, resulting in locally wind-generated waves behind the dam becoming dominant in the area. On the offshore side of the dam, significant wave heights are increased as a result of reflection of incoming waves. The maximum water level during the storm decreases in the nearshore area.

As the area behind the dam is transformed into an area resembling an estuary, the dominant hydrodynamic and, consequently, the morphodynamic processes are changed. The dam blocks all incoming waves from the west and northwest, which are the dominant wave directions in the area. Because of this, the wave energy within the area decreases significantly under storm conditions. At the same

time, the tidal amplitude is expected to be amplified within the area. These changes cause the area to become more tide-dominated. As a result, a decrease in the onshore directed sediment transport into the area is expected. The entrance of the estuary is expected to become more flood-dominant, as a result of which more inflow of sediment into the created estuary is expected. Dominant sediment transport mechanisms with the estuary are also changed, but for a more accurate view of the extent to which this happens, a complete morphological model is necessary, which has not been applied in this study.

In summary, a DTP dam oblique to the Dutch coast can provide a substantial amount of energy, although it is significantly less when compared to a perpendicular dam and to previous studies. A further advantage of this dam is that the area behind is sheltered against storm wave conditions and extreme water levels, thus increasing the coastal safety. It is foreseen that the area attracts more sediment by the creation of the dam, but this needs to be confirmed by a future morphological model assessment.

Contents

Preface	i
Summary	ii
Nomenclature	vii
1 Introduction	1
1.1 Problem context	1
1.2 Objective	3
1.3 Research questions	3
1.4 Research method	3
1.5 Thesis outline	3
2 Literature review	4
2.1 Dynamic Tidal Power	4
2.1.1 DTP theory	4
2.1.2 DTP: other studies	5
2.2 DTP turbines	6
2.3 Coastal safety Delta coast	8
2.4 Morphological processes in the Voordelta	9
2.5 DTP modelling approach	9
2.6 Conclusion	10
3 System Analysis	11
3.1 Location analysis	11
3.1.1 Geographical characteristics	11
3.1.2 Hydrodynamic conditions	12
3.1.3 Morphological processes	14
3.2 Recent development of the Voordelta	15
3.3 Coastal safety assessment of the Dutch Delta coast	16
3.3.1 Dune coasts	16
3.3.2 Eastern Scheldt Barrier	17
3.4 Conclusion	17
4 Reference layout of the DTP dam	18
4.1 Design requirements	18
4.2 Reference Design	19
4.3 Influence DTP dam on the tidal wave	20
4.4 Influence of the dam design on the wave climate	22
4.5 Influence of the dam design on wind set-up	22
4.6 Conclusion	23
5 Energy Yield Assessment	24
5.1 Methodology	24
5.2 FINEL flow model	25
5.2.1 Modelling software	25
5.2.2 FINEL model input	25
5.2.3 Validation hydrodynamic flow model	26
5.3 Results energy yield assessment	28
5.3.1 Optimal open ratio	28
5.3.2 Results oblique dam	29
5.3.3 Results perpendicular dam	30

5.3.4	Comparison of the perpendicular and oblique dam	30
5.3.5	Comparison influence of meteorological input	31
5.4	Discussion	32
5.5	Conclusion	33
6	Coastal Safety Assessment	34
6.1	Methodology	34
6.2	Storm model	35
6.2.1	Modelling software	35
6.2.2	Calibration	35
6.2.3	Validation	37
6.3	Storm Schematisation	38
6.3.1	FINEL Model Input Storm	38
6.3.2	SWAN Model Input Storm	40
6.4	Results	40
6.4.1	Change in Maximum Values	40
6.4.2	Time Series Measurement Locations	43
6.4.3	Overview results	44
6.5	Discussion	46
6.5.1	Discussion northwestern storm	46
6.5.2	Discussion southwestern storm	48
6.5.3	Effect on load characteristics	48
6.5.4	Effect of MSLR	50
6.6	Conclusion	50
7	Development of the Voordelta	51
7.1	Change in Morphological Processes	51
7.2	Morphological model	53
7.2.1	Modelling approach	53
7.2.2	FINEL model input	53
7.2.3	Results	54
7.2.4	Discussion	55
7.3	Conclusion	56
8	Discussion	57
8.1	Analysis of the results	57
8.1.1	Effect of dam orientation on energy output	57
8.1.2	Desirability of the project	58
8.2	Validity	59
8.3	Usability of the study	60
9	Conclusion and recommendations	61
9.1	Conclusion	61
9.1.1	Main Research Question	61
9.1.2	Sub-Questions	62
9.2	Recommendations	63
	References	65
A	North Sea Program 2022 - 2027	70
B	Calculation reflection standing wave	72
C	Model calibration and validation	73
C.1	Calibration of the coastal safety model	73
C.1.1	Calibration Results Water Level	74
C.1.2	Calibration Results Significant Wave Height	75
C.1.3	Calibration Results Peak Period	76
C.2	Validation of the combined FINEL-SWAN model	77
C.2.1	Validation Results Water Level	77

C.2.2	Validation Results Significant Wave Height	78
C.2.3	Validation Results Peak Period	79
C.3	Validation FINEL flow model	81
C.3.1	Validation FINEL model with ERA5 input	81
C.3.2	Validation FINEL model with CFSR input	83
D	SWAN input file	85
E	Results Coastal Safety	87
E.1	Change in Maximum Values	87
E.1.1	Scenario No MSLR	88
E.1.2	Scenario 25 cm MSLR	89
E.1.3	Scenario 80 cm MSLR	91
E.1.4	Southwestern Storm	93
E.2	Time Series	94
E.2.1	Significant Wave Height	94
E.2.2	Peak Wave Period	95
E.2.3	Maximum Water Level	95

Nomenclature

Abbreviations

Abbreviation	Definition
DTP	Dynamic Tidal Power
FECSM	FINEL European Continental Shelf Model
HW	High Water
KC	Keulegan-Carpenter
LW	Low Water
MHW	Mean High Water
MLW	Mean Low Water
MSL	Mean Sea Level
MSLR	Mean Sea Level Rise
NAP	Normaal Amsterdams Peil (Dutch Ordnance Datum)
RMSE	Root Mean Square Error

Symbols

Symbol	Definition	Unit
A	Flow area through the dam	$[m^2]$
A_{eq}	Equilibrium cross-section of the entrance channel	$[m^2]$
C	Energy loss coefficient	$[-]$
C_d	Discharge coefficient turbines (Chapter 2)	$[-]$
C_d	Wind shear stress coefficient (Chapter 6)	$[-]$
C_f	Resistance factor channel	$[-]$
D	Length of the DTP dam	$[m]$
D_{50}	Median particle diameter	$[m]$
D_{90}	90th percentile particle diameter	$[m]$
F	Fetch	$[m]$
g	Acceleration of gravity	$[m/s^2]$
H	Water head	$[m]$
$H_{1/3}$	Significant Wave Height	$[m]$
h	Waterdepth	$[m]$
k	Wave number	$[1/m]$
l	Length of the estuary	$[m]$
P	Power generated (Chapter 2)	$[W]$
P	Tidal prism (Chapter 7)	$[m^3]$
Q	Discharge	$[m^3/s]$
R	Hydraulic radius	$[m]$
T	tidal wave period	$[s]$
U_{10}	Wind velocity at 10 metres altitude	$[m/s]$
U_{eq}	Equilibrium velocity	$[m/s]$
V	Velocity	$[m/s]$
δh	Water level difference	$[m]$
ζ	Surface elevation of the tidal wave	$[m]$
η	Efficiency coefficient	$[-]$
λ	Wavelength	$[m]$
μ	Damping modulus	$[-]$
ρ	Density	$[kg/m^3]$

1

Introduction

1.1. Problem context

With the energy transition, the focus of Dutch and worldwide energy production is shifting fast towards renewable energy. The Netherlands has set the goal, that by 2050 all used energy will come from renewables. Currently, many projects are planned, especially for offshore wind energy, with the goal that by 2030, 16% of all power will be from offshore wind (Rijksoverheid, n.d.). The other methods focused on are onshore wind and Solar-PV (Rijksoverheid, 2019). However, these methods of generating renewable power take up a lot of space, but they also have the problem that the power generated is not constant. This means that during periods without sun or wind, a so-called *dunkelflaute*, insufficient power could be generated (Edwards et al., 2022). Therefore, it is necessary to ensure a way of generating a stable base load of renewable energy.

A possible new way of generating a large and more stable energy yield is a dynamic tidal power (DTP) dam. A DTP dam has a length in the order of magnitude of several tens of kilometres built in the sea, stretching from the bottom to just above the surface. A dam of sufficient length can create phase differences in the propagating tidal wave on either side of the dam, creating a water head difference over the dam. This head difference can be used to generate energy using large turbines installed in the dam. Recent research by TNO states that a single dam in front of the Dutch coast could account for up to 21 % of the total Dutch electricity production in 2050 (TNO, 2021). As the tidal wave is highly predictable, so is the expected energy yield, which is an advantage compared to other renewable energy alternatives. Besides this, the DTP dam can be built using existing techniques such as sluice caissons used in the Delta Works (Witteveen+Bos and CE Delft, 2019). Furthermore, a key asset of DTP compared to other sustainable energy generation methods is that it can combine several goals with energy generation.

At the end of 2022, the minister of Climate and Energy confirmed in a letter to parliament that Dynamic Tidal Power is promising for Dutch energy production and could contribute significantly to the national energy transition (Jetten, 2022). He also said however, that more research on the subject and its impact on the Dutch coast is needed before more investments are made. This decision to not invest in the technology at this moment was based upon a report by TNO on the various possibilities for generating renewable energy from water (TNO, 2021). The report was relatively positive towards the opportunities for DTP in The Netherlands. However, a 25 to 50 percent cost reduction is still needed for the project to be cost-efficient. Besides this, research must be done on the effects on coastal safety and sediment transport along the coast and other functions of the North Sea, such as ecology, shipping and fishery. Furthermore, as large parts of the Dutch coast are designated Natura 2000 protected areas, the influence of such a project on these areas should also be investigated.

Recently, there has been some new research on the possibility of constructing a DTP dam in The Netherlands. (Bitter, 2018; Svašek Hydraulics, 2020; TNO, 2021). Svašek Hydraulics (2020) notes that the most promising location of such a dam would be off the coast of Maasvlakte 2, with a southwest orientation, as shown in Figure 1.1. This location is deemed ideal because the dam is connected

to an industrial area, reducing the need for new energy infrastructure. Also, the tidal velocities are higher in the southern part of the Netherlands. Because the tidal velocity influences the water level at the dam, this should result in a higher water level difference over the dam, which in turn is beneficial for the expected energy output (Hulsbergen et al., 2005; TNO, 2021). The orientation is proposed because this way the interference with regions designated for Natura 2000, navigation routes and anchor areas as defined in the ‘Programma Noordzee 2022-2027’ (Ministerie van Infrastructuur en Waterstaat, 2022) is minimal. Besides that, this way can a tidal basin be created which should be beneficial for the head difference. Furthermore, as the largest waves measured off the coast of Zeeland are predominantly from the northwest, the proposed design of the DTP dam would shelter the coast from most of the highest waves, thus increasing the coastal safety of Zeeland while also reducing the wave-driven erosion of the Voordelta, the shallow area in front of the Dutch Delta coast. However, this orientation differs from previous research on DTP dams, which all assumed a DTP dam perpendicular to the coast. Because of this, the process explained by Hulsbergen et al. (2005) can change, which can impact the energy generated by the oblique dam compared to that of a perpendicular dam. No previous studies have been done into the energy generation of a oblique dam, meaning that this should be a key part of this study.

The most critical part of the coastal infrastructure in the Dutch Delta region is the Eastern Scheldt Barrier. Recent calculations show that due to the expected mean sea level rise in the North Sea, the Eastern Scheldt Barrier will have to be strengthened in the coming decades or must be protected against individual aspects of the design conditions, such as the wave heights or the wind setup. The proposed dam could potentially do this.

Furthermore, the construction of the Delta Works has greatly impacted the development of the Voordelta. As a result of damming the various estuaries, at several of the estuaries, the ebb-delta front has been eroded by waves. This resulted in a loss of intertidal areas, increased wave attack on the Schouwen coast, and increased shoreface erosion, resulting in the coast being strengthened more often. It is hypothesised that the design of this dam could increase the amount of sediment trapped in the area. As the area loses large amounts of sediment each year, this could positively influence the development of the Natura 2000 protected area, The Voordelta and protect the various ecotypes in the region against sea level rise. Moreover, as most of the sediment lost is deposited in the Euro-Maas deep-water shipping channel, the dam’s construction could significantly lower the volume of sediment dredged from the shipping channel annually.

The potential benefits of constructing an oblique Dynamic Tidal Power dam off the coast of Zeeland, starting at Maasvlakte 2, have not been thoroughly researched. This dam could address three different problems: providing stable and predictable renewable energy, reducing water levels and waves during design storms to enhance coastal safety and potentially decreasing the need for coastal strengthening measures, and improving sediment trapping in the Voordelta to counter long-term sediment loss. Existing research in the Netherlands has primarily focused on energy generation from perpendicular coastal dams, neglecting other aspects of the project. Additionally, no research has been conducted on the energy generation potential of a dam parallel to the coast, as depicted in Figure 1.1. Considering that a design with multiple problem-solving capabilities enhances the feasibility of such a large-scale undertaking, it is crucial to investigate the potential benefits of an oblique dam.

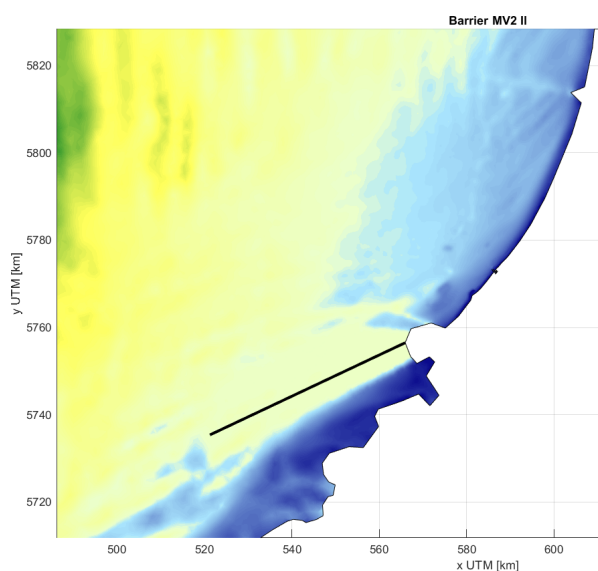


Figure 1.1: Proposed location and orientation of the DTP dam, from Svašek Hydraulics (2020).

1.2. Objective

The objective of this study is to provide a first-order assessment of a dynamic tidal power dam extending into the North Sea from Maasvlakte 2 with southwest orientation. The evaluation focuses on three aspects: the approximate energy yield of an oblique DTP dam compared to previous studies, the influence on the coastal safety of the Dutch Delta coast, and the expected hydrodynamic and morphological changes behind the dam.

1.3. Research questions

The main research question is formulated as follows:

How does the orientation of a dynamic tidal power dam starting at Maasvlakte 2 influence its energy yield as well as the coastal safety and development of the Dutch Delta coast, and is such a construction desirable from these perspectives?

To comprehensively address the main research question, the following sub-questions have been formulated:

- How does constructing an oblique DTP dam impact the hydrodynamic conditions in the Voordelta?
- What is the expected energy yield of an oblique DTP dam, and how does it compare to a perpendicular DTP dam and to literature?
- How is the coastal safety of the Dutch Delta coast influenced by the construction of an oblique DTP dam?
- What is the effect of an oblique dam on the development of the area between the dam and the coast?

1.4. Research method

The research method of this study consists of five main steps to address the research questions. First, a literature review was conducted to analyse existing knowledge on DTP and the area impacted by the proposed design. Next, an analysis of the system has been carried out, which encompasses the geographical characteristics as well as the dominant hydrodynamic and morphological processes of the area of interest, to provide an understanding of the relevant processes governing the dam's impact. After that, a set of specific requirements was proposed to which the DTP dam should adhere to make a reference layout of the dam, which has been used in the analytical calculations and numerical models. Then, two numerical models were set up. The first has been used to estimate the energy yield of the dam following the reference layout. The second model was used to assess the influence of the dam on the hydrodynamic conditions in front of the Dutch Delta coast to determine the dam's impact on the coastal safety in the region. Finally, a hypothesis on the expected morphological changes as a result of the DTP dam's construction has been formulated based on literature and the hydrodynamic models.

1.5. Thesis outline

Chapter 2 consists of a literature review of relevant scientific articles. In Chapter 3, the system analysis is conducted. Chapter 4 describes the reference layout of the DTP dam and its requirements, as well as the analytical calculations concerning the hydrodynamic impact of the dam. Chapter 5 describes the numerical modelling software used, the numerical models developed and their input, as well as the calibration and validation process of these models. Chapter 6 presents the results of the numerical model concerning the energy output of the DTP dam. In Chapter 7, the result of the numerical models assessing the impact of the dam on coastal safety is presented. In Chapter 8, a hypothesis on the morphological changes caused by the DTP dam is formulated. The results of this research are discussed in Chapter 9. The thesis is concluded in Chapter 10 with the conclusions and recommendations.

2

Literature review

In this chapter, the current level of knowledge on DTP dams and their influence on the surroundings is reviewed through an analysis of existing studies. First, in order to analyse the power generated by the DTP dam, an analysis is done of the concept, the relevant processes influencing the power generated and other literature concerning DTP. Then, as the energy is generated through the use of turbines, their integration and use in previous research are analysed. After that, as the influence of the dam on coastal safety is assessed, the relevant factors and characteristics to make this assessment in the relevant location, the Voordelta, are analysed. Subsequently, literature on the morphological processes in the area is considered to assess the development of the area surrounding the dam. Finally, the modelling software used in similar research is discussed.

2.1. Dynamic Tidal Power

2.1.1. DTP theory

The Dynamic Tidal Power dam concept was first described in an article by Hulsbergen et al. (2005). Considering the characteristics of the local tidal system in the Keulegan-Carpenter (KC) number, dams with a length in the order of tens of kilometres have a KC number of around 1, which means that the inertial forces on the dam are significantly larger than the drag forces, allowing for neglecting of the drag forces (Keulegan and Carpenter, 1958). The process is then turned around and pictured as an oscillating plate in a water tank with the same characteristics as the tide. As the drag forces are neglected, the only forces relevant to the dam are the inertial forces applied by the 'added mass' on both sides of the dam. Because of the oscillatory motion, the concept of added mass is applicable, which accelerates and decelerates along with the object. The result of this is a pressure build up at one side of the object, which is translated into a rising water level. Importantly, at the same time a negative pressure pulls on the other side of the dam (Hulsbergen et al., 2012). This pressure difference can be expressed in the hydraulic head over the dam, as described by Hulsbergen et al. (2005) in equation 2.1. This model was later analytically verified by Mei (2012).

$$\Delta h_{max} = \frac{4\pi D V_{max}}{gT} \quad (2.1)$$

In this equation Δh_{max} is the maximum water level difference over the dam. D is the length of the dam, V_{max} is the maximum tidal velocity, g is the gravitational acceleration and T is the wave period of the tidal wave.

The water level difference calculated with equation 2.1 is the maximum water level difference assuming there is no flow over or through the dam. However, along the length of the dam, openings are present with turbines installed to generate energy. The flow through these openings reduces the water head until an equilibrium is reached between the discharge through the dam and the water head over the dam. The flow through these openings is calculated using a discharge-water head (Q-H) relationship, a simplified version of which is used in Dai et al. (2017), shown in equation 2.2.

$$Q = C_d A \sqrt{2gH} \quad (2.2)$$

Where Q is the discharge through the dam, C_d is the discharge coefficient of the turbines, which varies with the type of hydraulic structure. A is the total flow area through the dam.

Dai et al. (2017) calculate the generated power P using equation 2.3.

$$P = \rho g Q H \eta \quad (2.3)$$

With ρ , the density of the water flowing through the dam, and η the efficiency coefficient of the turbines.

As the discharge through the dam depends on the total flow area through the dam A , an optimal flow area exists, defined as the open ratio of the dam. Dai et al. (2017) researched the optimal open ratio numerically and found an optimal open ratio of 8%. As this number is based on numerical models in a different location and, more importantly, on a dam perpendicular to the coast, the ideal open ratio with the conditions considered in this study may have a different value. This must therefore be analysed separately in this research.

2.1.2. DTP: other studies

Several other studies into DTP have been conducted, which can be divided in two relevant subjects: optimisation of the power output through the design of the dam and studies on the power output of DTP dams at different locations.

Liu and Zhang (2014) and Hulsbergen et al. (2005) investigate ways of increasing the maximum water head over the DTP dam, which results in an increased energy output. Hulsbergen et al. (2005) hypothesises that the addition of 'wings' at the tip of the dam, perpendicular to the main dam, increases the added mass region. They predict that this results in a head difference over the dam that would be up to 50 % larger than without these additions. Liu and Zhang (2014) confirmed the increased water head using numerical models, but found that for 50 km long dams in the Taiwan street, the gain in maximum water head was only 15 %. They also considered placing the wings under an angle, giving the dam a Y-shape, because this shape has tidal wave gathering effects. They find that an angle of 45° increases the water head by an additional 13%, as a result of increasing phase difference over the dam. Park and Youn (2020) investigated the effect of creating slits in the DTP dam on the created water head, effectively creating several separate dams, divided by channels with a width of several kilometres. They found that with more slits, the maximum water head decreased. They also found that the location of the slit in the dam had no influence on the water level, which means that slits do not have a positive effect on the power output.

Secondly, a series of studies has been conducted to find optimal locations for applying DTP. Park (2017), Hulsbergen et al. (2008) and Hulsbergen et al. (2012) all considered locations in Korea, as the tidal amplitude at that location is up 9.5 m during spring tide. All studies used two-dimensional numerical flow models to investigate the maximum water head over the dam, using the theory explained in Hulsbergen et al. (2005). However, none of these studies considered turbines in the model, but used an estimated 'leak factor' by which the water head decreases with an open ratio of 10 %, based on Hulsbergen et al. (2005). This had been found by making a gap in the dam close to shore, with a length equal to that of ten percent of the total dam surface, rather than distributing the openings over the length of the dam. They find an expected maximum power output of 23 TW (Park, 2017), 15 GW (Hulsbergen et al., 2012) and varying between 7 and 45 GW, depending on the location (Hulsbergen et al., 2008). All of these studies assumed 50 km long dams with a 40-50 km long perpendicular side dam. Liu and Zhang (2014), Shao, Feng, Xi, et al. (2017), Shao, Feng, and Xu (2017) and Dai et al. (2020), conducted the same research for locations in China and the Taiwan Strait. The first three only considered the maximum water level difference over the dam, none of those studies considered openings in the dam. The only studies which did consider turbine openings were Dai et al. (2017) and Dai et al. (2020), which has been discussed previously in this section. They found a peak energy yield of 2.72 GW for a 50-km long dam without additions. These studies all used two-dimensional flow models to calculate the water head as well.

Finally, Hulsbergen et al. (2005) and Witteveen+Bos and CE Delft (2019) researched the expected power output of DTP dams in the Netherlands. Based on the theory explained in the study, Hulsbergen et al. (2005) calculated a peak power output of 5 GW for a dam of 30 km with a 20 km long side dam. They used the leak factor described previously. Finally, Witteveen+Bos and CE Delft (2019) describe a 50 km long DTP dam with T wings of which the length is not indicated, which would result in a maximum water head of 2.9 metres and a corresponding maximum power output of 15 GW.

2.2. DTP turbines

The power output of DTP dams is power generated by large turbines embedded in the dam. More specifically, turbines with a low working head are necessary for DTP in the Netherlands, as tidal amplitudes in The Netherlands are relatively low compared to locations previously investigated. This section gives an overview of how these turbines and the energy generated have been modelled in previous research and what governing equations are relevant for the turbines in DTP dams.

Hulsbergen et al. (2005) based calculations of the expected energy output P of tidal dams on an estimated average water level difference over the entire dam length. However, because the power output of energy turbines is proportional to $H^{3/2}$, as follows from equations 2.2 and 2.3, this averaging method will underestimate the total energy output. Dai et al. (2017) applied a simplified turbine module that calculates the power output for each grid cell separately, which was a significant improvement compared to previous research. However, this module did not consider the energy loss within the turbine installation, influencing the calculated power output.

Bitter (2018) derived a parameterised form of turbine dynamics and related energy losses applied to conical turbines. The Q-H relation for this turbine and its inverse are shown in equations 2.4 and 2.5:

$$Q_i = A_{outer(i)} \sqrt{\frac{2g\Delta h_{sys}(1 - a_{turb})}{C}} \quad (2.4)$$

$$\Delta h_{sys} = C \frac{Q|Q|}{2g(1 - a_{turb})A_{outer(i)}^2} \quad (2.5)$$

Here Q_i is the discharge through each turbine i , $A_{outer(i)}$ is the cross-sectional area at the entrance and exit of the conical turbine tube, Δh_{sys} is the total instantaneous water level difference over the dam and C is a dimensionless energy loss coefficient. The parameter a_{turb} is defined as:

$$a_{turb} = \frac{\Delta h_{turb}}{\Delta h_{sys}} \quad (2.6)$$

a_{turb} is the ratio of the water level difference over the turbine only and the total water level difference over the dam. Δh_{turb} is the fraction of the total water level difference used for power generation. Equation 2.4 closely resembles 2.2, but rather than determining the relation between the discharge and the water head, is Equation 2.4 applied to each turbine. Besides that has in Equation 2.4 compared to Equation 2.2, the factor C_d been replaced by the factor $\sqrt{\frac{1-a_{turb}}{C}}$.

It should be noted that the cross-sectional area A_{inner} of the turbine itself is usually smaller than the entrance/exit area A_{outer} . How the loss coefficient C is defined depends on the actual definition of the cross-sectional area. Bitter (2018), determined a representative value of $C = 1.85$ based on reports on tidal turbines designed for the Grevelingendam, assuming A_{outer} at the definition of the cross-sectional area. This value of C represents the combined energy loss due to in- and outflow effects and energy dissipation inside the turbine.

Dai et al. (2017) did use a discharge-head relationship, shown in Equation 2.2, adapted from a previous study on tidal barrage systems, Zhou et al., 2014. This did include a discharge coefficient C_d , similar to the factor $\sqrt{\frac{1-a_{turb}}{C}}$ used by Bitter (2018). However, following Zhou et al. (2014), Dai et al. (2017) assumed the factor to have a value of 1.0, although they noted that the factor usually is higher than 1.0 if A is the throat area of the hydraulic structure.

Given the relation between discharge and water level difference over each turbine, the power generated is calculated using equation 2.7, which was also used by Dai et al. (2017):

$$P_i = \rho g Q_i \Delta h_{turb} \eta \quad (2.7)$$

When substituting equation 2.4 into equation 2.7, it follows that a maximum power output is gained for $a_{turb} = 2/3$, which has also been shown by Bitter (2018). In reality, the operational settings of a turbine determine which value of a_{turb} will occur in real-time.

Equation 2.7 differs from the equation used in Hulsbergen et al. (2005) and Park (2017), who instead used Equation 2.8.

$$P_i = \rho g \Delta h_{eff} A_{turb} V_{turb} \eta \quad (2.8)$$

With A_{turb} and V_{Turb} the net cross-sectional flow area of all turbines and the flow velocity through the turbines respectively, with the flow velocity calculated according to Torricelli's law: $V_{turb} = \sqrt{2g\Delta h}$. This means that they did not consider energy losses when calculating the energy yield, except for the efficiency coefficient η . This means that the power output calculated by these studies significantly overestimates the energy yield.

The efficiency factor of the turbines η was assumed to be 1.0 by Dai et al. (2017). However, Hulsbergen et al. (2008) and DTP Netherlands (n.d.) considered an efficiency factor of 0.85 to be more realistic. The latter factor is used throughout this study.

An energy yield model should be used to calculate the generated power for individual turbines rather than using averages over the whole dam, as nonlinear relationships determine the power output. For the same reason, the discharge through the dam should be calculated through individual turbines. The Q-H relationship used to do this should include a predetermined loss coefficient, such as calculated by Bitter (2018), to prevent overestimating the power discharge and, consequently, the power output.

2.3. Coastal safety Delta coast

One of the objectives of this study is to assess the impact of the parallel DTP dam on the coastal safety in the Voordelta. To determine the influence of the DTP dam on coastal safety, it must be clear how this coastal safety is defined and which characteristics should be considered. As constructing such a barrier has a long lifetime, climate change, the associated mean sea level rise, and the effect on other relevant factors should be considered.

The coast of the Dutch Delta can be divided into soft and hard coasts. The chance of failure of these and all other primary coastal defences in The Netherlands are described in the Waterwet (2021). For every section of the coast, a lower limit for storms that the defence should be able to withstand has been determined. In the Voordelta, this lower limit is 1/10000 per year for the Eastern Scheldt Barrier and the coast immediately south of Maasvlakte 2. The rest of the dune coast, as well as the Brouwersdam and the Haringvliet sluices, have a lower limit of 1/1000 per year (Slootjes and Van der Most, 2016). Den Bieman and Kieftenburg (2015) note that the most critical hydraulic conditions for the failure mechanisms of coastal structures are the surge height, significant wave height, wave period and loading duration. This follows findings by Van Rijn (2009), who showed that an increasing storm surge level, wave height and wave period corresponded to increasing dune erosion. Therefore, these factors should be considered when comparing the influence of coastal structures on the safety of hydraulic structures. Roscoe et al. (2010) calculated the extreme wave heights and wave periods using a generalised Pareto distribution based on 30 years of measurements at various locations near the Dutch shore.

According to the KNMI (2014), the sea level in the North Sea is expected to rise by up to 80 cm until 2080 and up to 2.8 meters in 2200 (Kopp et al., 2014). This sea level rise can have significant effects in relatively shallow coastal seas such as the North Sea, on processes such as tidal propagation, storm surges, wave heights, and on the future existence of intertidal areas in the Western Scheldt, Wadden Sea and the proposed Voordelta estuary. This impacts the coastal safety in the Netherlands through the obvious sea level rise, but Arns et al. (2017) describe how it can also enhance separate processes such as increasing wave impact.

De Winter et al. (2012) find a directional change of the yearly highest waves coming from the southwest more often than now. As the winds from the southwest have a shorter fetch than winds from the north and northwest, this results in the yearly maximum wave height and wave period being lower than the yearly maximum wave heights and wave period at this moment. However, Sterl et al. (2009) note that these south-western winds are not important for storm surges, meaning that the 1/10000 storm event is not affected by this change in wind direction, which is still expected to occur with a north-western wind. This is confirmed by De Winter et al. (2012), who did not find a significant change in the expected wave height and wave period with a return period of 10000 years.

The effect of MSLR on the tidal amplitude is highly dependent on location. As a greater water depth reduces energy dissipation at the bottom, this should result in a greater tidal amplitude in shallow areas. In addition to this, it is possible that since the tidal wave propagates faster in shallow areas as a result of sea level rise, shelf seas could reach resonance with respect to deep oceans (Green, 2010). Roos and Velema (2011) modelled the expected impact of MSLR on the southern North Sea tidal amplitude. They show an increase in the tidal amplitude in the German Bight. Along the Dutch coast however, the modelled amplitude of the M_2 tidal component increases about a centimetre at most when applying a 1-metre sea level rise. Pickering et al. (2012) find a slightly larger increase of 10 centimetres in Vlissingen when applying a 2 metres sea level rise. An important note considering the response of the tides and storm surges is that this could result in newly flooded areas, which will act as dissipative areas for tide and surge, dampening the tidal wave. In these models, a so-called fixed shoreline was applied, meaning that it was assumed that no such flooding would occur. This is considered a reasonable assumption for the Dutch coast, which will also be applied in this study. Finally, Rasquin et al. (2020) call attention to the fact that the tidal amplitude near the coast is influenced considerably by topographic features such as estuaries, tidal flats and channels and that these have a considerable role in the tidal dynamics on a more local scale. However, the previously noted papers do not adequately resolve these features, as shelf models typically have a cell size of 2 to 7 kilometres. As this research focuses on these smaller-scale topographic features, it is crucial to resolve this part of the model in a sufficiently small resolution. Despite this, and despite the models and the boundary conditions of the models

varying considerably, the models show very similar results for the tidal increase as a result of MSLR.

Concluding, to assess the influence of the DTP on coastal safety, the focus should be on changes in water level, significant wave height, wave period and duration of the loading. The incoming wave characteristics have been calculated for a return period corresponding to the highest safety levels in the area. Mean sea level rise should be included in the assessment, as this can increase several components of the hydraulic load. Wind conditions during extreme storms and tidal amplitude are not expected to change with climate change in this century. Finally, a small grid size should be used to include the local influence of small-scale topographic features.

2.4. Morphological processes in the Voordelta

In order to be able to evaluate the influence of the dam on the morphological processes in the Voordelta area, an analysis has been done of the studies describing the current dominant morphological processes in the area. The entire Voordelta area can be defined as being part of the Dutch shoreface, which extends to the limit of the effective wave influence on the seabed morphology (Van der Spek et al. (2022)). In The Netherlands, this limit is 20 metres below NAP (Mulder, 2000). Of this area, the area below 8 metres depth is defined as the lower shoreface (J. Van der Werf et al., 2017). Grasmeijer et al. (2022) state that peak tidal velocities and their asymmetry determine the sand transport rates along the Dutch coast, as well as density-driven and wind-driven flows, the former being the more significant. As a result, the three-dimensional flow structure can not be neglected.

Using a three-dimensional flow and wave model of the North Sea, Van der Spek et al. (2022) calculated that the annual net sand transport at the 20 m depth contour is directed north-east, with the alongshore-directed sand transport being a factor 10 larger than the cross-shore sand transport. Along the Delta coast, transports are directed towards shallower water. They also found that storm conditions play an important role for the net transport rates at the lower shoreface, with high waves changing the net transport direction. Elias et al. (2017) describes the evolution of the Voordelta, explaining that the construction of the Delta Works caused the loss of intertidal areas at the upper shoreface due to the disappearance of shore-normal tidal flow. Based on a sediment budget, they concluded that the area loses significant volumes of sediment yearly, mainly due to the alongshore sediment transport directed north. Therefore, trapping sediment at the northern boundary can counteract the negative trend in sediment balance. However, their assumption that no sediment exchange over the 20 m depth contour occurs is refuted by Van der Spek et al. (2022) and J. Van der Werf et al. (2017), meaning that the actual sediment loss can be even more considerable.

Based on these studies, research into the effect of an oblique DTP dam should initially focus on the sediment budget of the area and the trapping capacities of the dam and its blockage of transport at the lower shoreface. A modelling study should be performed by a three-dimensional flow model with waves modelled separately, including storm effects.

2.5. DTP modelling approach

To make an accurate estimate of the DTP dam's power output, it is essential to conduct an accurate simulation of the water levels surrounding the dam. To achieve this, a numerical model is necessary. The concept of DTP is based on large-scale structures, with the primary process influencing the water level being the tidal wave propagation through the basin. As the wavelength of the tide ($\mathcal{O}(10^5 \text{ m})$) is several orders of magnitude larger than the depth in the North Sea ($\mathcal{O}(10^2 \text{ m})$), a model based on the two-dimensional shallow water equations is suitable. This matches with the method used by previous studies on the effect of DTP dams on the water level, such as Dai et al. (2017), Liu and Zhang (2014) and Park (2017). For estimating the influence of the DTP dam on coastal safety, the water level and wave characteristics, which are the most critical parameters concerning coastal safety in The Netherlands (Chbab and De Waal, 2017), should be estimated. For this reason, a coastal or shelf-sea wave model should be used, which can be nested in the flow model.

2.6. Conclusion

Previous research on DTP has provided theoretical groundwork for the idea, and numerical models have demonstrated its proof of concept. However, these studies considered a dam perpendicular to the coast, limiting the application of their results in this case. Furthermore, all studies mentioned only took tidal forcing into account, as this is the primary forcing process, especially in locations such as the west coast of Korea, with a tidal range of up to eight meters. However, the tidal range is significantly smaller near the Dutch coast compared to Korean and Taiwan Strait locations. The influence of atmospheric conditions could therefore have a more significant influence on the average head difference over the dam and should therefore be included in this research. Finally, all these studies focus on the water head and related power generation without considering other functions of the construction.

The numerical models should consider individual turbines, including energy loss factors, rather than the water head over the entire dam. When considering the hydraulic conditions determining coastal safety, the focus should be on wave characteristics and water level. Mean sea level rise should be included in the assessment, but other aspects of climate change have a negligible effect on extreme storm conditions. Both models should have a flow model based on the two-dimensional shallow water equations as the basis, with a coastal wave model added to assess the coastal safety.

A modelling study on the morphological impact of the dam should be carried out using a three-dimensional flow model. The three-dimensional modelling of the morphological system is outside the scope of the present work. Instead, a hypothesis on the expected morphological changes in the area is formulated based on existing literature and the hydrodynamic simulations.

3

System Analysis

In this chapter, a comprehensive system analysis of the area of interest is conducted in order to provide a detailed understanding of the area and the governing processes. Specifically, this chapter discusses the location of interest and its geographical characteristics, the characteristics of the governing hydrodynamic and morphological processes. Finally, the chapter discusses the recent morphological development of the area as a result of human interference through the construction of the Delta Works.

3.1. Location analysis

In this chapter's first part, the geographical characteristics of the area of interest are described, as well as the dominant hydrodynamic and morphological processes.

3.1.1. Geographical characteristics

The Voordelta is the area that will be most heavily influenced by the construction of a dam southwest of Maasvlakte 2. The Voordelta is a Natura 2000 protected area comprising the shallow-sea area in front of the delta coast in the southwest of the Netherlands. It is located between the navigation channel towards the port of Rotterdam in the north and the Dutch-Belgian border in the south. On the east side, it includes beaches and dunes, while on the west side, it ends at the 20 metres NAP depth contour, which is considered the edge of the morphologically active region in the Netherlands. It consists of the ebb-tidal deltas of the five major (former) estuaries in the region: the Brielse Maas, the Haringvliet, the Grevelingen, the Eastern Scheldt, and the Western Scheldt. These ebb-tidal deltas form a shallow area off the southern Dutch coast up to 10 kilometres offshore. The average depth is the smallest in the north of the area, as is the surface area of the shoals. After the North Sea flood of 1953, most of these estuaries have been dammed entirely or partly, so only the southernmost two can still be considered tidal basins. The area and bathymetry are shown in Figure 3.1, as well as the different ebb-tidal deltas it consists of.

The sediment distribution consists of sand and mud, resulting from the former periodic exchange of sand and mud between the estuaries and the delta (Van de Kreeke and Haring, 1979). As a result of the dominant north-directed longshore transports, the mean sand diameter is largest in the south, with an approximate mean sediment diameter of 200 μm , which gradually decreases to 150 μm in the north of the area.

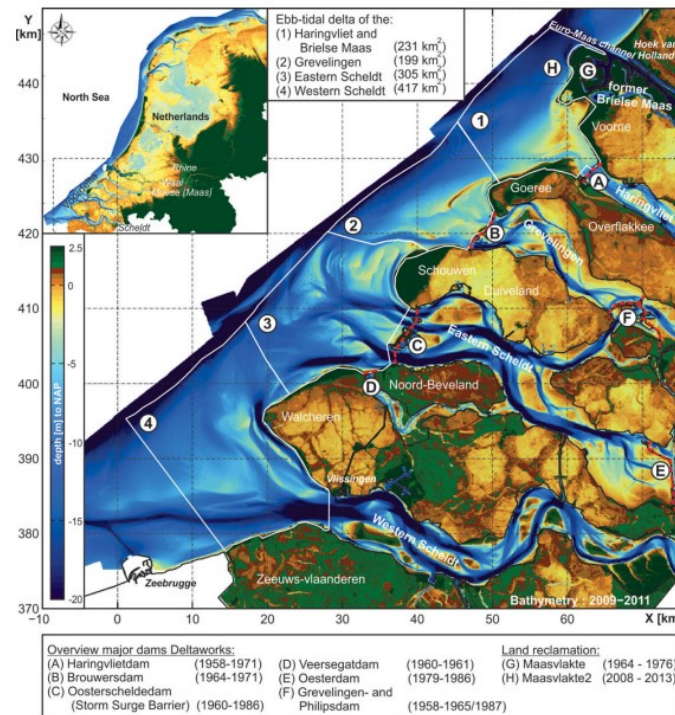


Figure 3.1: Overview of the Voordelta area and the different ebb-tidal deltas it consists of. From Elias et al. (2017). Note that this figure does not include the complete shape of the land reclamation Maasvlakte 2, which nowadays extends further into the North Sea at the location indicated with 'H'.

3.1.2. Hydrodynamic conditions

According to Elias et al. (2017), waves and tides are the dominant hydrodynamic forcing mechanisms in the Voordelta. The dynamic environment is characterized by shallow bars and shoals divided by deep tidal channels. Typically, the density gradients do not significantly affect the local morphology, except during large discharge periods from Haringvliet. A short overview of the tidal and wave environment will be given in the following subsections.

The tidal wave propagates counter-clockwise through the southern North Sea, from south to north along the Dutch coast. The mean high water measured in 2019 at the measurement location Roompot buiten, at the Eastern Scheldt barrier, is 1.59 m, and the mean low water measured is -1.26 m (Bosboom and Stive, 2021). The mean tidal range is 2.85 m, classifying the tide as a meso-tidal regime. The complete tide consists of a large number of constituents, the most critical four being the two main semi-diurnal components M_2 and S_2 and the two main diurnal components K_1 and O_1 . Of these four tides, the M_2 is the dominant constituent in the North Sea. Tide creates areas near the coast that are exposed during low water and submerged during high water, the so-called intertidal areas. The tidal wave is skewed and flood dominant, with a maximum flow velocity of about 1.25 ms^{-1} .

Waves near the Dutch coast come mainly from the northwest and southwest, with the highest waves coming primarily from the northwest, especially waves with a significant wave height greater than four metres, see Figures 3.2 and 3.3.

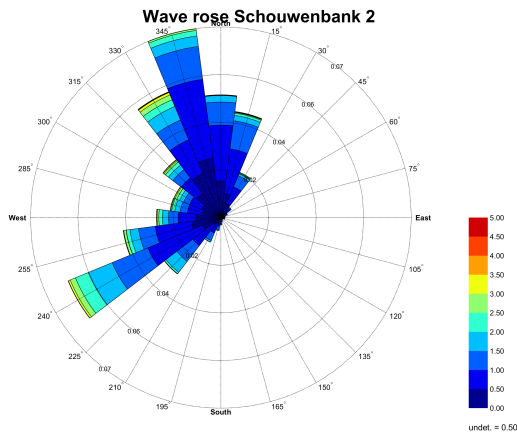


Figure 3.2: Wave rose at buoy Schouwenbank 2, off the coast of Zeeland. Based on wave data from 2021-2022.

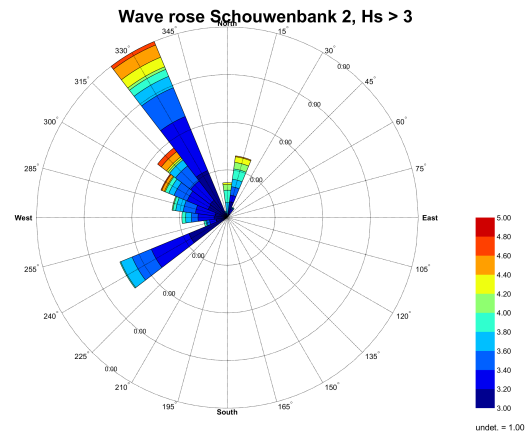


Figure 3.3: Wave rose of waves with a significant wave height over 3 m at buoy Schouwenbank 2, off the coast of Zeeland. Based on wave data from 2021-2022.

According to the classification used by Davies and Clayton (1980), the wave climate in the North Sea can be classified as a storm wave environment. It is classified as a high-wave environment in the north of the North Sea. However, the average significant wave height is lower further south and nearer to the Dutch coast. The measured average significant wave height at the Schouwenbank buoy in 2021-2022 is 0.93 m, classifying this part of the sea as a medium wave-energy environment. This means the wave heights are relatively large, while the wave periods are relatively low, around 5 seconds, although these can more than double during storm conditions. As can be seen in figure 3.4, the conditions are roughest during winter as a result of the higher wind velocities and storm conditions during these months, as in these months, the wave climate is the most energetic. The shape of the density spectrum resembles that of the JONSWAP spectrum for most months, which is logical since the JONSWAP spectrum is based on observations on the North Sea.

With these values for tidal range and wave height in mind, the coast near the Eastern Scheldt barrier can be classified as being on the border of low tide-dominated and mixed-energy with tide dominance, according to Davis Jr. and Hayers (1984). As the tidal range increases to the south and decreases to the north, the bigger part of the Voordelta coast currently has a mixed-energy environment with tidal dominance, and in the northernmost part it tends to a mixed-energy wave dominated environment.

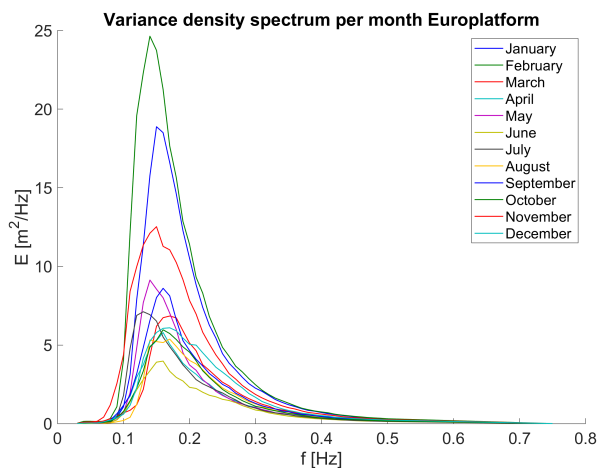


Figure 3.4: Variance density spectrum of the waves measured in 2014 at the Europlatform, off the coast of Zeeland. The plots show the averaged density spectra for each month separately.

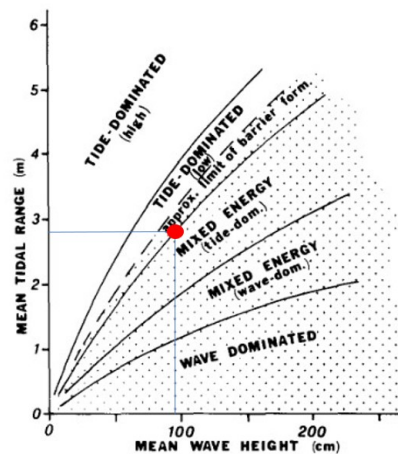


Figure 3.5: Classification of the conditions near the Dutch coast, adapted from Davis Jr. and Hayers (1984).

3.1.3. Morphological processes

As stated in the previous section, the area is predominantly influenced by tides and waves, which are also the most critical factors contributing to sediment transport in the area. Although the main part of the Voordelta can be qualified as a mixed-energy environment, Elias et al. (2017) describe how the morphology of the major inlets shows characteristics that are typical for a tide-dominated environment, specifically large ebb-tidal deltas and deep channels. They determine that this is the result of the area's relatively low wave energy combined with the estuaries' large tidal prisms.

A storm climate such as described in Section 3.1.2 is characterised by highly variable waves in height, period, and direction. This results in dynamic sandy coastal profiles corresponding with the Dutch coast (Bosboom and Stive, 2021). This also has as result that the active coastal zone extends to large water depths, as the waves break at relatively large water depths. In The Netherlands, the edge of the active coastal zone is assumed to be at 20 meters depth (Mulder, 2000).

As is the case for the Dutch coast, long-term longshore sediment transport towards the north is present, resulting from the dominant flood tidal currents directed north. Van der Spek et al. (2022) emphasise that the longshore sand transport is a factor 10 larger than the cross-shore sand transport and that these transports in the Voordelta are directed to shallower water. This also results in a coarser mean sand diameter in the south of the area compared to the north, which increases from circa 150 μm in the north to circa 200 μm near the mouth of the Eastern Scheldt (Van de Kreeke and Haring, 1979). In Grasmeijer et al. (2022) is stated that the net annual sand transport rates along the Dutch coast are determined by peak tidal velocities and tidal asymmetry, as well as density-driven flows, wind-driven flows and waves. The wind-driven flows are predominantly directed offshore near the bed, while the density-driven flows are predominantly directed onshore. They conclude that because of this, excluding the effects of density in modelling studies results in a significant decrease in onshore-directed transports.

Van der Spek et al. (2022) describe the sand transport on the lower shoreface in The Netherlands, the zone between 8 meters and 20 meters depth in The Netherlands. This area comprises a large part of the Voordelta area. The sand transport in this area is episodic and is determined by high-wave events. J. Van der Werf et al. (2017) note that the annual net cross-shore transport rates are 0-20 $\text{m}^3/\text{m}/\text{year}$ in the onshore direction at the 20 m depth contour for the Holland coast. At this depth, sediment transport is nearly completely comprised of near-bed transport. It is unclear, however, if this is also the case at the Delta coast, as the onshore transport described seems to be driven by density-driven currents resulting from the Rhine discharge, which primarily flows north. At the 8 meters depth contour, the edge of the upper shoreface, the net transport appears to be net zero, resulting from the onshore process being cancelled out by the offshore transport. Van der Spek et al. (2022) describe how sand is transported offshore in the lower shoreface due to downwelling currents during storm events, which then slowly return due to energetic wave conditions, described by J. J. Van der Werf et al. (2022) as conditions with significant wave heights above 3 m.

3.2. Recent development of the Voordelta

In the past half-century, the Voordelta has been changed heavily due to large-scale human interference in the system through the construction of the Delta Works. To gain insight into the anticipated changes resulting from the DTP dam construction, this section explores the area's recent development, resulting from this interference.

The morphology of the ebb-tidal deltas changed considerably after the damming of the estuaries. Kohsiek (1988) concluded that the ebb-tidal deltas of the Haringvliet and Grevelingen were reduced by 60%, as the deltas were no longer maintained by the tidal currents, the waves gained a larger influence on the morphology. This resulted in a process where the deeper parts of the ebb-tidal delta eroded, and the eroded material was moved onshore by the asymmetry of wave orbital motions, causing the bars to migrate landwards. When the bars reached the intertidal zone, the residual tidal current balanced landward transport by waves. Elias et al. (2017) also describe how shore normal tidal flow disappears due to the disappearance of the tidal inlets, causing the shore-parallel tidal currents to become dominant. Both the Haringvliet and Eastern Scheldt were kept partially open, but the combination of the elevated foundations of the barriers and the scour pits that developed on the sides of the barriers resulted in blockage of non-suspended sediment through the barriers. This, combined with a reduction of the tidal prism of these inlets, resulted in a decrease in sand supply by the ebb current. This combination of factors increased the relative magnitude of wave-driven sand transport, resulting in net sediment transport in landward direction. A significant result of these factors was the erosion of the shoals in front of the island of Schouwen. This resulted in decreased wave dissipation, causing a sustained wave attack on the island. As a result, the upper shoreface of the island has consistently been eroded, which has to be countered by nourishments carried out every five years on average (Vermaas et al., 2015).

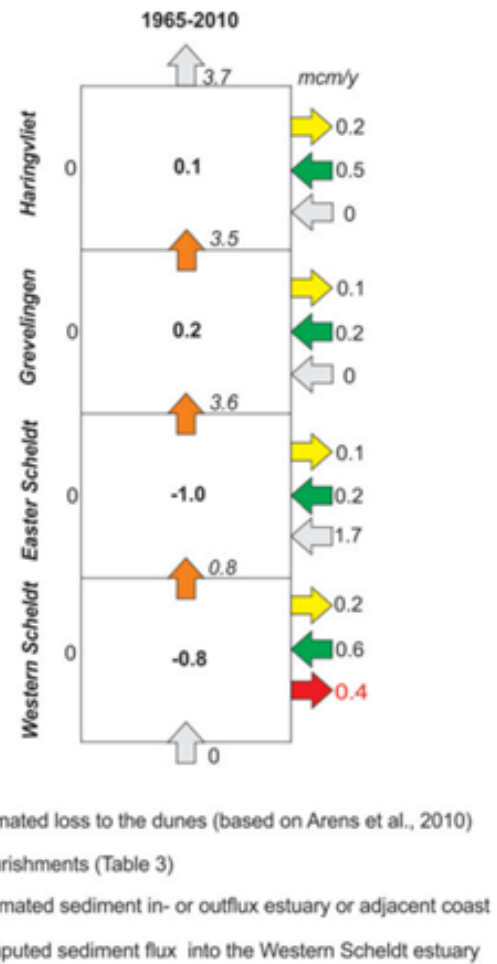


Figure 3.6: Sediment budget of the Voordelta, from Elias et al. (2017).

Since the completion of the Delta Works, the combined four ebb-tidal deltas have lost $0.5 \cdot 10^6$ cubic meters per year, even though a total volume of 95 million cubic meters has been nourished in that period (Elias et al., 2017). However, the differences between the ebb-tidal deltas were significant. Although the shoals moved further nearshore, especially at Grevelingen and the Haringvliet, these ebb-tidal deltas experienced an overall sediment gain since 1965. Elias et al. (2017) made a sediment budget of the four separate ebb-tidal deltas, shown in figure 3.6. To come to this model, they made a couple of important assumptions. First, since the depth of -20 m of the NAP is considered the lower limit of the active coastal system, it is assumed that there is no sediment exchange over this line (Mulder, 2000). The northern boundary condition is determined from the yearly dredged sediment volumes from the port of Rotterdam shipping channel, as Van Rijn (1997) determined that the combination of the harbour jetties and continuously dredged channel block all sediment exchange between the Voordelta and the Holland coast. Furthermore, no sand exchange was assumed through the eastern Scheldt barrier and Haringvliet, as well as a loss of nourishment to the dunes. Importantly, no influx over the southern boundary was considered due to the assumption that the harbour jetties at Zeebrugge, Belgium, block

all longshore transport. This means that no sediment influx into the system was considered possible except the Western Scheldt and as a result of nourishments.

3.3. Coastal safety assessment of the Dutch Delta coast

One of the objectives of this study is to assess the impact of the construction of the DTP dam on the coastal safety of the Voordelta. To be able to make this assessment correctly, the methods used to determine the strength of the coast and the characteristics commonly used to indicate coastal safety are discussed in this section.

The coast of the Dutch Delta can be divided into soft and hard coasts. The chance of failure of these and all other primary coastal defences in The Netherlands are described in the Waterwet (2021). For every section of the coast, a lower limit for storms that the defence should be able to withstand has been determined. In the Voordelta, this lower limit is 1/10000 per year for the Eastern Scheldt Barrier and the coast immediately south of Maasvlakte 2. The rest of the dune coast, as well as the Brouwersdam and the Haringvliet sluices, have a lower limit of 1/1000 per year (Slootjes and Van der Most, 2016).

3.3.1. Dune coasts

For the soft coasts, the coastal defence consists of a dune row combined with the beach in front of the dunes. To ensure the safety of these coasts, in 1990, the Dutch government adopted a policy called Dynamic Preservation. This policy had as its primary goal the preservation of the position of the coastline at the position it was at in 1990 (Ministerie van Verkeer en Waterstaat, 1990). To include the complete sand volumes on the beach in the analysis, the so-called momentary coastline was defined, which defines the coastline position as a function of the volume of sand in the nearshore zone. This momentary coastline is then compared yearly with its position in 1990. When a decreasing trend is apparent, and the beach position gets below the baseline, sand nourishments are applied (Van Koningsveld and Mulder, 2004).

Currently, the regions that should most be paid attention to in this research are the southwest side of Schouwen and the east side of Goeree, both of which show a considerable landward trend of the coastline. With a few minor exceptions, the other locations show either a minimal trend in either direction or a positive trend. (*Kustlijnkaarten 2023* (2022)).

The location of the dune foot varies relatively little, usually a few metres per year at most. However, during extreme storm events, the dune foot can be eroded metres during a single event. For example, the extreme storm of 1953 eroded the dune foot by 10 to 15 meters in several Dutch regions (Ruessink and Jeuken, 2002). Because of this, it is important that the expected characteristics of extreme events are also known at beaches. Van Rijn (2009) and others showed that dune erosion is determined by both characteristics of the dune itself and characteristics of the storm event, with primary influencing characteristics being the offshore wave height, the peak wave period, the wave angle and the storm surge level. Van Rijn (2009) also showed that an increasing storm surge level, wave height and wave period corresponded to increasing dune erosion, while dune erosion increases for wave angles of incidence of 0° to 10°. Larger angles of incidence did not show an increased rate of erosion. These characteristics should therefore be compared for storm conditions to examine the effect on coastal safety of large-scale interventions such as the proposed dam. Note that Van Rijn refers to offshore values, meaning an extensive beach model is not necessarily required in order to make an assessment of the coastal safety, this assumption is adopted in this study.

3.3.2. Eastern Scheldt Barrier

The coastal structures such as the Eastern Scheldt Barrier have been designed and constructed with certain hydraulic loads in mind that respond to the conditions in design extreme storm events. In the case of the Eastern Scheldt Barrier, this design water level was NAP + 5.8 meters, which included 50 centimetres to account for MSLR during the 200 years the barrier was designed to last. However, compared to more recent MSLR predictions for the North Sea, such in KNMI (2014), who estimated a MSLR of up to 85 centimetres in this century alone, it can be concluded that this design estimate turned out to be too low. In addition, the lower safety limit of the Eastern Scheldt has been increased from 1/4000 per year to 1/10000 per year (Waterwet, 2021). Den Bieman and Kieftenburg (2015) note that the most important hydraulic conditions for the failure mechanisms of coastal structures are the surge height, significant wave height, wave period and duration of the loading. Therefore, these factors should be considered when assessing the coastal safety.

3.4. Conclusion

In the system analysis was concluded that waves and tides are the dominant hydrodynamic factors in the area. As was explained in Chapter 2, the dam's energy yield depends on the long-term water level difference over the dam. This means that of the two named factors, tides are expected to be the dominant factor influencing the energy yield of the dam, which corresponds with the principle of the dam, which is based on tidal velocities.

It has been described how the hydraulic load on both hard and soft coasts depends on the same storm characteristics: significant wave height, wave period, surge height and duration of the loading. The dam's influence on the area's coastal safety can therefore be determined by determining the effect of the dam on these characteristics.

Among others Bosboom and Stive (2021), J. Van der Werf et al. (2017) and Grasmeijer et al. (2022) note how wind-induced currents, density-driven flows and other processes are three-dimensional processes, meaning that for a correct, small-scale representation of the sediment distribution in the estuary, a 3D morphological model is best.

4

Reference layout of the DTP dam

A reference layout must be determined to indicate the impact the dam will have on the surrounding area and its energy yield, which will be used in the remainder of the research. In this chapter, this reference layout is determined based on several requirements. Subsequently, the effect of the dam on the hydrodynamic processes in the Voordelta is investigated to give an indication of how the design of the dam influences the tide. To achieve this, first a set of requirements is formulated. Based on this set of requirements, a reference design is devised. Finally, a first analysis is made of the impact of this design on the hydrodynamic conditions in the area.

4.1. Design requirements

As described in Chapter 1, the proposed starting location of the dam is at the Maasvlakte 2, as at this location, a lot of the necessary energy infrastructure is readily available. Besides this, the energy generated by the DTP dam can be used by the port of Rotterdam, which takes up 10 to 20 percent of the total Dutch energy consumption (Hentschel et al., 2018). This means that the energy generated by the DTP dam can be used immediately at the location where it is generated, reducing the need for costly strengthening of the national power grid. The orientation of the proposed dam is southwards from the Maasvlakte 2 in order to have minimal overlap with areas in the North Sea designated for other purposes. These areas and their functions are defined in 'Structuurvisiekaart Noordzee', part of the Programma Noordzee 2022 2027 (Ministerie van Infrastructuur en Waterstaat, 2022). The complete map can be seen in Appendix A.

As shown in Figure A.1, several areas can be distinguished near the Maasvlakte 2 and the province of Zeeland. Most notable is the area in green, the Natura 2000 protected area Voordelta in front of the entire coast of Zeeland, which reaches to the 20 meters depth line. Any construction activities in this area should be prevented and construction should not harm this area. This is the most critical region to avoid in the dam's design. In the north of the map, the deep blue shipping channel of the port of Rotterdam can be seen. The dam should not interfere with the shipping route. Also, the dam should be built sufficiently far from this channel so that dredging and shipping activities do not pose a danger to the dam's structural integrity. It is, however, favourable to construct the dam within the vicinity of the channel, as it could be used as a wave breaker for part of the shipping channel, shielding it from waves from the south. In darker/greyish blue, three rectangular anchoring areas for the Port of Rotterdam can be identified. It is deemed acceptable to pass through the northern areas partly, but the other two should be avoided except in the case of a clear benefit to one of the goals of the dam. Finally, outside the Natura 2000 area, a large area with blue dots can be identified. This signifies the area reserved for sand mining. Moving through this area with the dam is deemed acceptable, as the total area reserved for this purpose is large. Immediately around the dam, a ban on sand mining should be placed, as this could interfere with the dam's structural integrity. This will only be a relatively small part of the area, meaning that most of the designated sand mining area will still be able to be used as such.

Lastly, the bathymetry of the coast should be considered. In front of the coast, several prominent sand ridges parallel to the coast can be found. In the dam's design, the choice was made to follow these ridges, as this can significantly lower the construction costs.

Based on this, several requirements have been formulated in order to design a reference layout for the purpose of this study. These are:

- The dam should start at the Maasvlakte 2.
- The dam should have a southwest orientation.
- The dam should have minimal overlap with regions designated as Natura 2000, navigation routes and anchor areas as defined in 'Programma Noordzee 2022-2027' (Ministerie van Infrastructuur en Waterstaat, 2022).

Furthermore, three additional choices have been made in the design. These are:

- The length of the dam should be in the order of magnitude of 50 kilometers, similar to designs considered in previous studies.
- The dam should block waves from the North Sea headed for the Eastern Scheldt Barrier during extreme storm conditions.
- Where possible, should the dam follow sand ridges in the North Sea.

The length of the dam has significant influence on the hydrodynamic conditions and processes within the estuary. However, as the objective of this study is to give a first assessment of the energy output of a DTP dam with this orientation, the choice was made not to optimise the design of the dam for energy generation. Instead, the length of the dam was chosen to be in the order of magnitude that has been used in previous studies on DTP dams, which means it should be between 30 and 65 kilometres long. Previous studies on DTP in the Netherlands assumed a length of 50 kilometres, which is therefore given as an aiming point for the length. A second criterion is that the dam should be long enough to block incoming waves during extreme storm conditions from reaching the Eastern Scheldt Barrier. This choice was made because this barrier is the part of the Dutch Delta coast with the highest safety criterion, which it is expected not to comply with in the near future.

Based on the three criteria and the minimal and maximum length, the possible locations for the reference layout of the dam are shown in Figure 4.1.

It can clearly be seen in Figure 4.1, that is not possible to have a dam with a southwest direction from Maasvlakte 2 without passing through the Natura 2000 area. In the reference design, the part of the dam which passes through the Natura 2000 area should be minimised.

Based on these requirements, the minimum and maximum length of the estuary are 30 and 65 kilometres. The created estuary would have a minimum width of 11 kilometres at the narrowest point and a maximum width of 40 kilometres in case of a dam with a west-southwest direction.

4.2. Reference Design

For this study, the choice has been made to base the length of the dam primarily on the requirement that it protects the Eastern Scheldt Barrier from the expected incoming storms. The largest waves have been determined to come from a direction between 285° and 15° north, so the dam should be long enough to block waves from these directions. To account for slight outliers, the choice was made to extend the dam to a length so that waves coming from a direction of 280° or more can not reach the most southern part of the Eastern Scheldt Barrier. This means the dam should extend to a point 57.5 km southwest of the Maasvlakte 2, which is the approximate length of the created estuary. The total length of the dam is 62.5 kilometres. In this design, the width of the opening of the estuary is 18 kilometres. The distance from the Eastern Scheldt Barrier to the dam is approximately 23 kilometres with this design, which is also the widest point of the estuary. The created estuary has an approximate basin area of 1000 km^2 and an average depth of 13 metres.

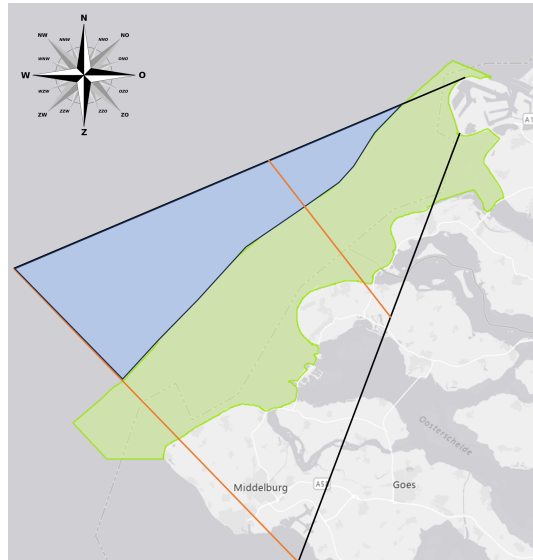


Figure 4.1: The areas in which the reference layout can be located based on the criteria. The green area shows the Natura 2000 area. The black lines show the west-southwest and south-southwest direction from Maasvlakte 2. The red lines show the 30 and 65 kilometre distance lines from Maasvlakte 2. Finally, the blue area shows the area the dam can be constructed in. Adapted from Natura 2000 (n.d.).

Considering the points discussed in section 4.1, the reference layout of the dam as has been used in this study can be seen in figure 4.2. This means that the dam will disturb a small part of the Natura 2000 area Voordelta. This lost nature area will have to be made up for, for example, by improving the remaining nature in the Nature 2000 area, such as has been done for the construction of the Maasvlakte 2. The dam loosely follows the edge of the Natura 2000 area, although it slightly deviates from it in order to follow the sand ridge.

4.3. Influence DTP dam on the tidal wave

It is expected that the tidal amplitude within the estuary could be changed, resulting from either tidal amplification or damping on the inside of the dam, which could result in a water level difference over the dam. As a result of the construction of the dam, two main processes cause the tidal amplitude to be dampened or amplified. Firstly there is the possibility of resonance. According to Webb (1974), shelf resonance occurs when the wave travelling from the shelf edge is reflected at the coast, which happens when the shelf is approximately $1/4$ wavelength or an uneven multiple of a quarter wavelength of the tidal wavelength, the so-called quarter-wavelength resonance. The same can be applied to estuaries when the estuary length is roughly $1/4$ of the tidal wavelength on the shelf or an uneven multiple of this. As on the European continental shelf, shallow water conditions can be applied to the tidal wave. The tidal wavelength can easily be approximated using equation 4.1.

$$\lambda = \sqrt{gh}T \quad (4.1)$$

In this equation, λ is the wavelength of the tidal wave, h is the waterdepth and T is the wave period of the tidal wave. For the tidal wave a wave period of 12.4 hours and a depth of 20 meters near the location of the dam, which is located in the deepest part of the estuary, are assumed. With these characteristics, the approximate wavelength of the tidal wave near the coast is 625 kilometres. This means that, as the estuary will have a length of 57.5 kilometres, no quarter-wavelength resonance is expected. To approximate the quarter-wavelength resonance of the tidal wave within the estuary, the DTP dam would need a length roughly twice that of the DTP dam in the reference layout.

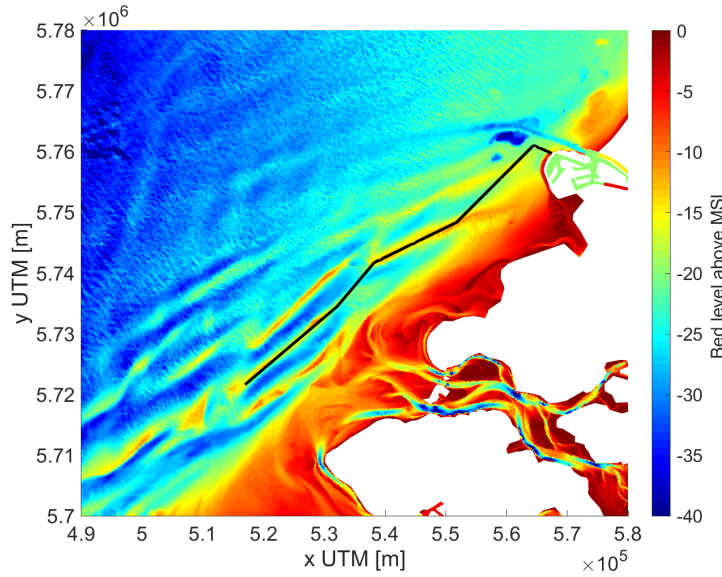


Figure 4.2: Bathymetry of the Voordelta area. In black, the DTP dam as used in the numerical models.

Although no quarter-wavelength resonance is expected, in coastal embayments, the quarter wavelength is only an approximation under natural conditions, as the bathymetry is not uniform across the estuary, meaning that the exact bathymetry can influence the extent of the tidal amplification (Godin, 1993). A second calculation can be done by considering the estuary as a semi-closed prismatic basin, with an opening at the seaside and a closed on the other side. On the open side, the water level in the estuary is determined by the harmonic movement of the tidal wave. This calculation is based on the propagation formulas for short waves in tidal basins as described in Battjes and Labeur (2017). These equations are based on the linearised one-dimensional momentum and mass balance equations. Battjes and Labeur (2017) state that for low waves in a prismatic conduit, the advective acceleration is relatively small and can be neglected in a first approximation. For a first approximation, the choice has been made to apply this simplification. It must be kept in mind that this is less applicable compared to natural estuaries because of the triangular shape of the inflow area, rather than a more or less rectangular shape that is more common, meaning that in the shallower part of the estuary, the tidal wave can not be classified as a low wave. Because this section aims to gain some first insights through a simplified approach, the choice has been made to assume an average depth.

As a result of this, the linearised momentum and mass balance equations can be used. An extensive derivation and explanation of the formulas used for this calculation can be found in Battjes and Labeur (2017). The equation used to calculate the so-called response factor is shown in equation 4.2.

$$r = \frac{\hat{\zeta}(l)}{\hat{\zeta}(0)} = \frac{1}{\sqrt{\sinh^2(\mu l) + \cos^2(kl)}} \quad (4.2)$$

In Equation 4.2, ζ is the surface elevation of the tidal wave, with position 0 at the opening of the estuary and position l at the landward end of the estuary. μ is the damping modulus, and k is the wave number. The complete calculation and the definition of all values can be found in Appendix B.

The calculations result in a response factor with a positive response in the order of 110 %, meaning that a slight amplification of the tidal wave is expected to occur in the estuary. As the quarter-wave resonance peaks at a value of $k_0 l = \frac{1}{2}\pi$, which is higher than the current value, it is expected that a longer dam would increase the amplification of the tidal wave within the estuary.

It is emphasised that this method is a severe simplification of reality, as the width and bathymetry change considerably along the length of the estuary. Besides this, this method does not consider the influence of the openings along the whole western side of the estuary.

The other often-occurring resonance process is called Helmholtz resonance. However, this resonance type only occurs in almost enclosed basins, with a narrow inlet connecting it to the ocean through which the tidal wave travels (Terra, 2005). As this is not the case, this type of resonance is not expected.

4.4. Influence of the dam design on the wave climate

This section discusses the expected influence of the dam on the waves attacking the Eastern Scheldt Barrier.

To calculate the impact of the dam on incoming swell waves during storm conditions, it is assumed that all waves coming from a northwestern direction are completely blocked. Because of this, wave heights at the barrier are solely determined by the wind velocity behind the dam, the distance to the barrier and the waterdepth in front of the barrier.

It must be noted that this calculation is a simplified first estimate, as it only considers wind generation, with depth-induced breaking as a reference. In reality, processes such as bottom friction, shoaling, current refraction and other processes significantly impact the wave height and wave propagation near the coast. For this first simple analysis, this calculation is deemed sufficient however. A numerical model will be used for more precise calculations, of which the results are presented in Chapter 6.

The wave growth behind the dam is determined using the equations and parameters to calculate the dimensionless wave height in limited-depth water for all sea states as described in Breugem and Holthuijsen (2006), with the deep water limited wave height \tilde{H}_{∞} defined at 0.24.

The dimensionless significant wave height, fetch and depth are calculated using equations 4.3, 4.4 and 4.5. For a more thorough explanation of wave growth in coastal waters, see chapters 6.3.2 and 8.3 from Holthuijsen (2017).

$$\tilde{H}_{1/3} = \frac{gH_{1/3}}{U_{10}^2} \quad (4.3) \quad \tilde{F} = \frac{gF}{U_{10}^2} \quad (4.4) \quad \tilde{h} = \frac{gh}{U_{10}^2} \quad (4.5)$$

With g the gravitational constant, $H_{1/3}$ the significant wave height, U_{10} the wind velocity at 10 metres altitude, F the fetch and h the waterdepth.

Using these equations, two calculations have been carried out, one assuming a waterdepth of 5.2 metres, which is the design water level according to 'Hydraulische Randvoorwaarden primaire waterkeringen' (Ministerie van Verkeer en Waterstaat, 2007), and one with an average water depth of 12 metres, which is the average depth added to the 5.2 metres. In the first case the calculated significant wave height at the barrier is 2.03 metres, in the second 3.12 metres. It is assumed that waves are depth-limited at the barrier without dam. When assuming a breaking parameter of 0.7, these values correspond to depths of 2.9 and 4.46 m, respectively. This means that in both cases the significant wave height is lower than the breaking wave height. This means that the waves are no longer depth-limited because of the dam, but limited by the distance between the barrier and the dam, which means that the dam significantly lowers the significant wave height in front of the Eastern Scheldt Barrier.

4.5. Influence of the dam design on wind set-up

A significant contributor to the hydraulic boundary conditions are the increased water levels caused by storm surges. These are produced by a combination of wind set-up caused by sustained high-velocity winds from the northwest and a lowered atmospheric pressure in the storm. Theoretically, it is possible to lower the wind set-up behind a dam. However, the water level reduces gradually behind the dam from the wind set-up water level. In the previous section, it was determined that the dam should only reach just past the Eastern Scheldt Barrier, meaning that the wind set-up will still impact the water levels behind the barrier. The wind set-up at the Eastern Scheldt barrier behind the dam is therefore not expected to be influenced by the dam. Further north however, the wind set-up is considered to have less impact during northwestern storms. During southwestern storms however, wind set-up is expected to increase as a result of the funneling effect. Furthermore, as Sterl et al. (2009) concluded, storm surges are not expected to increase in size due to climate change, neither because of increasing wind velocities nor from increased mean sea level.

4.6. Conclusion

In this chapter a reference layout has been devised which is used in all following calculations in this study. The derived reference layout has been devised based on a set of requirements set up for the purpose of this study, the most important of which are that the DTP dam should start at Maasvlakte 2, have a southwestern orientation and should have minimal overlap with Natura 2000 areas. The reference design for the DTP dam has a total length of 62.5 km and extends to a point 57.5 km south of Maasvlakte 2. The created basin has a minimum width of 11 km and a maximum width of 23 km. The created estuary has an approximate basin area of 1000 km^2 and an average depth of 13 m.

Based on a simple first calculation, some tidal amplification is expected within the estuary. No quarter-wavelength resonance is expected, as the estuary would have to double in length to reach that. Incoming swell waves coming from a northwestern direction are completely blocked from reaching the Eastern Scheldt Barrier, with as a result that under these conditions the significant wave height of incoming waves decreases significantly.

5

Energy Yield Assessment

This chapter describes the assessment of the energy yield of the oblique and perpendicular dam. First, the methodology used in this assessment is discussed. The second section consists of a description of the modelling software used and a discussion of the model that has been set up. Then, the results of the assessment are presented and, finally, these results are discussed and a conclusion to the research sub-question is given.

5.1. Methodology

This section gives a description of the steps taken to determine the energy output of the oblique and perpendicular dam, in order to answer the research question: *What is the expected energy yield of an oblique DTP dam, and how does this compare to a DTP dam perpendicular on the coast and to literature?*

The energy output of a DTP dam is determined by the water level difference over the dam, as explained in Chapter 2. The water level is most influenced by two physical phenomena: tidal forcing and meteorological effects, i.e. wind velocity and atmospheric pressure. For this reason, these two processes need to be captured in a numerical model that calculates the energy output of the dam. Therefore, a hydrodynamic two-dimensional flow model has been set up, in which the water level and the energy yield of the dam are calculated for extended periods.

This model has been used to estimate the energy yield that an oblique DTP dam from Maasvlakte 2 will generate and to compare it with the energy yield of a DTP dam perpendicular to the coast. The energy yield is calculated using a turbine module integrated into the numerical model.

The primary objective of this flow model is to provide information on the expected energy output of the DTP dam as described in Chapter 4. The second objective is to estimate the energy output of a DTP dam perpendicular to the coast under the same conditions so that the energy output of the proposed dam layout can be compared to that of the model proposed in previous research. To do this, two models have been set up, the first with a DTP dam as described in Chapter 4, the second with a DTP dam perpendicular to the coast from Maasvlakte 2 with the same length. The exact location of the DTP dams in their respective models is shown in figure 5.1. Apart from this, the input parameters of the two models are identical. For the calculation of the energy output of the oblique dam and the perpendicular dam, the same model parameters are used. Both models have been run for the same period of one year. As described in Chapter 2, because the tidal amplitude in the North Sea is lower, the meteorological input is expected to have a significant influence, compared to locations with a higher tidal amplitude, as previously studied. However, previous studies on DTP in the Netherlands did not include meteorological forcing in their models. For this reason a comparison has been made of the energy output calculated by the models with and without meteorological input.

The optimal open ratio of the DTP dam is used in the model to obtain an accurate result. However, because of potentially other governing hydrodynamic processes determining the water head over the oblique dam compared to the dam as used in Dai et al. (2017), the value for the optimal open ratio they found must be confirmed. For this reason, the optimal open ratio is investigated, which is then used in this study.

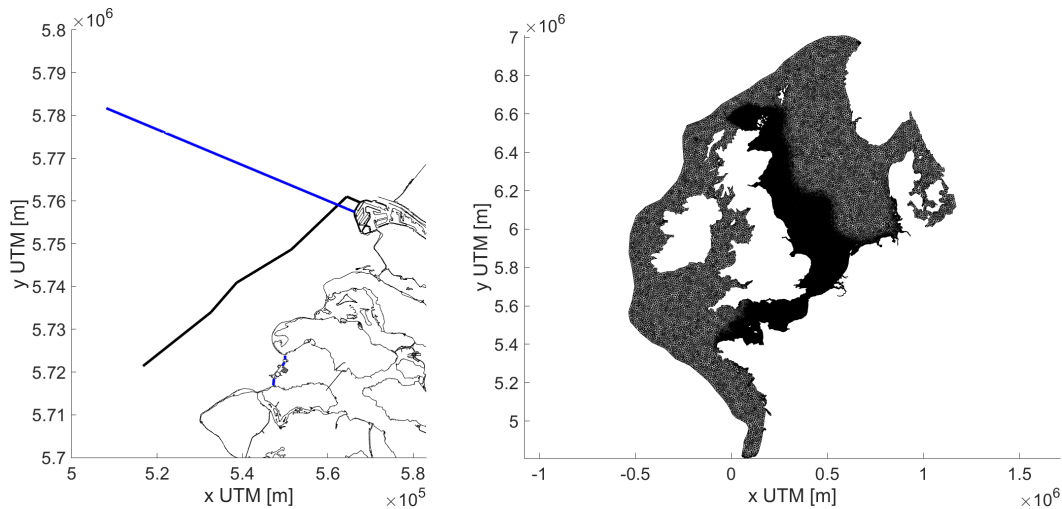


Figure 5.1: The two locations of the DTP dam used in the FINEL and SWAN models. The blue line shows the dam perpendicular to the coast. The black line shows the Voordelta dam.

Figure 5.2: 2D view of the computational grid of the FINEL North Sea flow model.

5.2. FINEL flow model

This section gives a description of the numerical model set up for the energy yield assessment. First, the used modelling software is described, followed by a description of the used model input and boundary conditions applied. Finally, the validation results of the model are presented.

5.2.1. Modelling software

For the energy assessment, the FINEL modelling software has been used. FINEL is a process-based model based on the shallow water equations, which are solved through the finite element method. FINEL is used in the two-dimensional, depth-averaged mode. Using this method, the water level variations over the dam can be represented accurately. A more comprehensive overview of the governing equations in FINEL2D is given in Dam et al. (2007). A benefit of the use of the finite element method rather than finite difference methods is that this method offers a significant amount of flexibility for the triangular grid generation, which allows for a high grid resolution in the area of interest and lower grid resolutions in the far-field, without having to use grid nesting (Kroon and Loman, 2015). A further reason to have chosen FINEL modelling software is the availability of a turbine module which uses Equations 2.4 and 2.7, as discussed in Section 2.2.

5.2.2. FINEL model input

The basis for the hydrodynamic flow model used is the FINEL European Continental Shelf (FECSM) model developed by Svašek Hydraulics. This FINEL2D model has been set up for the North Sea with tidal forcing and includes 32 tidal components that have been applied at the 71 boundary sections along the edge of the continental shelf. The tidal amplitudes and phases have been extracted from the global FES2014a world tide database. This model has been calibrated by Svašek Hydraulics by adjusting the Manning roughness throughout the model. The resulting calibrated roughness map can be seen in Figure 5.3. This calibration was executed for the period from May 2020 to June 2020. This period was chosen because it is a sufficiently long period for tidal models, including entire spring-neap cycles.

As mentioned, tidal forcing has been applied at the model boundary at the edge of the continental shelf. A fixed shoreline has been applied at the coast, similar to Pickering et al. (2012) and related studies.

In addition, a discharge boundary is applied at the Haringvliet, which is the river that flows into the Voordelta. The discharge volume is based on historical data, corresponding with the data implemented for the tidal and meteorological forcing. As of 2019, the Haringvliet sluices are opened slightly during high tides to allow salt water to flow into the Haringvliet and restore nature dependent on saline water in the Haringvliet, the so-called "Kierbesluit". However, the opening of the sluices has several restrictions to ensure that salt water does not propagate too far into the freshwater basin. This includes the requirement that freshwater discharge from the Rhine system is sufficiently large and that only a few sluices are partially opened at a time (Reeze et al., 2020). Because of this, the total discharge from the Voordelta toward the Haringvliet is considered small enough not to impact the hydrodynamics within the Voordelta. For this reason, the "Kierbesluit" will not be considered in this study. This means that the Haringvliet estuary is not included in the model and that only flow from the Haringvliet into the North Sea is considered as boundary condition.

Furthermore, since the Eastern Scheldt significantly influences the tidal wave in the projected estuary, the Eastern Scheldt has been included in the FINEL model. However, the Eastern Scheldt Barrier affects the flow into and out of this estuary. Therefore, this barrier has also been included in the model. The barrier has been modelled as three separate barriers, one for each opening. At each opening, the sill height used is the average sill height of the section. The gate height for all gates is 1 m above NAP (Rijkswaterstaat, 1986). The sill heights are:

- Roompot : 8.60 m
- Hammen : 6.32 m
- Schaar : 5.75 m

As the Eastern Scheldt Barrier closes on average once a year (Rijkswaterstaat, n.d.-b), the closures are not considered to affect the energy yield under average conditions significantly. For this reason, barrier closures have not been included in the model. Instead, the barrier is assumed to be open at all times.

Importantly, a turbine module is integrated in the model, which calculates the power output at every interface between two elements along the length of the dam. In the model, no water is assumed to flow over the dam. Instead, the flow through the turbines in the dam is modelled, depending on the water level difference over the dam and the open ratio of the section, using Equations 2.4 and 2.7. The total flow through the turbines is calculated separately for every section. Within FINEL, tidal power dam segments are always located at the interface between two triangular elements, meaning the dam is modelled as a sub-grid feature. At every interface, the number of turbines is calculated based on the open ratio of the dam. As the present hydrodynamic processes differ from those within the study by Dai et al. (2017), a sensitivity analysis regarding the optimal open ratio of the present tidal power dam has been performed, which is presented in section 5.3.1. In this study, a turbine diameter of 8.5 m is assumed. It is assumed throughout this study that the operational turbine settings can be dynamically adjusted so that the optimal value of a_{turb} for energy generation is always approached, meaning that a value of 2/3 is assumed in this study. The efficiency of the turbines, η , is assumed to be 85 % in this study.

On the entire model, meteorological data is applied. This data consists of wind velocities and directions, as well as pressure fields. Data from two different data sets were available, these have been compared in order to find the dataset that, when applied on the FINEL model, gives the best fit compared to measured data. This comparison is described in Section 5.2.3.

5.2.3. Validation hydrodynamic flow model

The model as described has been validated with historical data at several measurement locations in this research area. The validation has been carried out by comparing the model results to measured water level data of the astronomical tide. Compared to the calibrated FECSM model, the grid size was adjusted to optimise the computation time and accuracy of the results in the area of interest. The resulting chosen grid near the area of interest consists of elements with an element side length of

circa 1500 metres. For smaller grid sizes, no significant change in the root mean square error (RMSE) between the modelled and measured data was observed. In the area immediately surrounding the dam, a smaller grid size, with elements with a side length of 250 metres, was applied to ensure that the model could adequately determine flows around and through the dam. The distribution of the grid sizes across the complete model can be seen in Figure 5.2.

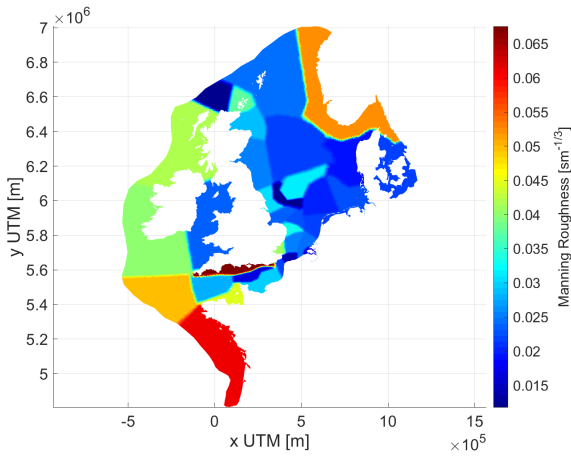


Figure 5.3: Roughness map of the tidal model as calibrated by Svašek Hydraulics.

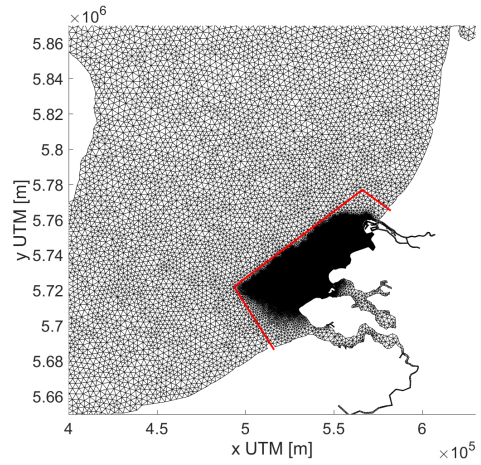


Figure 5.4: The seaward boundaries (shown in red) of the SWAN model as nested within the FINEL model. Notice that roughly within the SWAN model, the grid size decreases significantly.

Thereafter, the performance of the flow model including both tidal and meteorological effects was considered. To this end, wind and pressure fields have been applied in the FINEL model. For meteorological input, two different datasets have been considered in this study: CFSR and ERA5. The model including the meteorological data has been validated at the same locations to compare the two data sets. The model was validated for the period December 2017 to January 2018, as this period contains data including a northwestern storm, a southwestern storm, and calm periods in between. The RMSE of the water level is consistently lower for the ERA5 database, a difference in the order of 2 - 4 cm, at locations relevant to this research. For this reason, the ERA5 database has been used in this research. The validation results for the entire period can be found in Appendix C.3.

Table 5.1: Validation results of the FINEL2D model including tidal forcing and meteorological data in period 01/01/2017 - 30/01/2018. In every set of columns, the left column shows the results of the model with meteorological input from the CFSR dataset and the right column the results of the model with meteorological input from the ERA5 dataset. The values show the RMSE and Bias of the two models compared to measured data and the mean displacement in time and space of the low and high water values. Blue values mean that the water level modelled is lower than measured, and red values mean that the water level is modelled higher than measured.

station	RMSE (m)		BIAS (m)		HW, dt (min)		HW, dh (m)		LW, dt (min)		LW, dh (m)	
	CFSR	ERA5	CFSR	ERA5	CFSR	ERA5	CFSR	ERA5	CFSR	ERA5	CFSR	ERA5
Europlatform	0.16	0.12	0.10	0.07	2	3	-0.10	-0.09	2	3	0.06	0.06
HoekvanHolland	0.16	0.13	0.01	-0.03	5	6	-0.12	-0.11	5	6	0.03	0.03
Scheveningen	0.18	0.13	0.11	0.06	6	7	-0.11	-0.09	6	7	0.03	0.03
Westkapelle	0.21	0.17	0.11	0.07	-7	-6	-0.20	-0.18	-7	-6	0.09	0.06
OS11	0.21	0.16	0.13	0.10	-4	-4	-0.18	-0.17	-4	-3	0.09	0.09
Roopot buiten	0.21	0.16	0.14	0.10	-6	-5	-0.11	-0.10	-6	-5	0.07	0.07
Lichttaidland Goeree 2	0.19	0.15	0.13	0.09	7	8	-0.12	-0.11	7	8	0.07	0.07

Table 5.1 compares the results of the FINEL models with the different meteorological data sets applied to the measurements. It shows the RMSE, BIAS of the calculated values, the time difference in reaching High Water (HW) and Low Water (LW) and the height difference of the High Water and Low Water. As seen in Table 5.1, the model consistently underestimates the peaks of the tidal wave, especially the highest water levels. This could result in an underestimation of the power generated.

5.3. Results energy yield assessment

In this section, the results of the FINEL flow model as described in the previous sections are presented. These results concern the water levels on either side of the dam and the calculated power output of the turbines. The results of three models are presented: the results of a dam with the layout as has been determined in Chapter 4, the results of a dam perpendicular to the coast and finally, a comparison of models with and without meteorological input applied, to assess the influence of meteorological input.

5.3.1. Optimal open ratio

As described in section 2.1, Dai et al. (2017) determined the ideal open ratio for a DTP dam perpendicular to the coast in southeast China to be eight percent. However, this can not be assumed to be the case for the dam in this research because of the different locations of the dam as well as the potential different hydrodynamic processes relevant for creating the head difference over the dam. It is assumed that a DTP dam would be constructed with an optimal open ratio for energy production. Because the open ratio affects the hydrodynamic processes on both sides of the dam, the optimal open ratio for the reference layout of the dam is determined and used in all the following numerical calculations. To do this, numerical model simulations were performed with only tidal forcing applied. The dam's schematisation and other input parameters, such as bathymetry, are identical to the parameters used in the later simulations. Still, the grid size is larger compared to models used later, to keep modelling times reasonable. The runtime of the model for which the power output has been calculated is 15 days. This means the energy output is calculated for a complete spring-neap tidal cycle. The only parameter varied was the open ratio over the dam's total length, which was varied between zero and twenty percent. The results of these simulations can be seen in Figure 5.5.

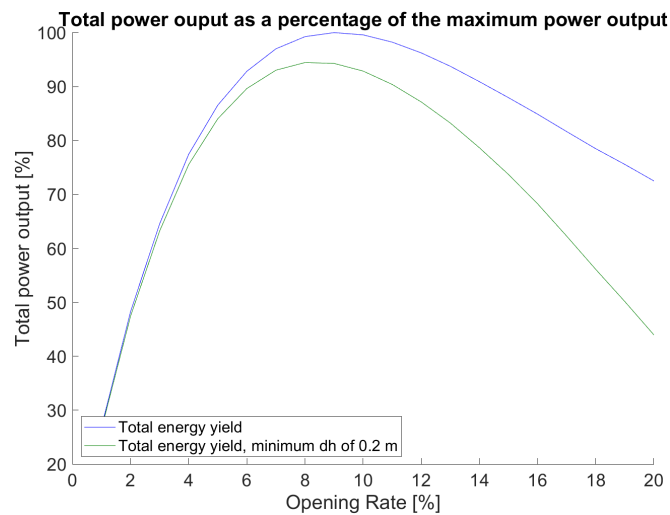


Figure 5.5: Calculated total power output for various open ratios of the dam, expressed as a percentage of the maximum power output calculated.

The optimal open ratio is 9 percent when no minimum necessary height difference over the turbine is assumed, which concurs with the findings by Dai et al. (2017). It could be that for a final design of a DTP dam, the choice would be made to install fewer turbines to build the most economical version of the dam, thus reducing the open ratio of the dam. In this research, however, the choice is made to use the open ratio of 9% in the numerical calculations.

Dai et al. (2017) mention that the turbines need a minimum working water head difference of 0.20 m. This can impact the dam's power output considerably, especially for larger open ratios. This impact is also shown in figure 5.5. However, Dai et al. (2017) do not include the working head in the calculation of the power output. Instead, they only consider it when determining the maximum open ratio of the dam at that location. As previous studies have not considered a minimum working head, the choice has been made not to include a minimum working head in this study for comparability reasons. However, it should be kept in mind that the actual power output can be lower than calculated because of this, as can be seen in Figure 5.5.

5.3.2. Results oblique dam

In this section, the results of the model with the oblique dam are presented. Figure 5.6 shows the water levels at both sides of the dam at a location halfway along the length of the dam, and compares it to the water levels at a nearby location without dam. Figure 5.7 shows a time series of the water level on the inside of the dam at the same location as well as the water level difference. Figures 5.8 and 5.9 show the time series of the power output of a single turbine at the same location and of the whole dam, respectively. Finally, Figures 5.10 and 5.11 show the cumulative power output of the entire oblique dam over a month and over a year.

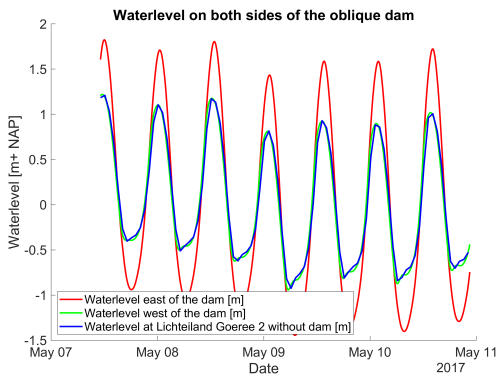


Figure 5.6: Water levels on the east and west of the DTP dam during part of the simulation.

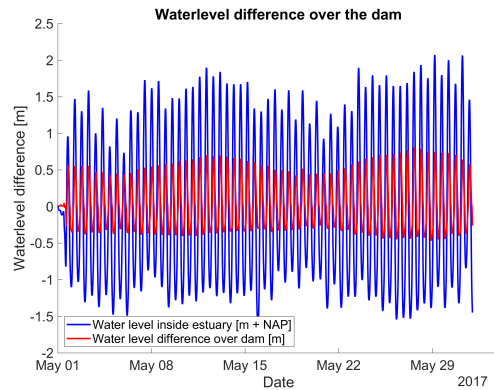


Figure 5.7: Water level on the east side of the dam (in blue) and water level difference over the dam (in red) in May 2017.

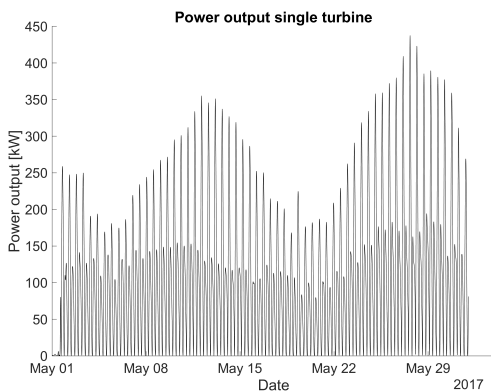


Figure 5.8: Time series of the power output of a single turbine located at the middle of the DTP dam.

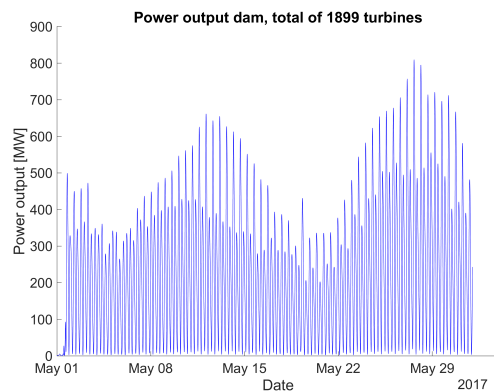


Figure 5.9: Time series of the sum of the power output of all turbines in the DTP dam.

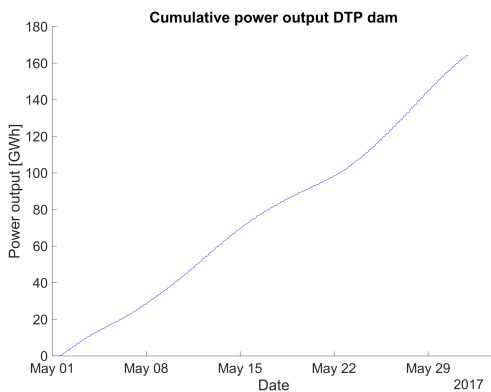


Figure 5.10: Cumulative power output of all turbines in the DTP dam during one month

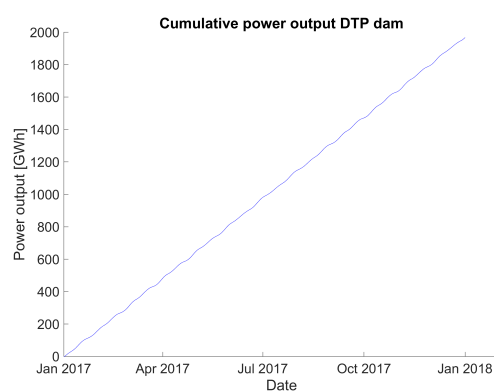


Figure 5.11: Cumulative power output of all turbines in the DTP dam during one year.

5.3.3. Results perpendicular dam

This section shows the results of the model in which the DTP dam has been constructed perpendicular to the Dutch coast, as shown in Figure 5.1. Figure 5.12 shows the water levels on the north and south side of the perpendicular dam as well as the water levels at a nearby location without construction of the dam. Figure 5.13 shows the water level on the south side of a point halfway along the length of the dam, as well as the water level difference over the dam at the same location. Figures 5.14 and 5.15 show the time series of the power output of a single turbine at that location and of the whole dam, respectively.

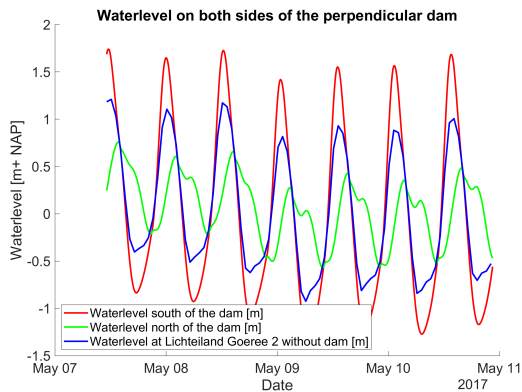


Figure 5.12: Water levels on the south and north of the perpendicular dam during part of the simulation.

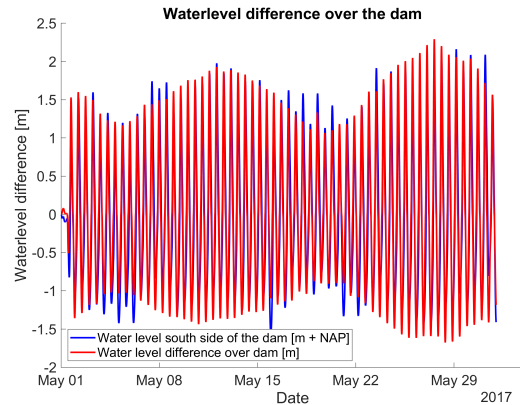


Figure 5.13: Water level on the south side of the dam (in blue) and water level difference over the dam (in red) in May 2017.

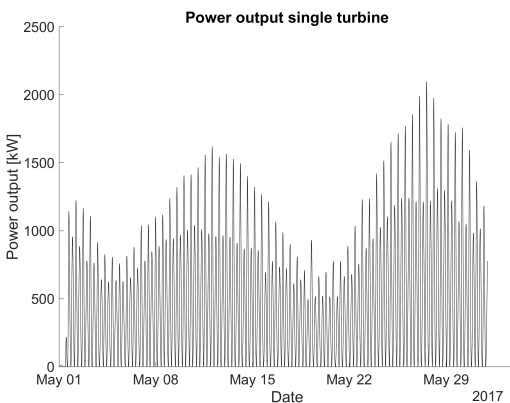


Figure 5.14: Time series of the power output of a single turbine located at the middle of the perpendicular dam.

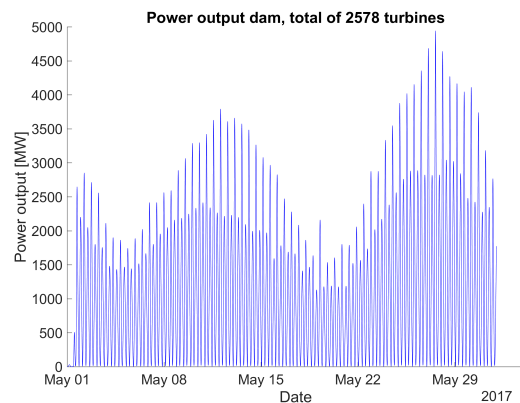


Figure 5.15: Time series of the sum of the power output of all turbines in the perpendicular dam.

5.3.4. Comparison of the perpendicular and oblique dam

This section shows some comparisons of the results from the model with the perpendicular dam and the model of the oblique dam. Figure 5.16 shows the yearly cumulative power output of the entire oblique and perpendicular dam, as calculated for the year 2017. 5.17 shows a time series of the power output of the entire perpendicular and oblique dam for the period of a month. Finally, Figures 5.18 and 5.19 show the development of the maximum water level difference over the dam along the entire length of the oblique and perpendicular dam.

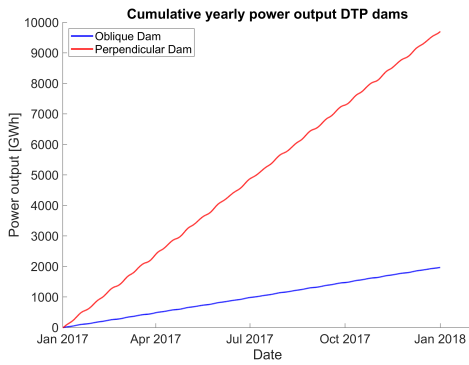


Figure 5.16: Cumulative energy generation of the perpendicular and oblique dam during one year.

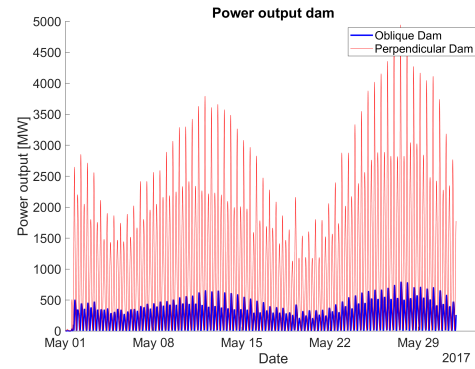


Figure 5.17: Time series of the sum of the power output of all turbines in the oblique and perpendicular dam.

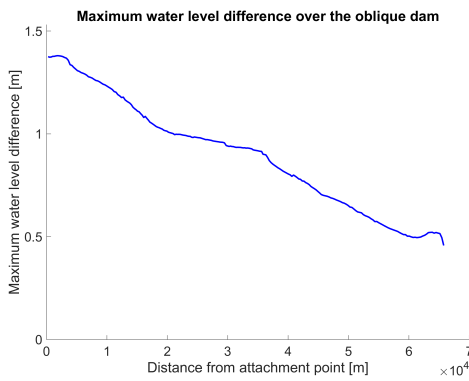


Figure 5.18: Maximum water level difference over the length of the oblique dam.

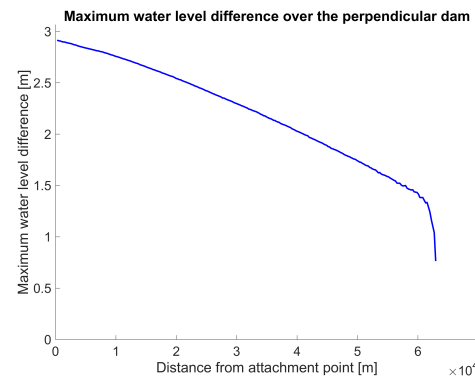


Figure 5.19: Maximum water level difference over the length of the oblique dam.

5.3.5. Comparison influence of meteorological input

Previous research did not include meteorological forcing in the model but only included tidal forcing. In this research, two meteorological data sets have been used during calibration, as described in Section 5.2.3. The models discussed in this chapter, with an oblique DTP dam and a DTP dam perpendicular to the coast, have been run without meteorological input. The total energy output of these models is presented in Figures 5.20 and 5.21 and compared to the simulations with meteorological input. In the simulations used to determine the power output, meteorological input from the ERA5 data set was applied.

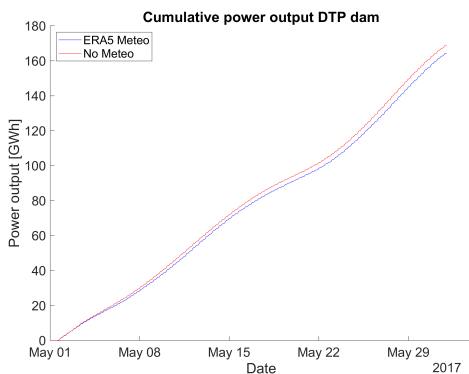


Figure 5.20: Cumulative power output of the oblique DTP dam, from the models run with and without meteorological input.

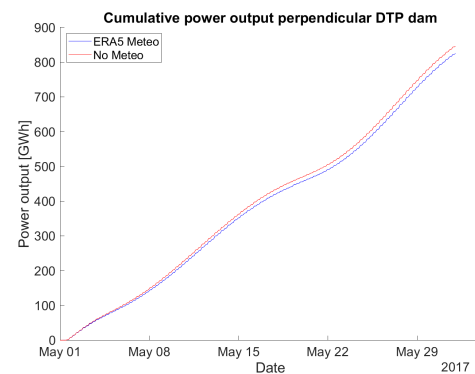


Figure 5.21: Cumulative power output of the DTP dam perpendicular on the coast, from the models run with and without meteorological input.

5.4. Discussion

In this section, the results presented in this chapter are discussed. Two processes are responsible for a water level difference over the oblique dam, as shown in Figure 5.6. First, it can be seen that the water level on the inside of the dam is higher than that on the outside, signifying that the tidal amplitude in the estuary is amplified. This is due to the reflection of the incoming tidal wave at the closed end of the estuary. This is the main reason for the water level difference over the dam. Besides that, a small phase difference between the peaks of the tidal wave can be seen, with the peak of the tidal wave on the outside of the dam occurring circa 20 minutes before the peak of the tidal wave on the inside. In the shown period, the maximum water level difference over the dam halfway along the dam is 0.95 m, while the maximum water level at that location on the inside of the dam is 2.20 m, meaning that the maximum water level difference is only 43% of the maximum water level above MSL. The reason that the maximum water level is smaller than the maximum water level above MSL, is a result of the slight phase difference over the dam, as illustrated in Figure 5.7. Figures 5.8 and 5.9 shows the calculated power output of a single turbine and the sum of the power output of all the turbines in the dam. Both graphs show a clear biweekly pattern in the power output, which coincides with the tidal spring-neap cycle at the location.

When comparing the results of the oblique and the perpendicular dam, it is clear that the dam perpendicular to the coast has a significantly higher power output. The maximum power output at one single moment and the cumulative power output over one year are nearly five times as high as the power output from the oblique dam. Two processes are mainly responsible for this phenomenon. Firstly, the number of turbines present in the perpendicular dam is circa 35 % larger than the number of turbines in the oblique dam. This is because the number of turbines has been calculated based on the open ratio and the water depth for every section of the dams. As the depth increases further offshore, the average depth of the perpendicular dam is larger than that of the oblique dam. The second reason for this difference is that for the perpendicular dam, the phase difference between the water levels on either side of the dam is substantially larger than for the oblique dam. As was described in the previous paragraph. The head difference over the oblique dam is a fraction of the water level on either side of the dam. In contrast, in the case of the perpendicular dam, the head difference is in the same order of magnitude as the tidal amplitude. Figure 5.12 shows that the phase difference between the water level on both sides of the perpendicular dam is substantially larger. Compared to the normal tide, not influenced by a DTP dam, the tidal amplitude on the south side increases, while the tidal amplitude on the north side decreases. This concurs with the findings of Hulsbergen et al. (2005) and Dai et al. (2017). The tidal amplitude inside the oblique dam is also amplified and in the same order of magnitude as that of the perpendicular dam. However, as there is no change in the tidal amplitude on the outside of the DTP dam, as seen in Figure 5.6, this is believed to be the result of the reflection of the the incoming tidal wave wave at the closed end of the estuary.

As shown in Figure 5.16, the cumulative power output throughout the year evolves nearly linearly. This suggests that the influence of meteorological effects is small. Because during winter the wind velocities are higher than during summer, a larger effect of meteorological input would be expected. However, no significant effect of this is apparent in the figure. This hypothesis is confirmed by Figures 5.20 and 5.21, which shows that the power yield calculated by the model without meteorological input is about 2.5% higher than that with meteorological input. Based on that can be concluded that previous studies were justified in their choice not to include meteorological forcing, as the effect on the final result is small.

The total power output of the oblique and perpendicular dams is compared in Figures 5.16 and 5.17. Based on this, for a DTP dam with a length of 62.5 km with a southwest orientation starting at Maasvlakte 2, the expected yearly energy yield is in the order of magnitude of 2 TWh, while the maximum expected power output at one moment is in the order of $8 \cdot 10^2$ MW. In comparison, based on these models, the expected yearly energy yield of a DTP dam perpendicular to the coast at Maasvlakte 2 with a length of 62.5 km is in the order of 10 TWh, with an expected maximum power output at one moment of 5 GW. As the total amount of electricity generated in The Netherlands in 2021 was 117.9 TWh (Centraal Bureau voor de Statistiek (CBS), 2022), this means that the oblique dam could generate one to two percent of the total electricity demand of The Netherlands, while a dam perpendicular to the coast with a length of 62.5 km could generate about 9% of the total electricity demand. This could further increase with the addition of 'wings' as researched by Hulsbergen et al. (2005) and Liu and Zhang (2014), who found that

the maximum head difference could be increased by 50% through the addition of T-shaped extensions of the dam, and even more by placing the extensions in a Y-shape. This can only be confirmed for the perpendicular dam, as their effect on an oblique dam has not been studied.

The expected yearly energy yield of the dam with southwest orientation is in the order of 2 TWh and the maximum power output is in the order of $8 \cdot 10^2$ MW. This is considerably smaller than the expected power output as calculated in Hulsbergen et al. (2005), who estimated a maximum power output of 5 GW for a dam with a length of 30 km, assuming a maximum tidal flow velocity of 1.0 m.s^{-1} . This power output estimated by Hulsbergen et al. (2005) would be even larger for a dam with a length of 50 or 60 km, such as the dams considered in this study. In the FINEL flow model without dam, a maximum flow velocity of 1.02 m.s^{-1} was found at location Lichteiland Goeree 2, close to the location of the dams. Using the equations from Hulsbergen et al. (2005), a maximum water level difference of 2.90 m and a maximum power output of 13.7 GW is found for a perpendicular dam with a length of 62.5 km, when assuming a max tidal velocity of 1.02 m.s^{-1} and an average depth of 20 m. This is nearly a factor three higher than the maximum power output of the perpendicular dam in this study.

In Figures 5.18 and 5.19, the maximum water level difference over every section of the dam is shown. The perpendicular dam shows a clear decrease with a steep drop at the end of the dam. This concurs with the findings of Mei (2012), who found that the head difference across the dam diminishes in the shape of an eclipse and vanishes at the offshore tip, instead of that the head difference is shaped like a circle, which was assumed in previous research. This is also described in Hulsbergen et al. (2012). The oblique dam shows a more linear decrease in the maximum water level difference. The decrease is less smooth because of the layout of the dam, which follows the sand ridges in the original bathymetry, as shown in Figure 4.2. Neither of the graphs show a maximum water level difference of zero at the final element. Of course, in reality at the tip the water level difference can not be different from zero. The reason that this is shown in this graph is that the water level difference is calculated at the center of each grid element, circa 125 meter from the tip. The other reason is that in the model, between the two final elements between which a dam is located, free flow proceeds through three more elements around the tip. The further water level difference is decreased through those elements.

TNO (2021) estimates a maximum power output of 15 GW for a dam with a length of 50 kilometres perpendicular to the coast. When accounting for the fact that this model includes a T-shaped wing, which increases the maximum head by 50% according to Hulsbergen et al. (2005), the representative power output for a dam without wings is 10 GW. This means that their estimate is also a factor 2 larger than the calculated output of the perpendicular dam in this study.

This large difference in results can partly be explained by the fact that both these studies use simplifications such as a mean head difference over the length of the dam. Hulsbergen et al. (2005) assume the head difference at the coast to be the head difference over the whole length of the dam, where in reality, this decreases significantly when moving further from the attachment point. Also, both studies do not consider energy losses due to flows through the turbine. As was described in Chapter 2, has an optimal power output been found for a factor a_{turb} of $2/3$, meaning that in this optimal scenario, $1/3$ of the potential energy in the total water level difference is lost due to flow losses.

5.5. Conclusion

This chapter has presented the numerical model used for the assessment of the energy yield and its results. The objective of this model is to answer the sub-question, "What is the expected energy yield of the proposed DTP dam, and how does this compare to a perpendicular DTP dam and to literature?"

The proposed DTP dam, with a length of 62.5 km and a southwest direction from the Maasvlakte 2, has been modelled to have a maximum power output in the order of $8 \cdot 10^2$ MW and a yearly power output in the order of 2 TWh. The dam perpendicular to the coast starting at the Maasvlakte 2 with a length of 62.5 km has a maximum power output in the order of 5 GW and a yearly power output in the order of 10 TWh. This is significantly lower than the values estimated in previous studies and used in reports, who had estimates a factor two to three higher than this study. The energy yield of the oblique dam is significantly lower than that of the DTP dam built perpendicular to the coast and the direction of the tidal propagation, the difference in energy yield is a factor five.

6

Coastal Safety Assessment

This chapter describes the assessment of the impact of the oblique DTP dam on the coastal safety in the Voordelta. First, the methodology used in this assessment is discussed. The second section consists of a description of the modelling software used and a discussion of the model that has been set up. Then, the results of the assessment are presented and, finally, these results are discussed and a conclusion to the research sub-question is given.

6.1. Methodology

This section describes the methods used to determine the impact of the dam on coastal safety in the Voordelta, to answer the research question: *How is the coastal safety of the Dutch Delta coast influenced by the construction of an oblique DTP dam?*

In Chapter 3, Van Rijn (2009) and Den Bieman and Kieftenburg (2015) were cited, stating that the most important factors to consider for the coastal safety of both dunes and hydraulic structures are wave height, wave period, storm surge level, and storm duration. Due to this, coastal safety is analysed based on these factors in this study.

In order to make this assessment, a wave model has been set up and coupled to the hydrodynamic flow FINEL model. With this model setup, the hydraulic conditions during a storm event are simulated. In the area of interest, the Eastern Scheldt Barrier has the highest safety level. It should withstand a storm with a return period of 10000 years. For this reason, the combined flow and wave models that have been run simulate a storm with a return period of 10000 years. The storm schematisation is explained in Section 6.3.1.

To assess the impact of the DTP dam on the hydraulic conditions during a design storm, two versions of the model have been run: one model with the DTP dam as designed in Chapter 4 and one model without the DTP dam.

A second objective of this model is to assess the impact of the DTP dam on coastal safety in the future, as the construction, when built, would have a considerable lifetime. For this reason, two other scenarios have been considered. First, with the sea level as it is at this moment. Besides that, two other scenarios have been considered, to which a higher sea level has been applied. The MSLR applied in these scenarios is 25 cm and 80 cm, respectively. These are the lower and upper limits of the MSLR in 2085 as calculated in KNMI (2014). In chapter 2 is described that in previous research was concluded that MSLR will have minimal to no impact on the tide or the wind velocities during extreme storm conditions. For this reason, these parameters are not adjusted in the models, meaning that the input of the models is identical except for the MSLR applied. As in the first scenario, a model with and without a DTP dam has been run for both scenarios.

6.2. Storm model

In this section, the numerical model used to schematise the storm conditions is described. First, the modelling software used to do this is described and subsequently, the calibration and validation of this model are discussed.

6.2.1. Modelling software

Just as with the assessment of the energy output, a two-dimensional FINEL flow model was used. However, because for the assessment of storm conditions, waves should be considered as well, a wave model must be included.

For assessing the coastal safety, a SWAN wave model has been coupled to the FINEL model, creating a feedback loop between the two models, which is repeated at regular intervals. SWAN is a third-generation wave model developed at Delft University of Technology, which can be used to simulate waves in coastal areas. The model is based on the spectral wave action balance equation. An elaborate explanation of the model can be found in Booij et al. (1999), while an extensive overview of the use of the model and all additions to the model since its initial development is given in *SWAN User Manual* (2023). In this research, version 41.41 of SWAN has been used.

The SWAN modelling software is applied to calculate the waves in the Voordelta. The SWAN wave model is set up and coupled to the FINEL flow model to do this. This means that at a regular interval, FINEL generates current, and water level files, which are then used as input for the SWAN model to calculate the waves. The calculated wave forces by SWAN are subsequently fed back into FINEL, which incorporates these into the flow computations. This interaction between the wave and flow model occurs at every timestep. The exact characteristics of the SWAN model have been varied during the calibration process. An example of the SWAN input file as used in the final model can be found in Appendix D. Figure 5.4 shows the boundaries of the SWAN model nested in the FINEL model. At the seawards boundary, the incoming waves are applied as a boundary condition. Over the whole grid, meteorological data is applied, equal to that applied in the FINEL model. Similar to the FINEL flow model, the grid of the SWAN wave model consists of elements with a side length of 250 metres.

6.2.2. Calibration

As no measurement data is available for a design storm, the model has been calibrated using data from recent storms. First, the model has been calibrated for the storm of January 31 and February 1, 2022. Subsequently, the model with the best fit was validated for the storm of February 9 to February 11, 2020. These two storms were chosen because these are the two most recent storms during which the Eastern Scheldt Barrier was closed (Rijkswaterstaat, n.d.-a). In these models, at the western border of the SWAN model, the wave characteristics as measured at Europlatform have been applied, as well as the meteorological data of that period.

For the calibration period, the wave characteristics at five locations in the area of interest were compared to available measurements. Three rounds of calibration have been performed. First, by varying the meteorological data input between the ERA5 or CFSR data set. Although the design storm is based on a schematised storm rather than ERA5 or CFSR data, the available data was the foundation for the rest of the calibration models. Second, the physics input of the SWAN model was varied. Finally, the wave breaking parameter was varied to try and increase accuracy nearshore. A short overview of the calibration and validation results is shown in Tables 6.1 and 6.2 and 6.3. Appendix C.1 provides a complete overview of the calibration and validation results. The data in the table have been calculated for the period of the actual storm taking place, from 30-01-2022, 16:00 to 01-02-2022, 08:00.

For locations Domburger Rassen and Schouwenbank, no comparison of the maximum wave height is shown, as no measurement data are available of the storm itself, as can be seen in figures C.11 and C.10. Of four models considered, the calibration results are shown below. The exact input parameters of the different models are described in Appendix C.1.

Table 6.1: Calibration results of the FINEL models for significant wave height. The values show the RMSE of the significant wave height and the difference in the maximum measured significant wave height at five locations. Blue values mean that the significant wave height modelled is lower than measured, and red values mean that the significant wave height is modelled higher than measured. At the bottom, the RMSE of the values above is given for easy comparison. The gray cell shows the model with the lowest RMSE.

Station	RMSE (m)				Hs_max, dt (s)			
	Model 1	Model 2	Model 3	Model 4	Model 1	Model 2	Model 3	Model 4
OS11	0.27	0.39	0.56	0.45	-0.53	-0.27	-0.79	-0.93
Domburger Rassen	0.24	0.41	0.73	0.41				
Schouwenbank	0.32	0.45	0.74	0.45				
Lichteiland Goeree 2	0.31	0.42	0.71	0.41	0.38	0.46	-0.91	0.44
Oosterschelde 4 boven	0.20	0.36	0.44	0.30	-0.19	0.41	0.53	0.08
RMSE	0.27	0.41	0.65	0.41	0.31	0.30	0.59	0.46

Table 6.2: Calibration results of the FINEL models for peak wave period. The values show the RMSE of the peak wave period and the difference in the maximum measured significant wave height at five locations. Blue values mean the peak wave period is lower than measured, and red values mean the peak wave period is modelled higher than measured. At the bottom, the RMSE of the values above is given for easy comparison. The gray cell shows the model with the lowest RMSE.

Station	RMSE (s)				Tp_max, dt (s)			
	Model 1	Model 2	Model 3	Model 4	Model 1	Model 2	Model 3	Model 4
OS11	2.34	2.32	3.32	2.31	-0.51	-0.50	-4.26	0.20
Domburger Rassen	2.72	2.70	3.82	2.70	-0.90	-0.91	-4.33	-0.92
Schouwenbank	2.22	2.19	3.57	2.19	0.06	0.05	-4.53	0.05
Lichteiland Goeree 2	2.57	2.39	3.21	2.38	0.04	0.04	-4.48	0.04
Oosterschelde 4 boven	3.78	3.75	4.15	3.66	-0.09	-0.08	-1.65	-0.06
RMSE	2.78	2.73	3.63	2.70	0.47	0.47	4.00	0.42

Table 6.3: Calibration results of the FINEL models for water level. The values show the RMSE of the water level and the difference in the maximum measured water level at six locations. Blue values mean the water level is lower than measured, and red values mean the water level is modelled higher than measured. At the bottom, the RMSE of the values above is given for easy comparison. The gray cell shows the model with the lowest RMSE.

Station	RMSE (m)				HW, dh (m)			
	Model 1	Model 2	Model 3	Model 4	Model 1	Model 2	Model 3	Model 4
OS11	0.27	0.17	0.17	0.17	-0.48	-0.04	-0.05	-0.03
Roompot Buiten	0.30	0.22	0.22	0.22	-0.50	-0.08	-0.10	-0.08
Brouwershavensegat 2	0.27	0.18	0.18	0.18	0.25	0.66	0.67	0.68
Lichteiland Goeree 1	0.25	0.16	0.16	0.16	-0.20	0.19	0.21	0.19
Europlatform	0.24	0.15	0.15	0.15	-0.45	-0.03	-0.03	-0.03
Haringvliet 10	0.26	0.17	0.16	0.17	-0.51	-0.11	-0.11	-0.09
RMSE	0.27	0.18	0.18	0.18	0.42	0.29	0.29	0.29

An example of the input file used for the SWAN calculations can be found in Appendix D. The names of the different models refer to the SWAN input parameters, the models are shown in Table 6.4. Appendix C.1 explains these in more detail.

In Tables 6.1 and 6.2 can be seen that the Models 1 and 2 perform the best at replicating the wave characteristics. However, Model 2 performed significantly better when considering the maximum water level. Keep in mind that these meteorological data sets are not used in the final model. This will be elaborated on in Section 6.3.1.

Table 6.4: Model versions considered in the calibration of the FINEL-SWAN model.

Model	Wave growth method	Data set wind input	Breaker index γ
1	ST6	ERA5	0.73
2	ST6	CFSR	0.73
3	Komen	CFSR	0.73
4	ST6	CFSR	0.60

6.2.3. Validation

Based on these results, the physics input of Model 2 was chosen to use for validation and the models used in the research. An overview of the validation results is shown in Table 6.5, and the complete results are shown in Appendix C.2. Both the graphs and the validation show the data for the period 08-02-2020, 02:00 to 13-02-2020, 00:00.

Table 6.5: Validation results of the FINEL-SWAN model. The values show the RMSE of the model compared to measured data, as well as the difference in peak values measured and modelled. Blue values mean that the water level modelled is lower than measured, and red values mean that the water level is modelled higher than measured.

Station	RMSE (m)			dPeak		
	Hs	Tp	H	Hs (m)	Tp (s)	H (m)
OS11	0.66	1.28	0.17	-0.04	-1.31	-0.01
Domburger Rassen	0.63	1.10		0.39	-0.66	
Schouwenbank	0.70	1.12		0.16	-0.66	
Lichteiland Goeree 2	1.06	0.84		0.50	-0.20	
Oosterschelde 4 boven	0.45	1.14		0.12	-0.56	
Roompot Buiten			0.26			-0.07
Brouwershavensegat 2			0.15			-0.06
Lichteiland Goeree 1			0.19			-0.04
Europlatform			0.15			0.05
Haringvliet 10			0.20			-0.03
RMSE	0.66	1.01	0.13	0.27	0.70	0.03

The most important parameters are the peak of the measured values, as these are the factors determining the maximum hydraulic load. It is for this reason that these values are compared in this chapter. When comparing Table 6.5 to previous figures, it can be seen that the model performs similarly compared to the storm used for calibration. The values for maximum significant wave height and maximum water level are closely approached. This gives confidence that the model is capable of creating the conditions during a design storm in an sufficiently accurate manner.

6.3. Storm Schematisation

This section describes the characteristics of this schematisation and the corresponding input in the models. Because no historical data of a design storm with a return period of 10000 years are available, a schematised design storm is applied in the FINEL and SWAN models, which is discussed in this section.

6.3.1. FINEL Model Input Storm

The numerical model must consider both waves and tidal forcing to compare the three storm characteristics. At the same time, meteorological factors must also be considered, as these influence both water levels and wave heights. To achieve this, the FINEL model as has been described in Section 5.2.2 forms the basis of the modelling approach used for this part of the study, coupled to the SWAN model. In the FINEL model, however, several changes have been applied.

During storm conditions, the Eastern Scheldt Barrier is closed, meaning no flow through the barrier is possible. However, the barrier has been designed so that the crest height of the barrier is at the design water level (Mooyaart and Jonkman, 2017). As stated in section 3.3, this design water level was statistically calculated for a return period of 1/4000 years, while the new safety water level is that with a return period of 1/10000 years. This means that during a design storm, the water levels may be higher than the barrier height. For this reason, the Eastern Scheldt is included in this model. However, as opposed to the model used for calculating the energy yield, the Eastern Scheldt Barrier is modelled as a barrier with a sill height equal to their respective design heights, with no barrier gate applied. This corresponds to a sill height of 5.8 m + NAP for the two southern barriers and 5.6 m + NAP for the northern barrier, as defined in Rijkswaterstaat (1986). This way, no flow through the barrier is modelled, but during extreme storm conditions, flow over the barrier is possible, influencing the conditions in front of the barrier.

Storm surges in the southern North Sea occur due to low-pressure systems, which increase wind velocities and cause an atmospheric storm surge. These systems can be accompanied by large rainfall amounts, which can result in large river discharges (Khanal et al., 2019). Both Khanal et al. (2019) and Kew et al. (2013) conclude that the probability of storm surges and extreme discharge events happening simultaneously is three to four times higher than random chance. For this reason, the discharge from the Haringvliet applied to the model is that of an extreme discharge event to account for the worst possible conditions. Based on Van Krefeld et al. (2009), the discharge applied is equal to that measured during the flood events of 1995, which means that a discharge into the Voordelta of $9500 \text{ m}^3 \text{ s}^{-1}$ has been applied.

In Figure 3.3 is shown that the highest waves near the Dutch coast come from two directions: 330°N and 240°N . Sterl et al. (2009) notes that north-westerly winds are most dangerous for storm surges along the Dutch coast, as these have the longest fetch. However, the response of the hydraulic conditions on the presence of the dam is expected to be very different for the two directions. For this reason, the coastal safety assessment is made for storms coming from northwestern and southwestern direction. In the case of the northwestern storm, both the wave direction and the peak wind direction are 330°N and for the southwestern storm both are 240°N .

Instead of existing meteorological data, wind speed and direction applied in the model are based on the idealised shape of a design storm as described in Chbab and De Waal (2017). For the Dutch Delta and Holland coast, the wind profile is described as a trapezoid, of which the basis lasts 44 hours, while the peak of the storm lasts 2 hours. This shape of the wind profile as applied in the model is shown in black in Figure 6.1. Different from this figure, the maximum applied wind velocity is 35.0 m s^{-1} . Chbab and De Waal (2017) describe that at the Holland and Delta coast, the phase difference between the wind setup and the tide is 2.5 hours, meaning that the peak of the wind setup occurs 2.5 hours before high tide, which is applied in this model. The direction of the storm is also not constant but changes just before the middle of the storm's duration. The magnitude of the change in direction depends on the wind direction in the second part of the storm. For peak wind directions between 300°N and 360°N , the shift in wind direction is 70 degrees in the five hours leading up to the storm's peak. For peak wind directions between 240°N and 300°N , the shift is 50 degrees in the five hours before and after the storm (Kieftenburg and Chbab, 2012). This means that the northwestern storm is applied with an initial wind

direction of 260°N and a final wind direction of 330°N . For the southwestern storm, in Figure 6.1 can be seen that for peak wind directions between $240\text{--}300$ degrees, the wind direction shifts from peak wind direction -40 degrees to peak wind direction $+10$ degrees. Based on this, the wind direction in this design storm is assumed to shift from 200°N to 250°N . In figure 6.1, an example of the shift of the wind direction is shown, as well as the development of the wind velocity. Note that in the figure, the base of the wind velocity is 48 hours rather than the 44 hours used in this research. The 44 hours are based on later research and have replaced the 48 hours.

The peak of the wind speed applied is the wind speed with a return period of 10000 years, as calculated for the location Lichteiland Goeree. Chbab (2015) calculated that this is 35.0 m.s^{-1} for a direction between 315°N and 345°N , as well as for a wind direction between 225°N and 255°N .

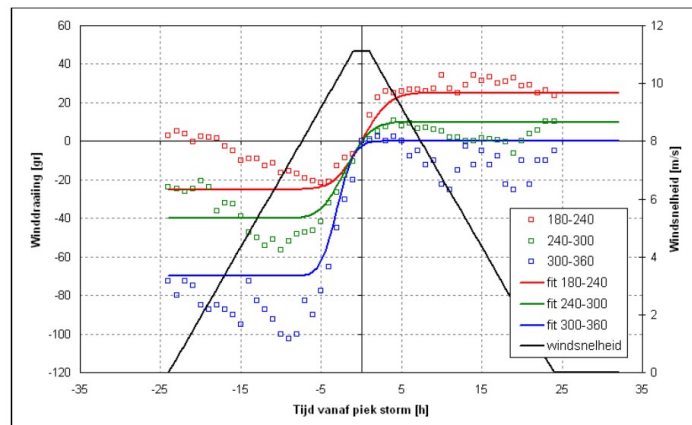


Figure 6.1: Development of the wind speed and direction during a design storm. From Kieftenburg and Chbab (2012). (In Dutch)

The wind shear stress coefficient C_d in FINEL is a variable coefficient depending on the wind speed. Up to a velocity of 7.8 m.s^{-1} , the coefficient has a value of 0.0014. For wind speeds greater than 50.0 m.s^{-1} , the coefficient has a value of 0.0039. The coefficient increases linearly between the two wind speeds (Bak and Vlag, 1999). This is illustrated in Figure 6.2.

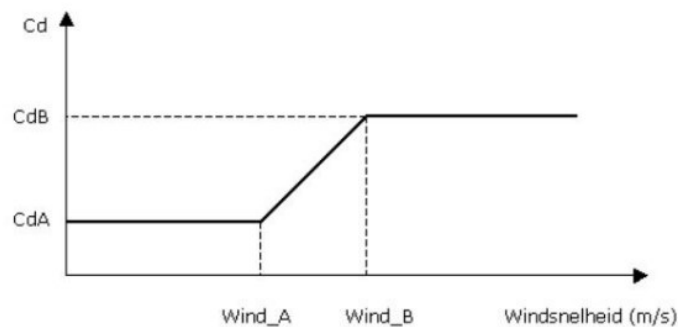


Figure 6.2: Development of the variable wind shear stress coefficient C_d . From Bak and Vlag (1999). (In Dutch)

6.3.2. SWAN Model Input Storm

Because the SWAN model is coupled to the FINEL model, the water levels and tidal currents are provided by the FINEL model. Likewise, the boundary conditions for the waves are provided at regular intervals. In the case of the storm model, these wave boundary conditions remain the same throughout the entire model. At the western boundary, the input parameters of the waves are based on the extreme hydraulic boundary conditions as calculated in Roscoe et al. (2010). They calculated the extreme wave heights and wave periods using a generalised Pareto distribution based on 30 years of measurements. Based on this, the wave boundary conditions applied in the SWAN wave model are:

- Significant wave height: 7.40 metres.
- Peak wave period: 12.98 seconds.

In their calculations, Roscoe et al. (2010) did not take wave direction into account, meaning that the calculated wave characteristics are unidirectional. For that reason, the same wave characteristics are applied as boundary condition in the SWAN wave model. Meaning that in the model for a storm coming from a northwestern direction the waves come from a direction of 330 °N and for the storm coming from a southwestern direction the waves come from a direction of 240 °N. Finally, the directional spread of the waves is modelled at 30 degrees. Furthermore, schematised wind conditions are applied in the model as explained in Section 6.3.1.

Unlike FINEL, it is not possible to integrate turbine modules in SWAN. Because of this, in SWAN, the dam has been modelled as an impermeable barrier. This is considered sufficient because it is assumed that no wave energy can be transported through the turbines. Keep in mind that this is only the case for the wave energy, as the currents and water levels are calculated by FINEL, which does include the turbine module. The complete input file of the SWAN model is shown in Appendix D.

6.4. Results

This section presents the results of the assessment of the impact of the DTP dam on the coastal safety in the Voordelta. The results are divided in three subsections. First, the change in the maximum characteristic, the significant wave height, the peak wave period or the maximum water level, is shown. This is done for both the northwestern and southwestern storm. Then, time series of these characteristics at selected locations are shown. These graphs include results from both the northwestern and southwestern storm, as well as the results from the models including MSLR. Finally, an overview of the results is presented.

6.4.1. Change in Maximum Values

This section shows the results of the change in maximum value of the significant wave height, peak wave period and water level, throughout the entire area of interest. For these graphs, the maximum value has been determined at every location. The graphs show the change in maximum value between the model with and without the dam.

In this section, only figures showing the absolute difference are shown to preserve the chapter's readability. Other graphs, showing the changes as a percentage of maximum calculated value without dam, can be found in Appendix E. For the same reason, only the figures showing the impact of the dam at current water levels are shown. The results with MSLR applied can be found in Appendix E. The figures are shown with the results of both the northwestern and southwestern storm.

6.4.1.1 Northwestern Storm

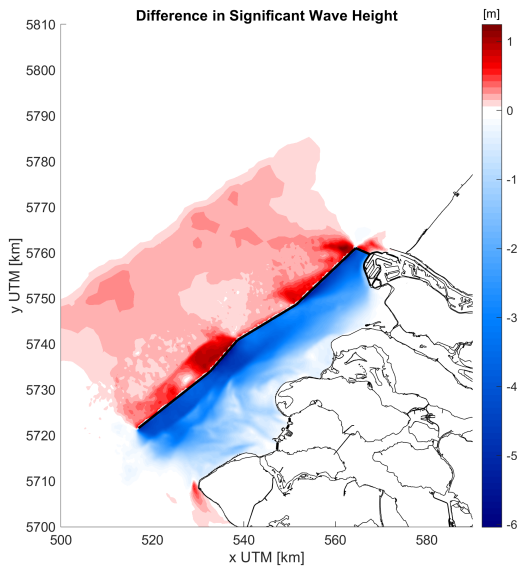


Figure 6.3: Absolute difference in maximum significant wave height in simulations with and without dam for a northwestern storm with a return period of 10000 years. Areas in blue show a decrease in significant wave height after dam construction compared to the situation without the dam. Red shows an increase in significant wave height.

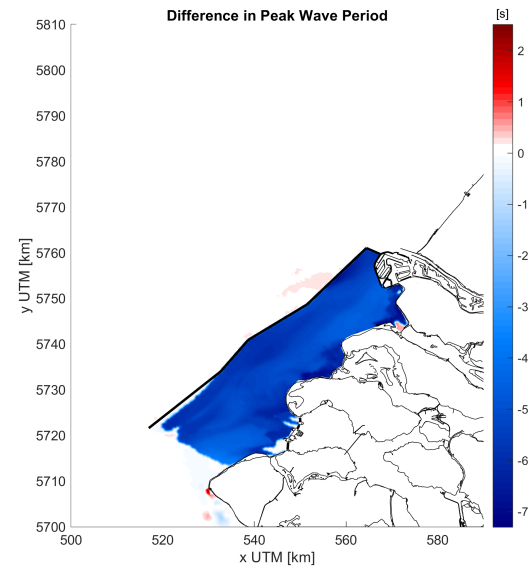
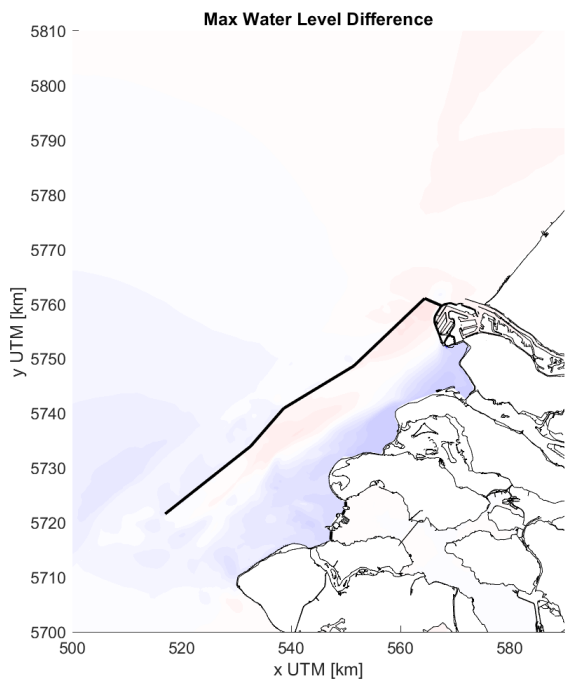
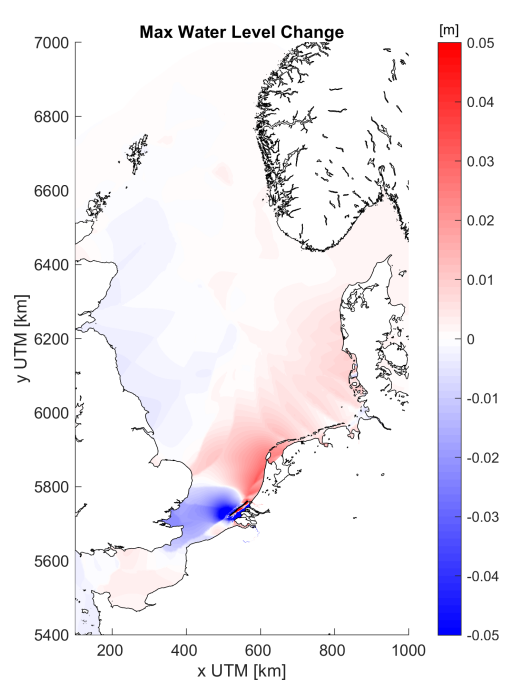


Figure 6.4: Absolute difference in maximum peak wave period in simulations with and without dam for a northwestern storm with a return period of 10000 years. Areas in blue show a decrease in the peak wave period after dam construction compared to the situation without the dam. Red shows an increase in the peak wave period.



(a)



(b)

Figure 6.5: Absolute difference in maximum water level in models with and without dam for a northwestern storm with a return period of 10000 years. Figure (a) shows the Voordelta and Figure (b) shows the entire North Sea. Areas in blue show a decrease, while red shows an increase in maximum water level compared to the situation without dam. Note that Figure (b) has a much smaller scale on the colour bar compared to Figure (a).

6.4.1.2 Southwestern Storm

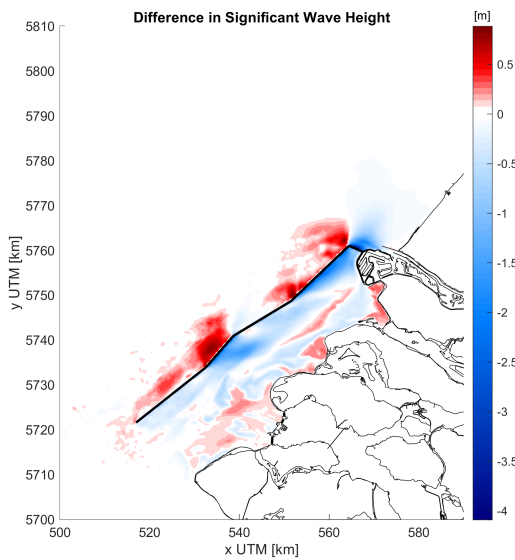


Figure 6.6: Absolute difference in maximum significant wave height in simulations with and without dam for a southwestern storm with a return period of 10000 years. Areas in blue show a decrease in significant wave height after dam construction compared to the situation without the dam. Red shows an increase in significant wave height.

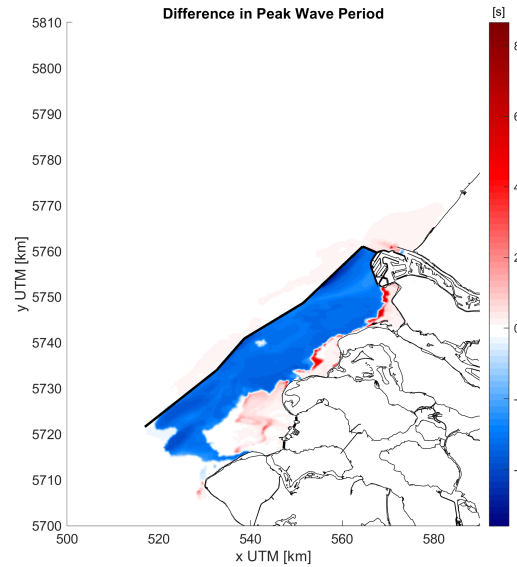


Figure 6.7: Absolute difference in maximum peak wave period in simulations with and without dam for a southwestern storm with a return period of 10000 years. Areas in blue show a decrease in the peak wave period after dam construction compared to the situation without the dam. Red shows an increase in the peak wave period.

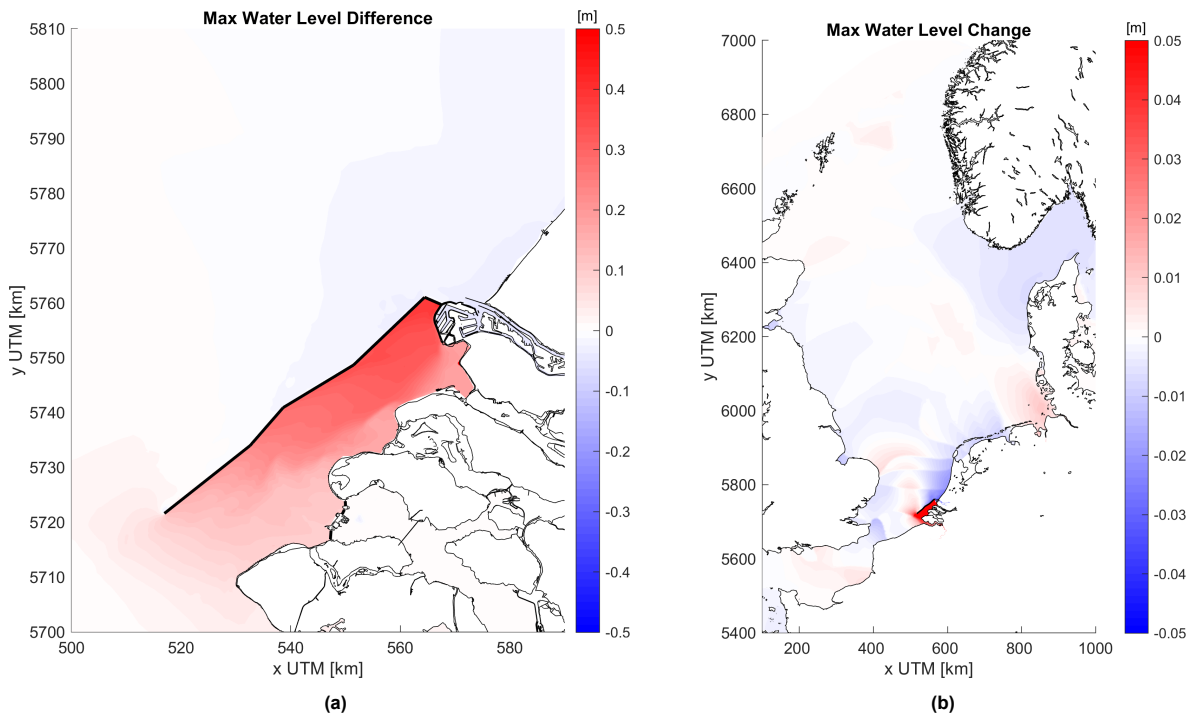


Figure 6.8: Absolute difference in maximum water level in simulations with and without dam for a southwestern storm with a return period of 10000 years. Figure (a) shows the Voordelta and Figure (b) shows the entire North Sea. Areas in blue show a decrease, while red shows an increase in maximum water level compared to the situation without dam. Note that Figure (b) has a much smaller scale on the colour bar compared to Figure (a).

6.4.2. Time Series Measurement Locations

In this section, graphs showing the time series of the water level, significant wave height and peak period at two locations: Brouwershavensegat 2 and Roompot Buiten. The graphs of the other measurement locations are shown in Appendix E. The location of the measurement locations as well as the location of the dam are shown in Figure 6.9.

Each graph shows the time series of eight different models. These are the models with and without dam for each of the three water level inputs: current water level, MSLR of 25 cm and MSLR of 80 cm, all with a northwestern storm applied; and the models with and without dam with current water level and a southwestern storm applied.

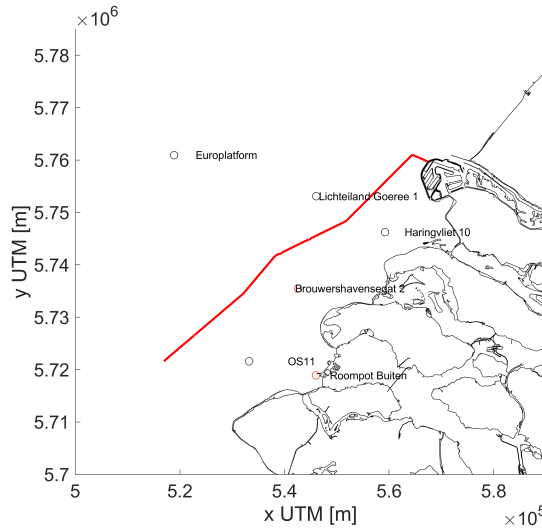


Figure 6.9: Locations of the measurement locations of the SWAN model. In red the locations of which the figures are shown in this chapter, in black the locations of which the results are shown in Appendix E.

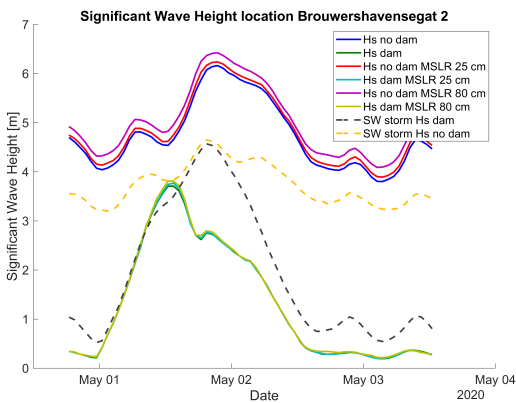


Figure 6.10: Time series of the significant wave height modelled for a design storm with a return period of 10000 years at location Brouwershavensegat 2. The full lines show the results of the northwestern storm, the dotted lines show the results of the southwestern storm.

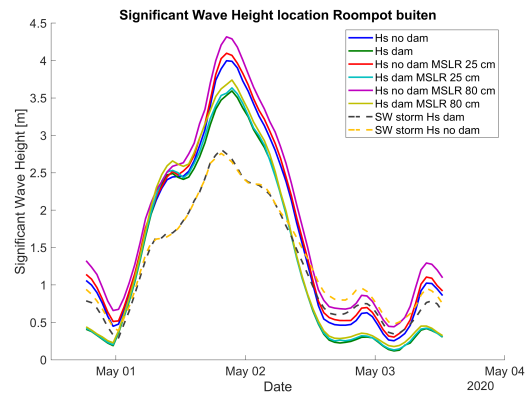


Figure 6.11: Time series of the significant wave height modelled for a design storm with a return period of 10000 years at location Roompot Buiten. The full lines show the results of the northwestern storm, the dotted lines show the results of the southwestern storm.

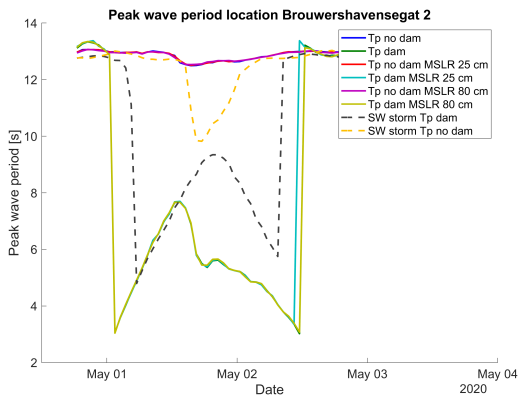


Figure 6.12: Time series of the peak wave period modelled for a design storm with a return period of 10000 years at location Brouwershavensegat 2. The full lines show the results of the northwestern storm, the dotted lines show the results of the southwestern storm.

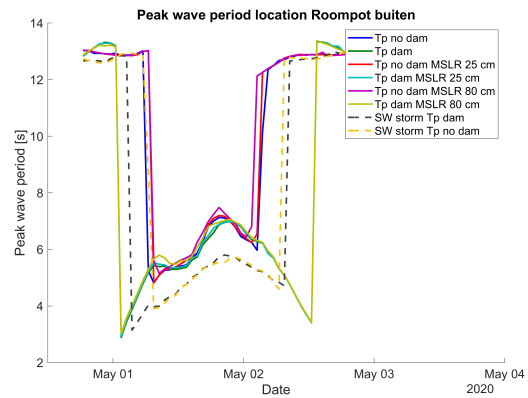


Figure 6.13: Time series of the peak wave period modelled for a design storm with a return period of 10000 years at location Roompot Buiten. The full lines show the results of the northwestern storm, the dotted lines show the results of the southwestern storm.

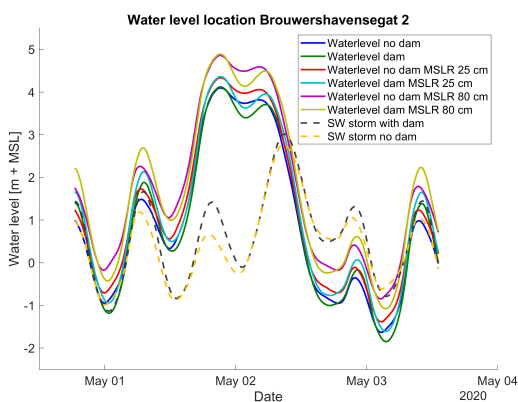


Figure 6.14: Time series of the water level modelled for a design storm with a return period of 10000 years at location Brouwershavensegat 2. The full lines show the results of the northwestern storm, the dotted lines show the results of the southwestern storm.

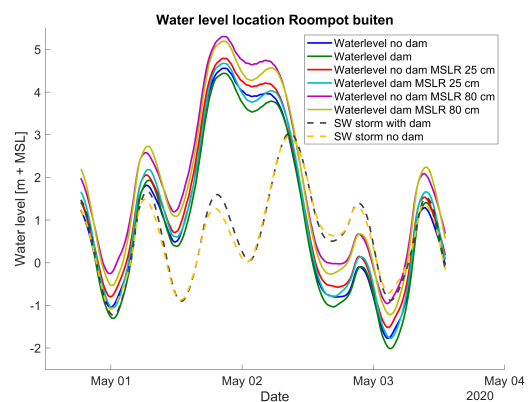


Figure 6.15: Time series of the water level modelled for a design storm with a return period of 10000 years at location Roompot Buiten. The full lines show the results of the northwestern storm, the dotted lines show the results of the southwestern storm.

6.4.3. Overview results

Finally, this section shows an overview of the results at output locations. Table 6.7 shows the results of the models at several output locations, with water levels without MSLR as input. The load duration time is defined as the consecutive period during which the water level at that location is higher than the mean high water (MHW) level at that location. The MHW without dam for each of the locations has been calculated and are shown in Table 6.6. The table shows the maximum value modeled at the locations for each of the four parameters, for both the model with and without dam. The third column shows the difference between the two, with a negative value indicating a decrease after the dam construction compared to before and vice versa. The final column shows the difference as a percentage of the measured value without the construction of the dam.

Because a structure of this size is built with a considerable lifetime in mind, MSLR in this century should be taken into account when assessing the influence on coastal safety. For this reason, the model of the northwestern storm has been run including an applied MSLR of 25 and 80 cm. Tables 6.8 and 6.9 show the results of these models and compare the results to the model without MSLR applied. The tables show the impact of the dam on the coastal safety after MSLR and give a comparison if the impact of the dam increases or decreases with rising sea levels. Every first column shows the absolute increase maximum value modelled of the significant wave height, peak wave period, water level and load duration, respectively, compared to the same model without MSLR applied. The second column shows the increase as a percentage of the value at that location without MSLR applied.

Table 6.6: Mean High Water calculated at measurement locations based on results of the FINEL model without dam applied.

Location	MHW [m + MSL]
OS11	1.70
Roompot Buiten	1.75
Brouwershavensegat 2	1.69
Lichteiland Goeree 2	1.64
Europlatform	1.22

Table 6.7: Maximum wave and water level parameters modelled with and without dam at several locations.

Location	Hs [m]				Tp [s]				H [m + MSL]				Load duration [h]			
	Dam	No Dam	Dif	%	Dam	No Dam	Dif	%	Dam	No Dam	Dif	%	Dam	No Dam	Dif	%
OS11	3.40	4.97	-1.57	-31.5%	7.95	13.10	-5.15	-39.3%	4.20	4.29	-0.08	-1.9%	18.83	19.00	-0.17	-0.9%
Roompot Buiten	3.59	4.00	-0.40	-10.1%	6.98	7.13	-0.14	-2.0%	4.44	4.56	-0.12	-2.6%	19.17	19.50	-0.33	-1.7%
Brouwershavensegat 2	3.71	6.16	-2.45	-39.8%	7.67	13.01	-5.34	-41.0%	4.12	4.10	0.02	0.6%	18.67	18.67	0.00	0.0%
Lichteiland Goeree 2	9.02	8.82	0.20	2.2%	13.04	12.88	0.16	1.3%	3.90	3.90	0.00	-0.1%	19.67	19.67	0.00	0.0%
Europlatform	8.12	7.97	0.15	1.9%	12.77	12.75	0.02	0.2%	3.97	4.00	-0.02	-0.6%	18.50	18.50	0.00	0.0%
Haringvliet 10	3.73	5.66	-1.93	-34.1%	8.32	13.05	-4.73	-36.2%	4.16	4.16	-0.01	-0.2%				
Domburger Rassen	4.29	6.68	-2.38	-35.7%	7.89	12.92	-5.04	-39.0%	4.14	4.17	-0.03	-0.8%				
Oosterschelde 4 boven	3.31	4.06	-0.76	-18.7%	6.79	13.13	-6.34	-48.3%	4.37	4.50	-0.13	-3.0%				

Table 6.8: Modelled increase in maximum wave and water level after applying a mean sea level rise of 25 cm. The table shows the absolute modelled increase and the increase as a percentage of the value without MSLR applied.

Location	Hs [m]				Tp [s]				H [m]				Load Duration [h]			
	Dam	%	No Dam	%	Dam	%	No Dam	%	Dam	%	No Dam	%	Dam	%	No Dam	%
OS11	0.05	1.6%	0.09	1.9%	0.04	0.6%	0.04	0.3%	0.24	5.7%	0.24	5.5%	0.50	2.7%	0.67	3.5%
Roompot Buiten	0.04	1.1%	0.10	2.5%	0.01	0.1%	0.52	4.1%	0.23	5.2%	0.23	5.1%	0.67	3.5%	0.67	3.4%
Brouwershavensegat 2	0.06	1.6%	0.08	1.2%	0.02	0.3%	-0.03	-0.2%	0.24	5.8%	0.24	5.8%	0.50	2.7%	0.67	3.6%
Lichteiland Goeree 2	0.04	0.5%	0.02	0.2%	-0.01	-0.1%	0.01	0.1%	0.24	6.2%	0.24	6.2%	0.83	4.2%	0.83	4.2%
Europlatform	0.01	0.1%	-0.09	-1.1%	0.00	0.0%	0.00	0.0%	0.24	6.1%	0.24	6.1%	0.83	4.5%	0.67	3.6%
Haringvliet 10	0.04	1.1%	0.08	1.4%	0.02	0.2%	0.00	0.0%	0.24	5.8%	0.24	5.7%				
Domburger Rassen	0.02	0.5%	0.10	1.5%	0.00	-0.1%	0.00	0.0%	0.24	5.8%	0.24	5.7%				
Oosterschelde 4 boven	0.02	0.5%	0.09	2.2%	0.05	0.7%	0.00	0.0%	0.24	5.4%	0.23	5.1%				

Table 6.9: Modelled increase in maximum wave and water level after applying a mean sea level rise of 80 cm. The table shows both the absolute modelled increase and the increase as a percentage the value without MSLR applied.

Location	Hs [m]				Tp [s]				H [m]				Load Duration [h]			
	Dam	%	No Dam	%	Dam	%	No Dam	%	Dam	%	No Dam	%	Dam	%	No Dam	%
OS11	0.21	6.2%	0.29	5.9%	0.08	1.1%	-0.01	-0.1%	0.76	18.2%	0.75	17.6%	2.00	10.6%	2.17	11.4%
Roompot Buiten	0.15	4.1%	0.32	8.0%	0.07	1.1%	0.53	4.3%	0.75	16.9%	0.75	16.4%	2.00	10.4%	2.50	12.8%
Brouwershavensegat 2	0.10	2.8%	0.26	4.2%	-0.01	-0.1%	-0.02	-0.2%	0.77	18.6%	0.76	18.6%	2.17	11.6%	2.50	13.4%
Lichteiland Goeree 2	0.17	1.9%	0.13	1.5%	0.00	0.0%	-0.01	-0.1%	0.76	19.5%	0.76	19.5%	3.50	17.8%	3.33	16.9%
Europlatform	0.04	0.5%	-0.05	-0.7%	0.01	0.1%	0.01	0.0%	0.78	19.6%	0.78	19.6%	2.83	15.3%	2.83	15.3%
Haringvliet 10	0.14	3.7%	0.28	5.0%	0.01	0.1%	-0.02	-0.2%	0.77	18.4%	0.76	18.1%				
Domburger Rassen	0.15	3.5%	0.26	3.8%	0.01	0.1%	-0.01	0.0%	0.77	18.5%	0.76	18.2%				
Oosterschelde 4 boven	0.10	3.0%	0.28	7.0%	0.16	2.3%	0.01	0.1%	0.76	17.4%	0.75	16.6%				

6.5. Discussion

In this section, the results as presented in the previous section, as well as the additional results shown in Appendix E, are discussed.

6.5.1. Discussion northwestern storm

When looking at the northwestern storm, Figure 6.3 clearly shows a considerable decrease in significant wave height east of the DTP dam. The largest impact is immediately behind the dam, while the impact on the significant wave height decreases closer to the shore. This can be explained by the decreased water depth closer to shore, illustrated in Figure 4.2. As nearshore the water depths decrease, depth-induced breaking becomes the deciding factor for the significant wave height, decreasing the influence of the dam. However, also near-shore, a considerable decrease is still visible at most locations, as can be seen in Figure 6.15. The other reason for this result is that waves closer to shore have a longer fetch, which is roughly equal to the distance of the location to the dam, meaning that the waves closer to shore have a longer distance to grow behind the dam.

An increase in significant wave height can be seen at the east- and north-side of the dam. This is most pronounced near the sections of the dam which are more perpendicular to the wave direction. The increased significant wave height results from the reflection of incoming waves on the dam. A particular area of interest where this happens is at the short northern side of the dam, next to the Maasvlakte 2. In the model, the significant wave heights increase by nearly 1 m, which can significantly impact the coastal safety at that location. In this SWAN model, the reflection coefficient has been defined as 1.0, meaning that the incoming significant wave height is completely reflected. The actual reflection coefficient of the dam would depend on the design and should be determined in later studies. Finally, an increase in significant wave height can be seen at the coast near Westkapelle. At this location, both hard and soft coasts are present. The higher significant wave height could mean an increased erosion rate of the soft coast, while on the hard coast the hydraulic loads would increase.

Over the whole area behind the dam, the peak wave period during the storm is halved compared to the situation without the dam. This can be explained by looking at the wave energy distribution spectra with and without a dam, as shown in Figure 6.16. The figures show the moment at which the peak wave period at that location is at its maximum. Without dam, the peak of the energy distribution spectrum has a very low frequency, which closely matches the wave period of the design storm set at the boundary. This means that the wave frequencies that contain the most wave energy are those applied at the offshore model boundary. In the case with a dam, as these waves come from a direction of 330 °N, the waves are blocked by the dam, meaning that waves coming from the southwest, which are not obstructed by the dam, become dominant. As shown in Figure 6.1, a shift in wind direction is applied before the peak of the storm. As this happens, the waves applied at the boundary cease to directly enter the estuary and wind waves generated behind the dam become dominant, further decreasing the peak wave period, as can be seen in Figure 6.19. This is also displayed in Figure 6.17, which shows that the dominant wave direction is the west rather than the northwest, as is the case without dam. Three exceptions to this process can be distinguished. At Westkapelle, just like with the significant wave height, the peak wave period increases by about 10 percent compared to the situation without dam instead of decreasing, which can be seen in Figure 6.4. Secondly, near the Eastern Scheldt Barrier, no significant change in the peak wave period is visible, as opposed to the maximum significant wave height, which is reduced. This can be explained when comparing Figures 6.12 and 6.13. Further offshore, at location Brouwershavensegat 2, the waves coming from the boundary are dominant, meaning that the peak in the wave energy comes from the waves entering the model at the boundary. These waves therefore determine the peak wave period at that location. When these are broken, wind waves with a much lower peak wave period become dominant, explaining the sharp decrease in the peak wave period. However, it is seen that at location Roompot Buiten, located in the area near the Eastern Scheldt Barrier where no change is visible, the peak wave period also experiences a sharp drop in the models without barrier. This means that the waves coming from the northwest are still broken before reaching this location but by the sandbanks formed in the ebb-tidal delta of the Eastern Scheldt. Finally, near the Haringvliet sluices, a slight increase in the peak wave period can be seen. It is hypothesised that the reason for this is that at this location waves are depth-limited. Because the maximum water levels rise at that location, the peak wave period during the storm increases.

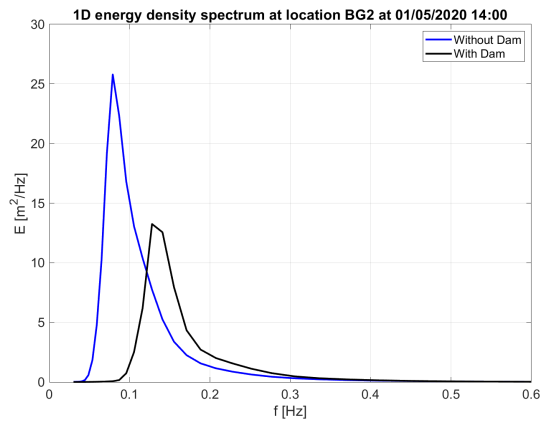


Figure 6.16: 1D Energy Density Spectrum at location Brouwershavensegat 2 during the peak of the storm, for the models of a northwestern storm with a return period of 10000 years with and without dam.

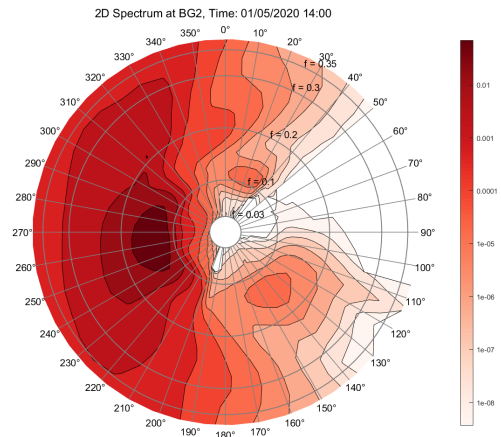


Figure 6.17: 2D Energy Density Spectrum at location Brouwershavensegat 2 during the peak of the storm, for the model of a northwestern storm with a return period of 10000 years with dam.

In Figure 6.5, four areas can be distinguished based on the location and change in maximum water level. First, the region immediately east of the dam. In this area, the maximum water level during the storm increases by a few percent, or several decimeters at most. The amplification as determined in Section 4.3 can most likely explain this. However, the increase in maximum water level seen is lower than the factor 1.13 calculated, which the influence of the turbine openings can explain. Then, in the area inside the estuary closer to shore, a decrease in the maximum water level is found. As a gradual shift from increase to decrease in maximum water level from the DTP dam to the coast can be discerned, it is hypothesised that the dam does influence the wind setup. As the wind setup is inversely proportional to the depth, this increases closer to shore, meaning a decrease in wind setup would be more pronounced close to shore.

Finally, Figure 6.5b shows that along the entire western coast of the North Sea north of the dam, the maximum water level is increased slightly, in the order of several centimetres. Although the impact is slight, this does show that this project impacts the hydrodynamics throughout the North Sea basin, and its impact in the basin should be researched precisely. It is hypothesised that as the western side of the North Sea basin and south of the dam the maximum water level decreases, while north of the dam, along the entire eastern side of the North Sea basin the maximum water level increases, the dam influences the tidal Kelvin wave propagating counterclockwise through the North Sea basin. This is strengthened by the fact that the influence is least in the middle of the basin, nearer the amphidromic points where the tidal amplitude is lowest. Further investigation of this result is outside the scope of this research.

6.5.2. Discussion southwestern storm

Compared to the northwestern storm, the impact of the dam on the significant wave height for the northwestern storm is less homogeneous. The most important result seen in Figure 6.6 is an increase in the significant wave height in all ebb-tidal deltas, in the order of up to 0.5 metres. This can be explained by the fact that the maximum water level in the estuary rises, as can be seen in Figure 6.8. As the significant wave heights are depth-limited near the coast in the ebb-tidal deltas, the increased water level has larger significant wave heights as result. Similar to the northwestern storm, an increase in significant wave heights on the outside of the dam can be observed, resulting from the reflection of the waves on the dam.

Around the ebb-tidal deltas an increase in the peak wave period can be observed, most pronounced at the edges. This can also be explained by the increased maximum water level. As a result of this, the edge at which the waves break moves closer to shore, which is shown by the bright red parts in Figure 6.7.

Finally, as discussed previously, the maximum water level in the entire basin can be observed to increase, most significantly at the northern end of the basin. This is a result of the wind set-up behind the DTP dam in the formed estuary. As the wind is directed immediately towards the opening of the estuary, the water is pushed into the estuary, resulting in an increased wind set up. Based on this model, it can be concluded that the DTP dam increases the hydraulic load on the majority of the Dutch Delta coast during southwestern storms.

6.5.3. Effect on load characteristics

It can be seen in Figure 6.10 that, in the models for the northwestern storm, the peak significant wave height occurs considerably later in the models without dam compared to the models with dam. Appendix E shows that this is the case for all offshore locations protected by the dam. The changing wind direction can explain this. As explained in Section 6.3.1, the storm's initial wind direction is 70 degrees lower than the final wind direction. This means that the wind direction changes from 260 to 330 degrees North. This is displayed in Figure 6.18, which clearly shows that the peak of the significant wave height occurs when the wind direction is approximately 280 °N behind the dam, while without the dam, the wave height continues to increase until the peak of the storm, which happens when the wind direction reaches 330 °N, without dam. This can also be seen in Figure 6.17, which shows the energy density spectrum at the moment of the peak wave period at the location and which shows the dominant waves coming from the west. For the southwestern storm, it can be seen that the peak significant wave height occurs later than for the northwestern storm in the models with dam. This can be explained by the fact that during the southwestern storm, the location Brouwershavensegat 2 is not sheltered by the dam, meaning that the waves can directly enter the estuary and reach the location up till the peak of the wind velocity, resulting in higher significant wave heights. At location Roompot Buiten, all models show a maximum significant wave height at the same moment. This is due to the fact that at this location the water depth is lower than at location Brouwershavensegat 2, meaning that at this location the waves are depth-limited. As a result of this the maximum significant wave height occurs during high water for all models.

Similar to the previously mentioned figures, in Figures 6.19 and 6.20, the wind direction is overlaid on the graphs of the peak wave period and water level at location Brouwershavensegat respectively. It can be seen that the change in the wind direction does not seem to affect the water level significantly. This, along with the minimal differences in water level visible between the models with and without dam, confirm the hypothesis that the dam will not significantly affect storm surge levels. The graph of the peak wave period, however, shows the same pattern as the significant wave height, with the peak occurring shortly after the wind direction starts shifting. In Appendix E, the relevant graphs show that this is the case for the other locations behind the dam as well, implying that the extreme wave climate behind the dam is strongly influenced by waves coming from the southwest, which dominate the waves formed by the wind behind the dam in terms of both peak wave period and significant wave height.

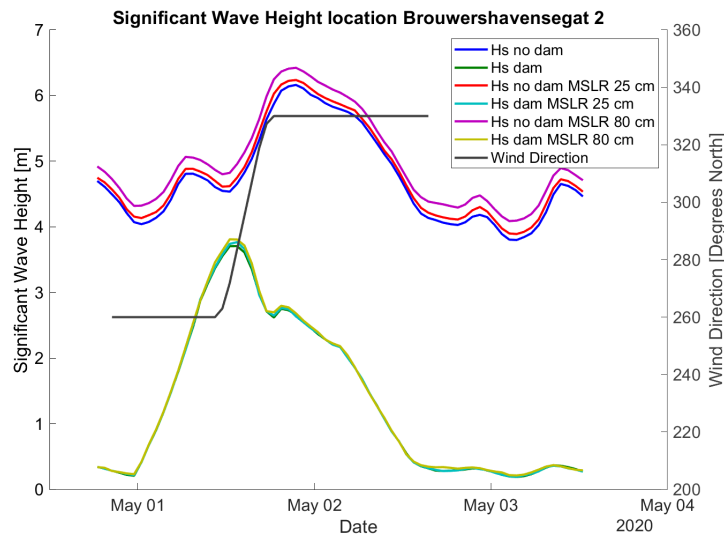


Figure 6.18: Significant Wave height and wind direction modelled for a northwestern storm with a return period of 10000 years at Brouwershavensegat 2.

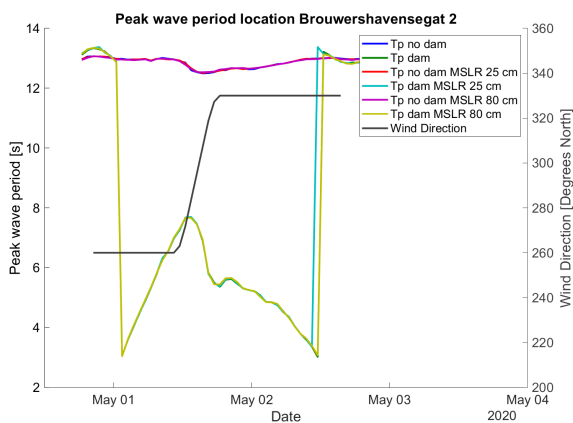


Figure 6.19: Peak wave period and wind direction modelled for a northwestern storm with a return period of 10000 years at Brouwershavensegat 2.

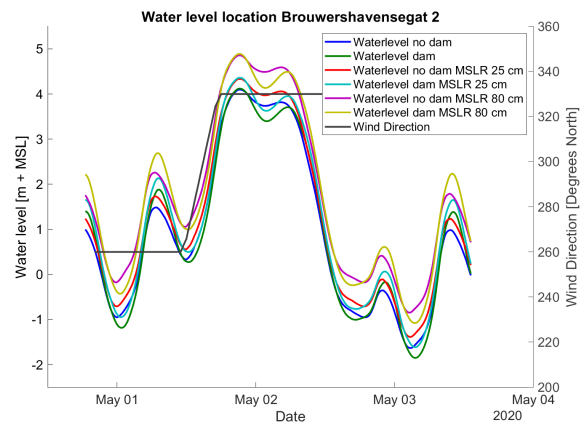


Figure 6.20: Water level and wind direction modelled for a northwestern storm with a return period of 10000 years at Brouwershavensegat 2.

Figures 6.12 and 6.13 show a sudden steep drop in the peak wave period. These lowered peak periods occur at the same moment that the wind input is increased, which is zero at the beginning and end of the model. The explanation for the drop in the peak wave period is that at that moment, the waves generated by the wind at that location have a larger peak in the energy density spectrum, suddenly changing the dominant wave period to those instead of the wave period that has been applied as the boundary condition. As the wind decreases later, the boundary waves become dominant again, and the peak wave period experiences a sudden increase. Because in this study, the peak wave periods during storms is analysed, Figure 6.4 compares only the peak wave periods of the wind-driven waves, as the peak wave conditions applied at the boundary are expected to occur during the height of the storm, when these waves are dominant.

It was concluded in the previous section that the dam has an increasing effect on the wave characteristics and the maximum water level during the southwestern storm. However, when comparing the models of the northwestern and southwestern storm, it can clearly be seen that the values for the maximum water level and maximum significant wave height are still considerably lower than those during the northwestern storm, see Figures 6.10 and 6.11. This agrees with the statement by Sterl et al. (2009) that northwestern winds are most dangerous for storm surges along the Dutch coast. It also agrees with the fact that the highest waves in the area are primarily from the northwest, as seen in Figure 3.3.

It is important to note, that in both SWAN models the same wave boundary condition has been applied, based on the statistical analysis by Roscoe et al. (2010). This was acceptable, because their found values were unidirectional. However, when comparing this with Figures 3.3 and 3.2, it is clear that historically, the highest waves come from the northwest rather than the southwest. As the statistical analysis has been performed based on this historical data, it is safe to assume that the wave with a return period of 10000 years as calculated by Roscoe et al. (2010), comes from the northwest. This means that the wave boundary conditions applied in the model of the southwestern storm should be smaller, reducing the significant wave height and the peak wave period. Based on this and the figures in Section 6.4.2 and Appendix E.2, it can be concluded that the northwestern storm is normative for the coastal safety.

6.5.4. Effect of MSLR

Lastly, the influence of MSLR on the hydraulic conditions has been modelled. Both Table 6.8 and 6.9 show an increased maximum water level which is slightly lower than the MSLR applied on the model compared to the original model. The reason for this is twofold. First, as discussed in Chapter 2, no significant increase in the tidal amplitude is expected, which explains why the maximum water level increase is in the same order of magnitude as the MSLR. Secondly, as explained previously, is the wind set-up inversely proportional to the water depth. As the water depth increases over the whole area, is a decrease in wind set-up expected. This hypothesis is reinforced by the results that show that the relative increase in maximum water level is smallest at the locations nearest the shore and the largest at Europlatform, which is the location furthest offshore.

In the peak wave period modelled, hardly any change is seen for the models without dam. At all locations except one, the calculated peak wave period is nearly equal to the peak period applied at the boundary. The exception is the location near the Eastern Scheldt Barrier, where the influence of breaking at offshore sandbanks decreases after the sea level has risen. For both models, the significant wave height increases at all locations due to MSLR. However, in both scenarios, the percentile increase in significant wave height is lower for the models without a dam than the models with dam, thus decreasing the impact of MSLR on hydraulic conditions during storm conditions. Finally, the load duration increases with the increased water level, which is expected as the calculations have been carried out based on the original MHW, so an increased MSL would, per definition, mean that the original MHW would be passed for a longer period. The construction of the DTP dam does not significantly impact the load duration at locations both inside and outside of the estuary.

6.6. Conclusion

In order to answer the research question "How is the coastal safety of the Dutch Delta coast influenced by the construction of an oblique DTP dam?" a numerical model has been set up consisting of a two-dimensional flow model in FINEL, coupled with a SWAN wave model, to simulate the hydraulic conditions during an extreme storm event with a return period of 10000 years. It is concluded that the peak water levels and the peak significant wave height near the Voordelta coast are considerably higher during a northwestern storm than during a southwestern storm with the same boundary conditions applied. Taking that into account, based on the models can be concluded that the construction of an oblique dam causes a considerable decrease in significant wave height. This is in the order of 0.5 m near the coast increasing to several metres just landwards off the dam. The peak wave period east of the DTP dam is halved in nearly the whole estuary. An exception is the coast near Westkapelle, where an increase in maximum significant wave height and peak wave period was found. A decrease in the maximum water level has been modelled near the Delta coast, in the order of 10 to 20 cm. However, an increase in maximum water level was found at Maasvlakte 2 and along the Holland coast. Near the Eastern Scheldt barrier, the maximum water level decreases by about 10 cm. The maximum significant wave height decreases in the range of 0 to 30%, depending on the location. The peak wave period does not decrease in front of the barrier. The effect of the dam on the maximum significant wave height is larger when applying MSLR, there is no significant difference in its impact on the maximum water level and the peak wave period when applying different mean water levels.

7

Development of the Voordelta

The final objective of this study is to investigate the development of the Voordelta. As has been described in Chapter 2, the exact morphology within the estuary is heavily influenced by three-dimensional processes. This means that to properly simulate the morphological development of the area, a three-dimensional flow model is necessary. To keep this study manageable, the choice has been made not to develop a three-dimensional model for the morphological development of the area but to formulate a hypothesis on its development based on existing literature and the results from the two-dimensional flow models used in this study. Additionally, a simplified sand transport module has been added to the two-dimensional flow model. In this chapter, an analysis of the development of the area is conducted. First, an analysis is done of the changed hydrodynamic conditions in the area as a result of the construction of the dam and the expected influence this will have on the morphological processes, based on the literature treated in Chapter 2. Thereafter, the used two-dimensional flow model and the added sediment module are discussed and the results of this model are presented and discussed.

7.1. Change in Morphological Processes

According to Elias et al. (2017), the dominant hydrodynamic processes in the Voordelta are the waves and tides, which are responsible for most of the sediment transport in the area. As both these processes are changed significantly after the construction of the DTP dam, the ratio of which of the two is dominant is expected to shift. Besides this, are density-driven flows expected to become more dominant, as is the case in estuaries (Savenije, 2005). The processes responsible for sediment transport in the Voordelta and the expected change in these processes are discussed in this section.

As discussed in Chapter 3, the majority of the waves in the Voordelta come from either a northwestern or a southwestern direction, with, as was shown in Figure 3.3, nearly all waves with a significant wave height above 3 m coming from the northwest. In Chapter 6, it was concluded that during storm conditions, waves coming from the northwest are blocked by the constructed DTP dam. The result of this is that, during northwestern storm conditions, significantly less wave energy is present within the created estuary, as can be seen in Figure 6.16. As Van der Spek et al. (2022) concluded that the high-wave events are the cause of the onshore transport at the lower shoreface, it can be deduced that this onshore-directed transport is halted within the estuary, decreasing the sediment coming into the system while also reducing the volume of sediment which is transported to the upper shoreface.

It has been hypothesised that the construction of the DTP dam at an angle can significantly increase the sediment available within the system by trapping the sediment. Because the dam effectively blocks the transport direction without openings at the bed level, it can be assumed that the bed level transport is trapped. However, with the turbine openings in the dam, suspended sediment could still proceed through the dam. As Kleinhans and Grasmeijer (2006) concluded that at the Dutch lower shoreface, the bed load transport is a factor five smaller than the suspended sediment transport, a first estimate would be that only a small part of the total sediment lost would be trapped, while simultaneously the inflow of sediment over the 20 m depth contour would be halted. A morphological model is necessary

to indicate better the DTP dam's effect on the sediment budget in the Voordelta.

The tidal amplitude within the estuary is expected to be amplified as a result of the reflection of the standing wave, as determined in Section 4.3. With increased tidal amplitude, the tidal prism also increases. The equilibrium velocity at the entrance of the estuary is dependent on the tidal prism, as can be seen in equation 7.1, from Bosboom and Stive (2021). A_{eq} is the equilibrium cross-section of the entrance channel, and T is the period of the tide in seconds. P is the tidal prism of the area, defined as the surface area of the estuary multiplied with the tidal amplitude.

$$\hat{U}_{eq} = \frac{\pi P}{A_{eq} T} \quad (7.1)$$

This means that as the tidal prism increases, either the equilibrium velocity in the estuary increases, which results in more erosion in the channels, or the equilibrium cross-section of the entrance must become larger, increasing erosion at the entrance.

With the majority of the incoming waves broken by the DTP dam, the wave energy present within the system decreases significantly compared to the current situation. This means that, in the classification of Davis Jr. and Hayers (1984), the dominant environment within the estuary is expected to shift towards tide-dominated. It is important to note that although the tidal range is expected to stay within the meso-tidal range, it can still be classified as tide-dominated. Also, it is expected that the wave energy of waves coming from a southwestern direction will not change considerably in the opening, as can be seen in Figure 6.6. Therefore, it is hypothesised that the coast near the entrance and the entrance will remain wave-dominated. However, going further north in the created estuary behind the dam, as wave action from southwestern waves is lessened due to friction and with lower northwestern waves incoming, sedimentation patterns become more tide-dominated (Dalrymple et al., 2012).

In tide-dominated estuaries, the tidal wave is normally asymmetric, as the crest migrates onshore more quickly than the trough, because the celerity of the tidal wave is dependent on the waterdepth, which is larger during flood periods. This results in a shorter duration of the flood tides, resulting in the flood currents being larger than the ebb currents, which creates flood dominance and a net onshore movement of bed material (Dalrymple et al., 1990). Normally, estuaries contain an inner part where an ebb dominant regime is leading, as the river outflow dominates the tidal influence at this location. However, because the tide does not only propagate along the length of the created estuary as is normally the case, but also flows in and out through the barrier, it is expected that this area will be very small, close to the Haringvliet barriers. Of course, this area's exact location can change depending on the river outflow through the Haringvliet.

As described by Van der Spek et al. (2022), the net transport from the lower shoreface to the upper shoreface is mainly driven by waves, while the transport the other way around is driven by downwelling currents during storm events. The wave impact is expected to decrease significantly, while this is not expected for the wind setup. Because of this, the equilibrium between these two processes is expected to change, possibly causing more sediment to move to the deeper part of the estuary, creating a more even bathymetry, especially in the area further north.

In conclusion, it is expected that the wave influence in the area will be reduced while the influence of the tide and that the density-driven flows will increase. As a result, the expected inflow of sediment into the area is expected to decrease, while at the same time, part of the sediment flowing out of the area is expected to be trapped. Several other processes have been discussed, with contradictory results. A three-dimensional morphological model is needed to get a better overview of the dominant processes within the estuary and the implications for sediment transport within the estuary.

7.2. Morphological model

In this section, the used two-dimensional flow model and the added sand transport module are explained and its results are presented and discussed.

7.2.1. Modelling approach

It has been foreseen that the hydraulic environment in the estuary will become more tide-dominated as a result of construction of the dam. In order to get a first insight into impact of the DTP dam on the sediment budget of the Voordelta, a morphological module has been added to the two-dimensional FINEL flow model, which was previously described in Chapter 5. To keep computational times manageable, several significant simplifications have been applied. Firstly, no morphological change is considered in the model. This means that the bathymetry in the model remains the same throughout the entire runtime, not taking into account sedimentation and erosion patterns. Second, only the tidal and meteorological input are applied in the model, which means that waves are not considered. Besides that is the flow model is two-dimensional. As a result of this, density driven flows are not included in the model. Furthermore, only sand is considered in this model, meaning that silt transport is not included. Importantly, the sediment concentrations and fluxes in this model have not been validated. This means that the calculated volumes are assumed not to be an accurate representation of reality. However, the erosion and sedimentation patterns are dependent on the hydrodynamic processes. As this part of the model has been validated, the model results are assumed to give an indication of the larger morphological trends. Because of the simplifications, the focus of the model discussion is on the sediment transport through the sides of the estuary. Also, the inner morphology of the estuary is not discussed based on this model.

7.2.2. FINEL model input

The hydrodynamic part of the FINEL model is identical to the model used to calculate the power generated, which has been described and validated in Chapter 5.

Added to the model is a morphological module, which calculates the sand transport in the area of interest. The model only considers sand, so silt is not included. Furthermore does the model not update the bathymetry based on the sediment transport, which means that the initial bathymetry is used throughout the entire run of the model. The sediment transport formula applied in the model is based on the theory as explained in Van Rijn (2007a), Van Rijn (2007b) and Van Rijn (2007c).

The sediment size is based on data from Deltares (2020), based on measurement data from 2007 near the opening of the estuary. The sediment sizes applied are:

- D_{50} 230 μm
- D_{90} 407 μm

The sediment size is applied uniformly over the model domain. This means that near the north of the estuary, the sediment size is higher than in reality, as it was previously established that in that area the average D_{50} is circa 150 μm (Van de Kreeke and Haring, 1979).

The model has been run twice, once with the DTP dam as designed in Chapter 4 and once without the dam.

7.2.3. Results

In this section, the results of the FINEL model are presented. The first section shows the measured discharges through the sides of the estuary, as well as the flow velocities at a location near the opening. The second section shows the cumulative sand fluxes in the estuary.

7.2.3.1 Flow results

In this section the results of the two dimensional flow model which are relevant for the morphological processes are shown. Figures 7.1 and 7.2 show a comparison of the water discharge through the sides of the estuary in the models with and without dam. Figure 7.3 compares the flow velocities at locations OS11, which is close to the opening of the estuary.

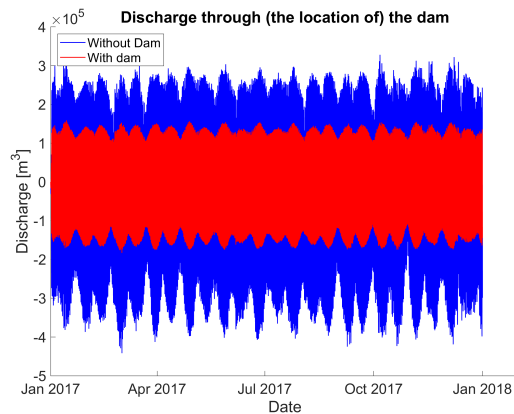


Figure 7.1: Discharge through the (location of the) dam during one timestep. Positive values mean a net discharge towards the estuary.

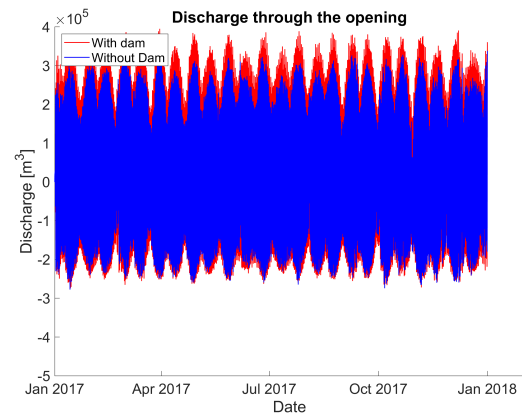


Figure 7.2: Discharge through the opening of the estuary. Positive values mean a net discharge towards the estuary.

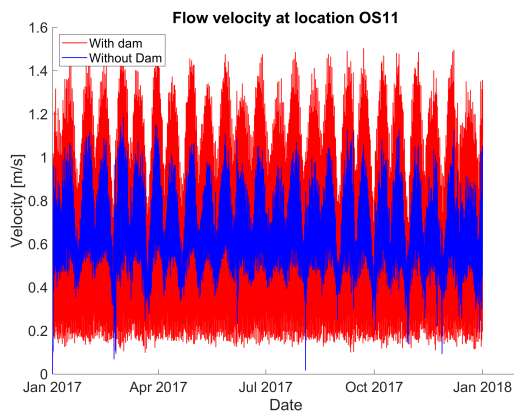


Figure 7.3: Flow velocities at measurement location OS11 in the models with and without dam.

7.2.3.2 Sand fluxes

Figures 7.4 and 7.5 show the cumulative sand flux through the location of the dam and through the opening of the estuary, comparing the results of the model with and without dam. Figure 7.6 shows the sum of the two previous models, showing the total sand flux through the edges of the estuary. In all cases, a positive value means a net sand flux towards the estuary.

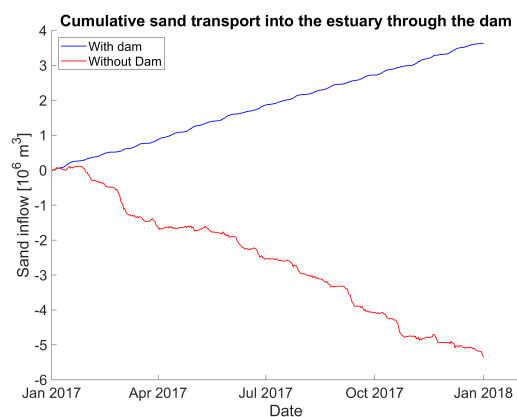


Figure 7.4: Cumulative sand flux through the (location of the) dam. Positive values mean a net flux towards the estuary.

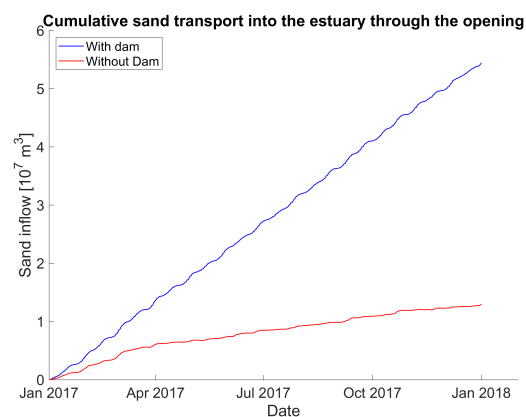


Figure 7.5: Cumulative sand flux through the opening of the estuary. Positive values mean a net flux towards the estuary.

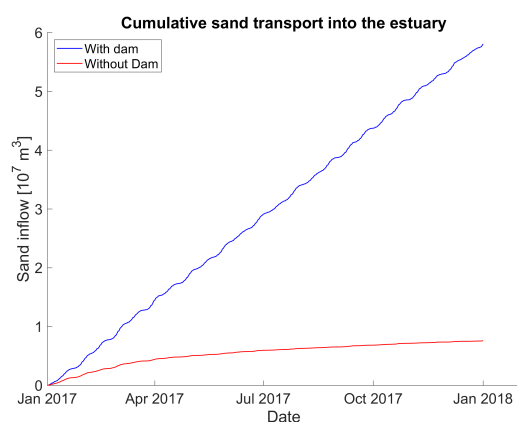


Figure 7.6: Cumulative sand flux through the sides of the estuary. Positive values mean a net flux towards the estuary.

7.2.4. Discussion

In this section, the results of the two-dimensional flow and morphological model are discussed, such as presented in the previous section.

7.2.4.1 Discussion of the results

The overall results of the models are shown in Figure 7.6. Based on this model, it is expected that the sediment flux into the Voordelta area will increase. Based on Figures 7.4 and 7.5, the majority of this sediment flux flows through the opening of the estuary, which significantly increases, while the sediment flux through the location of the dam is turned around and results in a net flux into the estuary as result of construction of the dam.

The hydrodynamic results of the models are more accurate than that of the morphological module, as the two-dimensional flow model has been calibrated and validated. The figures in Section 7.2.3.1 give an explanation for the increased sediment flux towards the estuary that is calculated in the model. When comparing Figures 7.1 and 7.2, several clear changes can be seen. In the model without DTP dam, the discharge into the area is similar over the western and southern boundary. The discharge out of the area is significantly larger through the western boundary through the southern boundary. However, after construction of the dam, the discharge through the dam is halved, both for in- and outflow. Figure 7.2 also clearly shows that, compared to the situation without dam, after construction of the dam the inflowing discharge increases more than the outflowing discharge. The result of this is that the flow velocities increase significantly in the opening, see Figure 7.3. As the inflowing discharge is larger than

the outflowing discharge, it follows that the inflowing velocities are larger as well. This results in a so-called peak-velocity asymmetry in the sediment transport. This means that the residual transport takes the direction of the highest peak velocity (Gatto et al., 2017). As bed-load transport is proportional to the flow velocity to the power 3-5 (Van de Kreeke and Robaczewska, 1993) and suspended transport is proportional to the flow velocity to the power 4 for non-cohesive fractions (Gatto et al., 2017). This corresponds with the expected flood-dominance in the estuary which was described in the previous section. Based on this, it can be concluded that the initial sediment flux towards the estuary is expected to increase after construction of the DTP dam.

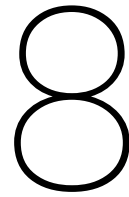
7.2.4.2 Interpretation of the calculated values

As mentioned above, because of the simplifications in this model, the values calculated by the model should only be used indicatively. However, in this section some interpretation of the values is given. The total sediment influx after a year without construction of a dam is a factor two to three larger than the volumes described in Elias et al. (2017). However Elias et al. (2017) assumed no inflow over the southern border, which is a major difference with this model.

The expected sand flux into the estuary is calculated to increase by a factor six by the model. One of the reasons for this large difference is that the bathymetry is not updated by the model. As a result of the construction of the dam, the flow velocities at the opening, especially the flows entering the estuary, are expected to increase significantly, as shown in Figure 7.3. As a result of this, severe erosion will occur at the opening with sedimentation of the eroded sand further inside the estuary. However, because the bathymetry is not updated in the model, this erosion process does not change and no equilibrium is reached, as was described in Section 7.1. The result of this is that the flux calculated by the model is larger than what will happen in reality. However, the results do give a first idea of the expected influence on the morphology, as the relative results show an increased import of sediment into the estuary.

7.3. Conclusion

The objective of this chapter is to answer the research question, "What is the effect of an oblique dam on the development of the area between the dam and the coast?". In the chapter, an analysis of the area and the changed conditions has been done based on literature and the results of the two-dimensional flow models used in this study, with an added module for sand transport. In the estuary, the influence of waves is expected to decrease, while the tidal amplitude is expected to increase. The result of this is an expected decrease of cross-shore sediment transport into the area. As is the case in most estuaries, the area is expected to become flood dominant, increasing the sediment transport towards the estuary, this was confirmed by the two-dimensional flow model. Other sediment transport processes are also changing compared to the current situation, but the exact results should be calculated using a three-dimensional morphological model.



Discussion

In this chapter, the study is discussed and reflected on. In the first section, an analysis of the results is performed. This analysis focuses on the impact of the design choices made in this study on the gained results. Then, an analysis of the validity of the research method used is done and the usability of the research in subsequent research is discussed..

8.1. Analysis of the results

In this study, the choice was made to make the assessment of a DTP dam under an angle based on one design. In the case of the assessment of the power generated, the comparison was made with a dam perpendicular to the coast, as this is the initial idea which has been used in previous studies. However, the choice for a single design has a large influence on the conclusions, as all considered aspects are influenced by the design. In this section, an assessment is made of the influence the design choices have on the results.

8.1.1. Effect of dam orientation on energy output

Firstly, the orientation of the dam is considered. The non-perpendicular orientation of the dam is the feature that most distinguishes the assessment of the energy generation from previous studies. It has been found that the power generated is significantly lower than that of a perpendicular dam with the same length. The first simple reason for that is that as a result of the larger water depths further from the coast, the perpendicular dam contains more turbines. The other, more important reason, is a result of the hydrodynamic processes responsible for the creation of a water level difference over the dam. The original idea for a dynamic tidal power dam is based on the oscillatory motion of the tidal wave. Because of the oscillatory motion, the concept of added mass is applicable, which accelerates and decelerates along with the object. The result of this is a pressure build up at one side of the object, which is translated into a rising water level. Importantly, at the same time a negative pressure pulls on the other side of the dam, which is seen as a decrease of the water level (Hulsbergen et al., 2012). The second process responsible for the water level difference is the creation of a phase difference in the tidal propagation over the dam, which further increases the water level difference over the dam. Figure 5.13 clearly shows both of these processes happening. The tidal amplitude on the southern side is amplified, while the tidal amplitude on the northern side is reduced, as a result of the first process, and a phase difference is seen in the tidal propagation on either side of the dam, further increasing the water level difference. However, Figure 5.7 shows an entirely different case. In the case of the oblique dam, amplification of the tidal wave does occur on one side of the dam, but the tidal wave is not dampened on the other side. This means that the pressure difference created by the movement of the added mass, as explained by Hulsbergen et al. (2012), is not present. Instead, the amplification of the tidal wave seems to be the result of reflection of the incoming tidal wave at the end of the estuary. The reason for this is that the designed dam has an orientation nearly parallel to the coast and therefore an orientation nearly parallel to the direction of the propagating tidal wave. As a result of this, hardly any pressure is exerted on the dam by the tidal wave, and the added mass area is nearly negligible.

No phase difference in propagation of the tidal wave on both sides of the dam occurs either, because the tidal wave reaches both sides of the dam at the exact same moment, meaning that any phase difference that is still found is the result of differences in depth on either side of the dam.

The added mass is at its maximum for a structure perpendicular to the flow direction. For angles in between, a representative added mass of the structure can be calculated, the method of which is outside the scope of this study. A more thorough explanation of the physics of added mass can be found in Brennen (1982). However, it can be concluded that the added mass, which is crucial for the creation of the pressure difference, is at its maximum at a dam perpendicular to the coast and minimum for a dam parallel to the coast. It is therefore expected that the water level difference and, consequently, the energy output, increases with an increasing angle with the coast.

8.1.2. Desirability of the project

It is clear that the choice for an oblique dam has a negative effect on the energy generated by the DTP dam. In fact, as it was determined that the processes for creating a water head difference over the dam are completely different from those described in Hulsbergen et al. (2005) and Hulsbergen et al. (2012), it can be concluded that the energy output generated by the DTP dam following the reference design is accidental. Nonetheless, a substantial energy yield is still expected to be generated by the DTP dam, with a yearly energy output in the order of 2 TWh.

The objective of this study was to make an assessment of the potential of a DTP dam based on more than just the energy criterion. The results of Chapter 6 clearly show that the hydraulic conditions during an extreme storm event become less severe across nearly the whole of the Voordelta, as a result of the construction of the DTP dam. This is a clear consequence of the dam being designed under an angle. If the angle of the dam with relation to the coast would be increased, the positive impact on the coastal safety would decrease. For a northwestern storm, a dam with the same length would protect a smaller part of the Delta coast from incoming waves, while the wind-driven waves behind the dam would increase on account of the increased fetch behind the dam. Wind setup at behind the dam would also increase because of the increased distance, most pronounced at the southern end of the created estuary.

Finally, an increased flood dominance is observed in the opening of the created estuary, shown by larger flow velocities flowing into the estuary. This results in an increased sediment flow towards the estuary. A construction of the dam under a larger angle would even further increase the size of the created estuary, as well as the size of the opening. It is expected that this would result in a decrease in the inflowing velocities compared to the design used in this study. This means that an increased angle is expected to decrease the sediment trapping capabilities of the area compared to the design used in this study.

Finally, one of the main reasons for the assessment of an oblique dam rather than a perpendicular dam is the decrease in interference with areas in the North Sea that have other functions, such as shipping. By choosing to design the DTP dam in such a way that it stays close to the Natura 2000 area, the interference with otherwise designated areas is at a minimum. This means that any design with an angle larger than the one chosen in this study, would result in more nuisance for other industries.

From this section can be concluded that the impact of the DTP dam as well as its energy yield are dependent on the design of the dam, most importantly the orientation. With an increasing angle the energy yield would increase, but at the cost of its positive impact on the Voordelta and at the cost of more nuisance in other areas. A smaller angle results in a more positive effect in the Voordelta, but results in a significantly smaller energy yield. This means that when considering this project, the first step must be a decision on what the most important objectives of the project are, and the design of the dam should be adapted based on the choices made. Additional to this should the impact of the dam on other fields such as ecological impact should be considered as well.

8.2. Validity

As can be seen in Chapter 6 and Appendix C, the model consistently underestimates the peak wave period. This underestimation seems to be the largest at the locations closest to shore. Because at these locations the peak wave period is smallest in the results, the model is assumed to overestimate the impact of the dam on the peak wave period. This overestimation is assumed to be at most $\frac{9}{12} - \frac{8}{12} = 8\%$, based on the measured maximum wave periods at location OS11, and assuming an underestimation of the peak wave period of 1 second in the model with dam. In this equation the 12 seconds are the peak wave period at location OS11 without dam, the 8 seconds are the calculated peak wave period and the 9 stands for the peak wave period when an underestimation of 1 second is assumed.

In contrast, the figures in Appendix C.2.2 clearly show that the model systematically overestimates the significant wave height, although it quite closely follows the development through time. The same can be seen in the figures in Appendix C.1. The exception to this is the location OS11, which is the only buoy nearshore, where the significant wave height is underestimated. Similar to the peak wave period, the overestimation offshore is in the order of 5%.

In the model used for determining the influence of the dam on storm characteristics, representative input parameters have been used that have been calculated statistically in previous research. Because of this, these input parameters have significant margins of uncertainty. For wind velocity, a value of 35 m s^{-1} was used, but the 95% certainty margin is between 31.9 and 38.1 m s^{-1} , according to Chbab (2015). As was concluded in Chapter 6, are the peak significant wave height and peak wave period determined by wind-generated waves growing behind the dam.

As explained by Holthuijsen (2017), the wind input term S_{in} is the sum of two factors, the first of which is proportional to u_{wind}^4 , and the second term to either u_{wind} or u_{wind}^2 , depending on the used theory. This means that the wind input term in the model is overestimated by up to $1 - (\frac{31.9}{35})^4 = 31\%$ or underestimated by up to $1 - (\frac{38.1}{35})^4 = 40\%$. As the wind input is relatively larger for the waves on the inside of the dam, this uncertainty can cause a significant overestimation or underestimation, respectively, of the impact of the dam on the peak significant wave height and the peak wave period. However, for the significant wave height the uncertainty is smaller nearshore, as there the wave heights are depth-limited rather than limited by the wind input term.

Similarly, the wave boundary conditions of the extreme storm event have been based on Roscoe et al. (2010). They state an uncertainty margin in the peak period between 11.41 and 21.09 s, and an uncertainty margin in the significant wave height between 6.18 and 9.95 m. These uncertainty margins were calculated using the bootstrap method with 1000 samples. However, these uncertainty margins were given before a final extreme value analysis. For the final return values, Roscoe et al. (2010) did not give an uncertainty margin, but it can be assumed that it is smaller than the one just mentioned. Nevertheless, an uncertainty in the significant wave height and wave period applied at the boundary condition can cause an under- or overestimation of the impact of the dam, because the difference between the wave characteristics before and after construction of the dam has been determined to be primarily dependent on the initial wave characteristics, which closely resemble the boundary conditions.

In the model used for calculating the energy output of the dam, the maximum water level is overestimated by about 10 cm. However, as this overestimation is the same across the whole area of interest, this is not expected to influence the energy output of the oblique dam. This is not the case for the perpendicular dam however. Because the energy output of this model is partly as a result of a phase difference over the dam, the overestimation of the maximum water level means that the energy output of the dam is also slightly overestimated.

In the calculation of the energy output of the dam, several assumptions regarding the parameters of the turbines were made. The parameter C from Equation 2.4, was assumed to be 1.85, based on previous studies on turbines in the Eastern Scheldt Barrier. However, these turbines are substantially different from the ones that will be used in the DTP dam, which have been assumed in this study to have a diameter of 8.5 meter, and which are completely encircled by the construction of the DTP dam, as opposed to the turbines in the Eastern Scheldt Barrier. Second, the assumption was made that the parameter a_{turb} can be kept at the optimum during operation. If this is not the case, the energy output of the barriers will be lower than calculated. Finally, the efficiency factor of the turbines was estimated to be 85%. Because the energy output is directly proportional to the efficiency factor, the actual value of

this factor will have a significant influence on the accuracy of the calculated power output in this study.

The calculations in this chapter are based on a model which had as input the tidal waves and meteorological data of 2017. This model does therefore not take into account the 18.6-yearly lunar nodal cycle which influences the tidal amplitude. However, as the tidal amplitude varies throughout this cycle, so is the energy output of the dam expected to vary. Thiébot et al. (2020) concluded that the annual energy production at a potential tidal barrier in northwest France was about 5% higher in 2017 than the long-term expected mean output, while the energy production can vary in the order of +/- 10% throughout the cycle. As in Section 5.3 a clear correlation between the tidal amplitude and the energy output of the DTP dam was found, it is expected that the energy output of the DTP dam will be affected by this cycle in the same order of magnitude, meaning that the mean energy output is expected to be in the order of 5% lower than calculated.

8.3. Usability of the study

In order to be able to reach the conclusions in this study, a reference layout for the dam had to be designed based on a few simple requirements. With the most important requirement being that the dam had a southwest orientation, the reference layout was sufficient for this step in the assessment. However, no further study has been made of optimisation of the layout, most importantly into the length and width of the estuary created and the optimisation of location of the turbines in the dam. In this research, the turbines were located at a fixed distance of each other, which was determined by the open ratio and the waterdepth. In a study on tidal energy generation using turbines in the Eastern Scheldt Barrier, Verbeek (2023) found that energy is harvested most efficiently when turbines were present in half the openings in the barrier. This could also be the case for the DTP dam, but this has not been researched. Similarly, the assumption was made that turbines are present along the whole length of the dam, even though water level differences are largest near the attachment point to the shore. Finally, along the whole length of the dam, the open ratio was the same. Changes in this open ratio along the dam could also have an effect on the efficiency of the energy generation. In a further design stadium, research should be done into optimisation of the distribution of turbines throughout the dam, and subsequently, of the impact this distribution has on the hydrodynamics in the estuary. Finally, no research has been done into the hydrodynamic effects of addition of wings, such as described in Section 2.1. Such changes in the layout could significantly change the resulting hydrodynamic processes around the dam. In the case of an oblique dam, addition of wings could increase a phase difference over the dam. However, the effect is expected to be less than for a perpendicular dam, because the main purpose of the added wings is to increase the added mass area, which is not applicable for the oblique DTP dam.

Following previous studies, this study has not considered a minimum water level difference necessary for the turbines to be functional. However, Figure 5.5 shows that a minimal necessary working head of 20 cm decreases the output by nearly 10%. DTP Netherlands (n.d.) and Witteveen+Bos and CE Delft (2019) mention the necessity for turbines which can function at water level differences as small as this or even smaller, which are still in development at this moment. More accurate estimates of the expected energy yield of DTP dams is therefore highly dependent on the working head of these turbines.

9

Conclusion and recommendations

In the first part of this chapter, the answers to the research questions posed in Chapter 1 are presented. After that, recommendations for further research are given in the second section.

9.1. Conclusion

In this section, the research questions are answered. The first subsection answers the main research question; a more detailed answer is given to the sub-questions in the second subsection.

9.1.1. Main Research Question

The aim of this study is to answer the research question:

How does the orientation of a dynamic tidal power dam starting at Maasvlakte 2 influence its energy yield as well as the coastal safety and development of the Dutch Delta coast, and is such a construction desirable from these perspectives?

Previous research on DTP dams and their influence on tidal flows was focused on DTP dams built perpendicular to the coast and to the direction of the tidal wave propagation. In order to study the influence of the orientation of the DTP dam, a reference layout has been determined with as the main requirement that it has a southwestern orientation, meaning that it is constructed under a small angle with the incoming tidal wave propagation. It was found that the construction of the DTP dam under this angle significantly decreases the phase difference in the propagation of the tidal wave on either side of the dam, as opposed to DTP dams built perpendicular to the coast. A second difference with a DTP dam perpendicular to the coast is that no dampening of the tidal wave on the northern/outside part of the dam is produced. Amplification on the southern/inside part of the dam occurs, similar to what happens with a DTP dam perpendicular to the coast. However, the process is different. For a perpendicular dam, the process responsible for this amplification is the inertial force of the added mass on the dam, which oscillates with the tidal wave. In the case of the dam under a small angle, the amplified tidal wave height seems to result from the reflection of the incoming tidal wave at the closed end of the estuary, with only a small part caused by the inertial force. The result of these occurrences is that the total energy yield of the dam under an angle is significantly lower than that of a dam perpendicular to the coast and the tidal wave propagation.

The impact on hydraulic conditions during a design extreme storm event of the DTP dam with the reference layout has been studied by comparing the relevant hydraulic conditions in the Voordelta area during such a storm without and with the dam applied in the model. This comparison yielded a decrease in both maximum significant wave height and peak wave period in most of the Voordelta area.

A DTP dam under an angle significantly changes the dominant hydrodynamic and morphological processes in the area in front of the Delta coast. The area becomes more tide-dominated, while density-driven flows also become more important. The extent to which this influences the morphological flows inside and through the area must be modelled using a three-dimensional morphological model, which has not been done in this study.

9.1.2. Sub-Questions

In order to answer the main research question, several sub-questions have been defined. The answers to these questions are summarised in the answer to the main research question and elaborated on in this section.

1. *How does the construction of an oblique DTP dam impact the hydrodynamic conditions in the Voordelta?*

The most important hydrodynamic forcing mechanisms in the Voordelta are tides and waves, both of which are influenced by constructing an oblique DTP dam.

The wave climate in the Voordelta consists of waves with two major directions: waves from the northwest and from the southwest. The highest waves all come from the northwest. The influence on the wave climate during storm events from the northwest has been modelled using a coastal wave model coupled with a two-dimensional flow model. The model showed that the wave energy in the Voordelta area decreased significantly during northwestern storms, with the dam breaking the incoming waves from the North Sea. As all waves coming from the northwest and west entering the Voordelta are broken, it is concluded that especially the high-energy wave events in the Voordelta decrease in number and severity as a result of the construction of the dam. The influence on the average wave climate has not been researched.

Based on several assumptions, an amplification of the tidal wave within the created estuary as a result of the reflection of the standing tidal wave was found to occur. This was confirmed with the use of a 2D flow model. Further amplification of the tidal wave is expected to occur when increasing the length of the dam and, thus, the estuary to approach the quarter wavelength of the tidal wave. However, assuming no changes in other parameters, it is estimated that the dam would have to double in length for quarter-wavelength resonance to occur. This has not been researched with the use of numerical models in this study.

2. *What is the expected energy yield of an oblique DTP dam, and how does this compare to a perpendicular DTP dam and to literature?*

A reference layout for the DTP dam has been designed with a southwest orientation starting at Maasvlakte 2. Of this dam, an analysis has been done of the open ratio, which optimises the energy yield. The changed orientation of the dam did not change the optimal open ratio, as the result was similar to that found by Dai et al. (2017). The energy yield of this oblique dam with optimised open ratio has been determined by calculating the discharge through each turbine using a 2D flow model with tidal and meteorological boundary conditions. This yielded an expected maximum energy output in the order of $8 \cdot 10^2$ MW and an expected yearly power output in the order of 2 TWh. A second model was made with a DTP dam perpendicular to the coast, starting at the same location. This dam had a modelled maximum power output and expected yearly output both a factor five higher than that of the oblique dam. Previous research has all been done assuming a dam perpendicular to the coast. When comparing the results of the perpendicular dam in this study to that in previous studies at the Dutch coast, it is found that previous studies find a power output which is a factor three higher than the power output found in this study.

3. *How is the coastal safety of the Dutch Delta coast influenced by the construction of an oblique DTP dam?*

Based on Den Bieman and Kieftenburg (2015) and Van Rijn (2009), the wave characteristics, peak wave period and maximum significant wave height, as well as the maximum water level and the load duration, were determined to be representative of the coastal safety of both hard and soft coasts in the Voordelta. A two-dimensional flow model with an integrated wave model was set up to compare these characteristics with and without the construction of an oblique DTP dam when applying the conditions representing a storm with a return period of 10000 years. It was found concluded that a northwestern storm is normative for coastal safety in the Dutch Delta coast. A decrease in significant wave height and wave period is seen along the entire delta coast. An exception to the decrease in the peak wave period is the Eastern Scheldt Barrier, where the dam does not influence the peak wave period. Near Westkapelle, both the significant wave height and the peak wave period increase. On the east and north sides of the DTP dam, a significant increase in wave height is seen due to wave reflection at the dam. The maximum water levels near the shore decrease by a few percent. The same results are seen when applying a higher water level as a result of mean sea level rise.

4. *What is the effect of an oblique dam on the development of the area between the dam and the coast?*

Based on a literature study and the results of the two-dimensional flow models used in this study, a hypothesis was made about the expected behaviour of the region after the construction of the DTP dam. The area behind the dam contains most characteristics of an estuary and can be classified as one, although the presence of openings along the side of the dam cause the dynamics within the area to be different from those seen in natural estuaries. The influence of waves in the area is expected to decrease as incoming waves from the northwest are blocked by the DTP dam, decreasing the wave energy inside the area. The flow velocities at the entrance of the created estuary increase significantly during flood, creating a system that is more flood dominant. The result of this is an increase in the net sediment transport into the Voordelta. A decrease in sediment entering the system is expected as flows over the 20 m depth contour are expected to decrease. On the other hand, the bed load transport leaving the area through the northern border is expected to be trapped. The exact impact on the sediment budget in the area must be modelled using a validated morphological model. The dominant processes determining morphological transport within the estuary will change due to the changing hydrodynamic processes. However, The extent of these changes and the resulting morphological transport must also be modelled with a three-dimensional morphological model.

9.2. Recommendations

In this section, the most important recommendations concerning further research into the construction of an oblique DTP dam in the North Sea are presented.

For a more detailed design of the DTP dam, it is important that first the objectives of the project are clearly defined and a choice is made in what the primary objective of the project should be. In this study was concluded that the orientation of the dam has large, conflicting influences on the energy yield and the impact on coastal safety. Similarly, the expected influence on the morphological development of the Voordelta is estimated to be larger for designs of the dam more parallel to the coast, such as studied in this research. These, and smaller requirements, will determine the final shape of the dam. Also, additions to the design of the dam such as wings at the tip, such as discussed in Chapter 2, have not been considered in this study. However, the expectation is that their influence will be considerably less for an oblique dam compared to a perpendicular dam, as the main impact of such wings is an increase in phase difference, it is still worth investigating if this is indeed the case. Furthermore, for a more final design, the reflection factor of the dam can be calculated more accurately, giving better insight into the effect of the dam on the wave heights west and north of the dam.

For a clear understanding of the impact of the dam on the morphological processes in the area a morphological model is necessary, as has been stated previously in this study. For a first insight into the large-scale impact of the dam, such as a global idea of the impact on the sediment budget in the Voordelta, a two-dimensional model is deemed sufficient. However, for a more accurate estimation as well as for an accurate insight into the morphological changes within the create estuary, a three-dimensional morphological model is advises, as concluded by, among others, Grasmeijer et al. (2022),

Van Rijn (2009) and Van der Spek et al. (2022). Such a study should also be done to assess the impact of a DTP dam on the alongshore sediment transport along the Holland coast.

For a more accurate estimation of the energy yield of the dam, the development of the low head turbines that could be used in such a dam must be finished, and of these turbines the loss parameters and efficiency should be determined.

Finally, for the realisation of such a project, many other studies must be carried out. Examples are a study determining the ecological impact of the dam and the turbines; a stakeholder study; a study on the impacts throughout the basin, which Figure 6.5b has shown are likely; and an economical feasibility study.

References

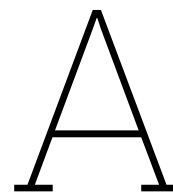
- Arns, A., Dangendorf, S., Jensen, J., Talke, S., Bender, J., & Pattiaratchi, C. (2017). Sea-level rise induced amplification of coastal protection design heights. *Scientific Reports*, 7(40171). <https://doi.org/10.1038/srep40171>
- Bak, C. I., & Vlag, D. P. (1999). *Achtergronden hydraulische belastingen dijken ijsselmeergebied, deel-rapport 5, modellering waterbeweging waqua* (tech. rep. RWS-RIZA rapport 99.042) [In Dutch]. RIZA. Lelystad.
- Battjes, J. A., & Labeur, R. J. (2017). *Unsteady flow in open channels*. Cambridge University Press.
- Bitter, G. (2018). *Dynamic Tidal Power (DTP), Energie uit getijdenstromen in de Noordzee*. (tech. rep.) [In Dutch]. Antea Group.
- Booij, N., Ris, R. C., & Holthuijsen, H. (1999). A third-generation wave model for coastal regions. *Journal of Geophysical Research*, 104(C4), 7649–7666. <https://doi.org/10.1029/98JC02622>
- Bosboom, J., & Stive, M. J. F. (2021). *Coastal dynamics*. TU Delft Open.
- Brennen, C. E. (1982). *A Review of Added Mass and Fluid Inertial Forces* (tech. rep. N62583-81-MR-554). Naval Civil Engineering Laboratory. Port Hueneme, CA, USA.
- Breugem, W. A., & Holthuijsen, L. H. (2006). Generalized Shallow Water Wave Growth from Lake George. *Journal of Waterway, Port, Coastal and Ocean Engineering*, 133(3), 172–182. [https://doi.org/10.1061/\(ASCE\)0733-950X\(2007\)133:3\(173\)](https://doi.org/10.1061/(ASCE)0733-950X(2007)133:3(173))
- Centraal Bureau voor de Statistiek (CBS). (2022). *Meer elektriciteit uit hernieuwbare bronnen, minder uit fossiele bronnen* [In Dutch]. Retrieved June 1, 2023, from <https://www.cbs.nl/nl-nl/nieuws/2022/10/meer-elektriciteit-uit-hernieuwbare-bronnen-minder-uit-fossiele-bronnen>
- Chbab, H. (2015). *Basisstochasten WTI-2017* (tech. rep. 1209433-012-HYE-0007) [In Dutch]. Deltares.
- Chbab, H., & De Waal, H. (2017). *Achtergrondrapport Hydraulische Belastingen. Wettelijk Beoordelingsinstrumentarium 2017* (tech. rep. 1230087-008-HYE-000 1) [In Dutch]. Deltares.
- Dai, P., Zhang, J., & Zheng, J. (2017). Predictions for Dynamic Tidal Power and Associated Local Hydrodynamic Impact in the Taiwan Strait, China. *Journal of Coastal Research*, 33(1), 149–157.
- Dai, P., Zhang, J., & Ziao, L. (2020). Temporal Evolution Assessment of Dyanmic Tidal Power Including Turbine Effects. *Journal of Coastal Research*, 36(5), 1050–1058.
- Dalrymple, R. W., Knight, R. J., Zaitlin, B. A., & Middleton, G. V. (1990). Dynamics and facies model of a macrotidal sand-bar complex, Cobequid Bay-Salmon River estuary (Bay of Fundy). *Sedimentology*, 37, 577–612. <https://doi.org/10.1111/j.1365-3091.1990.tb00624.x>
- Dalrymple, R. W., Mackay, D. A., Ichaso, A. A., & Kyungsik, S. C. (2012). Processes, Morphodynamics, and Facies of Tide-Dominated Estuaries. *Principles of Tidal Sedimentology*, 79–107. https://doi.org/10.1007/978-94-007-0123-6_5
- Dam, G., Bliet, A. J., Labeur, R. J., Ides, S., & Plancke, Y. (2007). Long term process-based morphological model of the Western Scheldt Estuary. *Proceedings of the 5th IAHR symposium of the River, Coastal and Estuarine Morphodynamics Conderence*, 1077–1084.
- Davies, J. L., & Clayton, K. M. (1980). *Geographical vaiation in coastal development*. Longman.
- Davis Jr., R. A., & Hayers, M. O. (1984). What is a wave-dominated coast? *Marine Geology*, 60, 313–329. [https://doi.org/10.1016/S0070-4571\(08\)70152-3](https://doi.org/10.1016/S0070-4571(08)70152-3)
- De Winter, R. C., Sterl, A., De Vries, J. W., Weber, S. L., & Ruessink, G. (2012). The effect of climate change on extreme waves in front of the Dutch coast. *Ocean Dynamics*, 62, 1139–1152. <https://doi.org/10.1007/s10236-012-0551-7>
- Deltares. (2020). *Deltares OPeNDAP*. Retrieved January 21, 2023, from <https://opendap.deltares.nl/thredds/catalog/opendap/tno/ncp/catalog.html>
- Den Bieman, J., & Kieftenburg, A. (2015). *Handreiking voor het afleiden van ontwerpwaterstanden en golfcondities* (tech. rep. 1209832-004-HYE-0001) [In Dutch]. Deltares.
- DTP Netherlands. (n.d.). *DTP Ontwikkeling inleiding* [In Dutch]. Retrieved April 12, 2023, from <https://www.dynamictidalpower.eu/DTP-ontwikkeling/>

- Edwards, P., Dobson, P., & Owen, G. (2022). The problem with renewables. *Physics World*, 35(4), 17. <https://doi.org/10.1088/2058-7058/35/04/17>
- Elias, E. P. L., Van der Spek, A. J. F., & Lazar, M. (2017). The 'Voordelta', the contiguous ebb-tidal deltas in the SW Netherlands: large-scale morphological changes and sediment budget 1965-2013; impacts of large scale engineering. *Netherlands Journal of Geosciences - Geologie en Mijnbouw*, 96(3), 233–259. <https://doi.org/10.1017/njg.2016.37>
- Gatto, V. M., Van Prooijen, B. C., & Wang, Z. B. (2017). Net sediment transport in tidal basins: Quantifying the tidal barotropic mechanisms in a unified framework. *Ocean Dynamics*, 67, 1385–1406. <https://doi.org/DOI10.1007/s10236-017-1099-3>
- Godin, G. (1993). On tidal resonance. *Continental Shelf Research*, 13(1), 89–107. [https://doi.org/10.1016/0278-4343\(93\)90037-X](https://doi.org/10.1016/0278-4343(93)90037-X)
- Grasmeijer, B., Huisman, B., Luijendijk, A., Schrijvershof, R., Van der Werf, J., Zijl, F., De Looff, H., & De Vries, H. (2022). Modelling of annual sand transports at the Dutch lower shoreface. *Ocean and Coastal Management*, 217. <https://doi.org/10.1016/j.ocecoaman.2021.105984>
- Green, J. A. M. (2010). Ocean tides and resonance. *Ocean Dynamics*, 60, 1243–1253. <https://doi.org/10.1007/s10236-010-0331-1>
- Hentschel, M., Ketter, W., & Collins, J. (2018). Renewable energy cooperatives: Facilitating the energy transition at the Port of Rotterdam. *Energy Policy*, (121), 61–69. <https://doi.org/10.1016/j.enpol.2018.06.014>
- Holthuijsen, L. H. (2017). *Waves in oceanic and coastal waters*. Cambridge University Press.
- Hulsbergen, K., De Boer, D., Steijn, R., & Van Banning, G. (2012). Dynamic Tidal Power for Korea. *Proceedings of the the 1st Asian Wave and Tidal Conference Series*.
- Hulsbergen, K., Steijn, R. C., Hassan, R., Klopman, G., & Hurdle, D. (2005). Dynamic Tidal Power (DTP). *Proceedings of the the 6th European Wave and Tidal Energy Conference*, 215–221.
- Hulsbergen, K., Steijn, R. C., Van Banning, G., Klopman, G., & Fröhlich, A. (2008). Dynamic Tidal Power (DTP) - A new approach to exploit tides. *Proceedings of the 2nd International Conference on Ocean Energy*.
- Jetten, R. A. A. (2022). Beantwoording Kamervragen over uitvoering van de motie van de leden Grinwis en Stoffer over onderzoek naar de opbrengst van Dynamic Tidal Power-energiesdampen in zee. [(In Dutch)].
- Keulegan, G. H., & Carpenter, L. H. (1958). Forces on cylinders and plates in an oscillating fluid. *Journal of Research of the National Bureau of Standards*, 60, 423–440.
- Kew, S. F., Selten, F. M., Lenderink, G., & Hazeleger, W. (2013). The simultaneous occurrence of surge and discharge extremes for the rhine delta. *Natural Hazards and Earth System Sciences*, 13(8), 2017–2029. <https://doi.org/10.5194/nhess-13-2017-2013>
- Khanal, S., Ridder, N., De Vries, H., Terink, W., & Van den Hurk, B. (2019). Storm Surge and Extreme River Discharge: A Compound Event Analysis Using Ensemble Impact Modeling. *Frontiers in Earth Science*, 7, 224. <https://doi.org/https://doi.org/10.3389/feart.2019.00224>
- Kieftenburg, A., & Chbab, H. (2012). *Achtergrondrapportage hydraulische belasting voor het ijsselmeer* (tech. rep. 1204143-003-ZWS-0024) [In Dutch]. Deltares.
- Kleinhans, G. M., & Grasmeijer, B. T. (2006). Bed load transport on the shoreface by currents and waves. *Coastal Engineering*, 53, 983–996. <https://doi.org/10.1016/j.coastaleng.2006.06.009>
- KNMI. (2014). *KNMI'14: Climate Change scenarios for the 21st Century – A Netherlands perspective*. (tech. rep. Scientific Report WR2014-01). KNMI. De Bilt, The Netherlands.
- Kohsiek, L. H. M. (1988). Reworking of former ebb-tidal deltas into large longshore bars following the artificial closure of tidal inlets in the southwest of The Netherlands. *Tide-Influenced Sedimentary Environments and Facies*, 113–122.
- Kopp, R. E., Horton, R. M., Little, C. M., Mitrovica, J. X., Oppenheimer, M., Rasmussen, D. J., Strauss, B. H., & Tebaldi, C. (2014). Probabilistic 21st and 22nd century sea-level projections at a global network of tide-gauge sites. *Earth's Future*, 2, 383–406. <https://doi.org/10.1002/2014EF000239>
- Kroon, A., & Loman, G. (2015). Application of FINEL2D model in hydro-morphological support of design & build of "Maasvlakte 2". *E-proceedings of the 36th IAHR World Congress*, 2205–2216.
- Kustlijnkaarten 2023* (tech. rep.) [In Dutch]. (2022). Rijkswaterstaat.

- Liu, Q., & Zhang, Y. (2014). Hydrodynamic study of phase-shift tidal power system with Y-shaped dams. *Journal of Hydraulic Research*, 52(3), 356–365. <https://doi.org/10.1080/00221686.2013.875071>
- Mei, C. C. (2012). Note on tidal diffraction by a coastal barrier. *Applied Ocean Research*, 36, 22–25. <https://doi.org/10.1016/j.apor.2012.01.005>
- Ministerie van Infrastructuur en Waterstaat. (2022). *Programma Noordzee 2022-2027*. (tech. rep.) [In Dutch].
- Ministerie van Verkeer en Waterstaat. (1990). *Kustverdediging na 1990, beleidskeuze voor de kustlijn-zorg* (tech. rep. Eerste kustnota) [In Dutch].
- Ministerie van Verkeer en Waterstaat. (2007). *Hydraulische Randvoorwaarden primaire waterkeringen* (tech. rep. voor de derde toetsronde 2006-2011 (HR 2006)) [In Dutch].
- Mooyaart, L. F., & Jonkman, S. N. (2017). Overview and design considerations of storm surge barriers. *Journal of Waterway, Port, Coastal, and Ocean Engineering*, 143(4), 06017001. [https://doi.org/10.1061/\(asce\)ww.1943-5460.0000383](https://doi.org/10.1061/(asce)ww.1943-5460.0000383)
- Mulder, J. P. M. (2000). *Zandverliezen in het Nederlandse kuststelsel. Advies voor Dynamische Handhaven in de 21 eeuw*. (tech. rep. Report RIKZ/2000.36) [In Dutch]. Rijkswaterstaat, National Centre for Coastal and Marine Management RIKZ.
- Natura 2000. (n.d.). *Voordelta kaart*. Retrieved July 5, 2023, from <https://geocontent.rvo.nl/Natura2000/Gebiedskaart/index.html?gebiednaam=Voordelta>
- Park, Y. H. (2017). Analysis of characteristics of Dynamic Tidal Power on the west coast of Korea. *Renewable and Sustainable Energy Reviews*, 68(1), 461–474. <https://doi.org/10.1016/j.rser.2016.10.008>
- Park, Y. H., & Youn, D. (2020). The study of a new tidal power for a practical use. *Journal of Coastal Research*, SI(95), 1500–1504. <https://doi.org/10.2112/SI95-289.1>
- Pickering, M. D., Wells, N. C., & Green, J. A. M. (2012). The impact of future sea-level rise on the European Shelf tides. *Continental Shelf Research*, 35, 1–15. <https://doi.org/10.1016/j.csr.2011.11.011>
- Rasquin, C., Seiffert, R., Wachler, B., & Winkel, N. (2020). The significance of coastal bathymetry representation for modelling the tidal response to mean sea level rise in the German Bight. *Ocean Science*, 16, 31–44. <https://doi.org/10.5194/os-16-31-2020>
- Reeze, B., De la Haye, M. A. A., Arts, F., Boudwijn, T. J., Van der Jagt, H. A., Van Kessel, N., Verweij, G. L., & Wegman, C. (2020). *Nulrapportage ecologische toestand Haringvliet en Voordelta 'Lerend implementeren Kierbesluit': 2009-2018* (tech. rep. No. 20-340) [In Dutch]. Bureau Waardenburg, Culemborg, The Netherlands.
- Rijksoverheid. (n.d.). *Windenergie op zee* [In Dutch]. Retrieved December 10, 2022, from <https://www.rijksoverheid.nl/onderwerpen/duurzame-energie/windenergie-op-zee>
- Rijksoverheid. (2019). *Klimaatakkoord*. (tech. rep.) [In Dutch].
- Rijkswaterstaat. (n.d.-a). *Alarmoproepen Oosterscheldekering* [In Dutch]. Retrieved May 16, 2023, from <https://waterberichtgeving.rws.nl/water-en-weer/specifieke-onderwerpen/alarmoproepen-osk>
- Rijkswaterstaat. (n.d.-b). *Oosterscheldekering* [In Dutch]. Retrieved March 31, 2023, from <https://www.rijkswaterstaat.nl/water/waterbeheer/bescherming-tegen-het-water/waterkeringen/deltawerken/oosterscheldekering>
- Rijkswaterstaat. (1986). *Ontwerpnota Stormvloedkering Oosterschelde. Boek 1: Totaalontwerp en ontwerpfilosofie*. (tech. rep.) [In Dutch].
- Rogers, W. E., Babanin, A. V., & Wang, D. W. (2012). Observation-Consistent Input and Whitecapping Dissipation in a Model for Wind-Generated Surface Waves: Description and Simple Calculations. *Journal of Atmospheric and Oceanic Technology*, 29, 1329–1346. <https://doi.org/10.1175/JTECH-D-11-00092.1>
- Roos, P. C., & Velema, J. J. (2011). An idealized model of tidal dynamics in the North Sea: resonance properties and response to large-scale changes. *Ocean Dynamics*, 61, 2019–2035. <https://doi.org/10.1007/s10236-011-0456-x>
- Roscoe, K., Caires, S., Diermanse, F., & Groeneweg, J. (2010). Extreme offshore wave statistics in the north sea. *WIT Transactions on Ecology and the Environment*. <https://doi.org/10.2495/friar100051>
- Ruessink, B. G., & Jeuken, M. C. J. L. (2002). Dunefoot dynamics along the Dutch coast. *Earth Surface Processes and Landforms*, 27, 1043–1056. <https://doi.org/10.1002/esp.391>

- Savenije, H. H. G. (2005). *Salinity and tides in alluvial estuaries*. Elsevier.
- Shao, D., Feng, W., Xi, F., & Xu, Y. (2017). Reinvestigation of the Dynamic Tidal Power Dams and their Influences on Hydrodynamic Environment. *Proceedings of International Conference on Environmental and Energy Engineering, 2017*. <https://doi.org/10.1088/1755-1315/63/1/012048>
- Shao, D., Feng, W., & Xu, Y. (2017). Hydrodynamic Investigation of Combinations of Double and Triple Dynamic Tidal Power Systems. *Proceedings of International Conference on Energy, Power and Environmental Engineering, 2017*, 149–154.
- Slootjes, N., & Van der Most, H. (2016). *Achtergronden bij de normering van de primaire waterkeringen in nederland* (tech. rep. Hoofdrapport) [In Dutch]. Ministerie van Infrastructuur en Milieu.
- Sterl, A., van den Brink, H., de Vries, H., Haarsma, R., & van Meijgaard, E. (2009). An ensemble study of extreme storm surge related water levels in the North Sea in a changing climate. *Ocean Science, 5*(3), 369–378. <https://doi.org/10.5194/os-5-369-2009>
- Svašek Hydraulics. (2020). *Dynamic Tidal Power (DTP): A review of a promising technique for harvesting sustainable energy at sea*. (tech. rep. Svašek Hydraulics Memo 2037/U20232/A/HTAL).
- Terra, G. M. (2005). *Nonlinear Tidal Resonance* (Doctoral dissertation). Universiteit van Amsterdam.
- The SWAN team. (2023). *Swan user manual*. Delft University of Technology.
- Thiébot, J., Guillou, S., & Droniou, E. (2020). Influence of the 18.6-year lunar nodal cycle on the tidal resource of the Alderney Race, France. *Applied Ocean Research, 97*(102107). <https://doi.org/10.1016/j.apor.2020.102107>
- TNO. (2021). *Stroom uit water. Onderzoek potentieel elektriciteitsopwekking uit water ten behoeve van de Verkenning Elektriciteit uit Water*. (tech. rep. TNO- rapport TNO 2020 P11977) [In Dutch]. TNO.
- Van de Kreeke, J., & Haring, J. (1979). Equilibrium flow areas in the Rhine-Meuse Delta. *Coastal Engineering, 3*, 97–111. [https://doi.org/10.1016/0378-3839\(79\)90012-7](https://doi.org/10.1016/0378-3839(79)90012-7)
- Van de Kreeke, J., & Robaczewska, K. (1993). Tide-induced residual transport of coarse sediment; application to the ems estuary. *Netherlands Journal of Sea Research, 31*, 209–220. [https://doi.org/10.1016/0077-7579\(93\)90022-K](https://doi.org/10.1016/0077-7579(93)90022-K)
- Van der Spek, A., Van der Werf, J., Oost, A., Vermaas, T., Grasmeyer, B., & Schrijvershof, R. (2022). The lower shoreface of the Dutch coast - An overview. *Ocean and Coastal management, 230*. <https://doi.org/10.1016/j.ocecoaman.2022.106367>
- Van der Werf, J., Grasmeyer, B., Hendriks, K., Van der Spek, A., & Vermaas, T. (2017). *Literature study Dutch lower shoreface* (tech. rep. 1220339-004-ZKS-0001). Deltares.
- Van der Werf, J. J., Schrijvershof, R. A., Brakenhoff, L. B., & Grasmeyer, B. T. (2022). Observations of near-bed orbital velocities and small-scale bedforms on the Dutch lower shoreface. *Ocean and Coastal Management, 218*, 106012. <https://doi.org/10.1016/j.ocecoaman.2021.106012>
- Van Koningsveld, M., & Mulder, J. P. M. (2004). Sustainable Coastal Policy Developments in The Netherlands. A Systematic Approach Revealed. *Journal of Coastal Research, 20*(2), 375–385.
- Van Krefeld, A., van Winden, A., Jacobs, P., Souwerbren, A., Gilber, A., te Linde, A., & Zwolsman, G. (2009). *Het benedenrivierengebied in tijden van klimaatverandering* (tech. rep. Klimaat voor Ruimte Rapport KvR 014/2009) [In Dutch].
- Van Rijn, L. C. (1997). Sediment transport and budget of the central coastal zone of Holland. *Coastal Engineering, 32*, 61–90. [https://doi.org/10.1016/S0378-3839\(97\)00021-5](https://doi.org/10.1016/S0378-3839(97)00021-5)
- Van Rijn, L. C. (2007a). Unified View of Sediment Transport by Currents and Waves. I: Initiation of Motion, Bed Roughness, and Bed-Load Transport. *Journal of Hydraulic Engineering, 133*, 649–667. [https://doi.org/10.1061/\(ASCE\)0733-9429\(2007\)133:6\(649\)](https://doi.org/10.1061/(ASCE)0733-9429(2007)133:6(649))
- Van Rijn, L. C. (2007b). Unified View of Sediment Transport by Currents and Waves. II: Suspended Transport. *Journal of Hydraulic Engineering, 133*, 668–689. [https://doi.org/10.1061/\(ASCE\)0733-9429\(2007\)133:6\(668\)](https://doi.org/10.1061/(ASCE)0733-9429(2007)133:6(668))
- Van Rijn, L. C. (2007c). Unified View of Sediment Transport by Currents and Waves. III: Graded Beds. *Journal of Hydraulic Engineering, 133*, 761–775. [https://doi.org/10.1061/\(ASCE\)0733-9429\(2007\)133:7\(761\)](https://doi.org/10.1061/(ASCE)0733-9429(2007)133:7(761))
- Van Rijn, L. C. (2009). Prediction of dune erosion due to storms. *Coastal Engineering, 56*(4), 441–457. <https://doi.org/10.1016/j.coastaleng.2008.10.006>
- Verbeek, M. C. (2023). *Optimizing the configuration of tidal turbines in storm surge barriers* (Doctoral dissertation). Delft University of Technology. <https://doi.org/10.4233/uuid:a370be10-b49d-4f4d-a074-39f464c3d8f9>

- Vermaas, T., Elias, E., & Van der Spek, A. J. F. (2015). Relocating Krabbengat channel; a tale of two developments. *Proceedings of the Coastal Sediments 2015*, 13–26. https://doi.org/10.1142/9789814689977_0242
- Webb, D. J. (1974). A model of continental-shelf resonances. *Deep-Sea Research*, 23, 1–15.
- Witteveen+Bos and CE Delft. (2019). *Perspectieven elektriciteit uit water: Nationaal potentieel voor 2030 en 2050*. (tech. rep.) [In Dutch]. Deventer, The Netherlands.
- Zhou, J., Falconer, R. A., & Lin, B. (2014). Refinements to the EFDC model for predicting the hydro-environmental impacts of a barrage across the Severn estuary. *Renewable Energy*, 62, 490–505. <https://doi.org/10.1016/j.renene.2013.08.012>



North Sea Program 2022 - 2027

On the next page the complete 'Structuurvisiekaart 2022-2027' is shown, from Ministerie van Infrastructuur en Waterstaat (2022). On this page a cut out of this map is shown, showing only the Voordelta area.

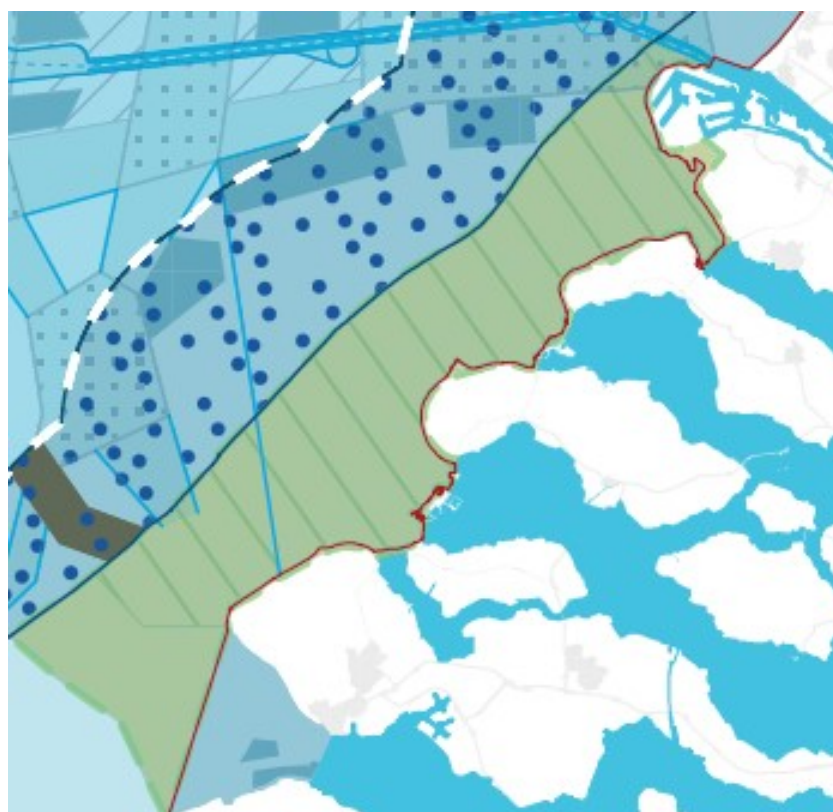


Figure A.1: Structuurvisiekaart Noordzee 2022-2027, zoomed in on the Voordelta. From Ministerie van Infrastructuur en Waterstaat (2022).

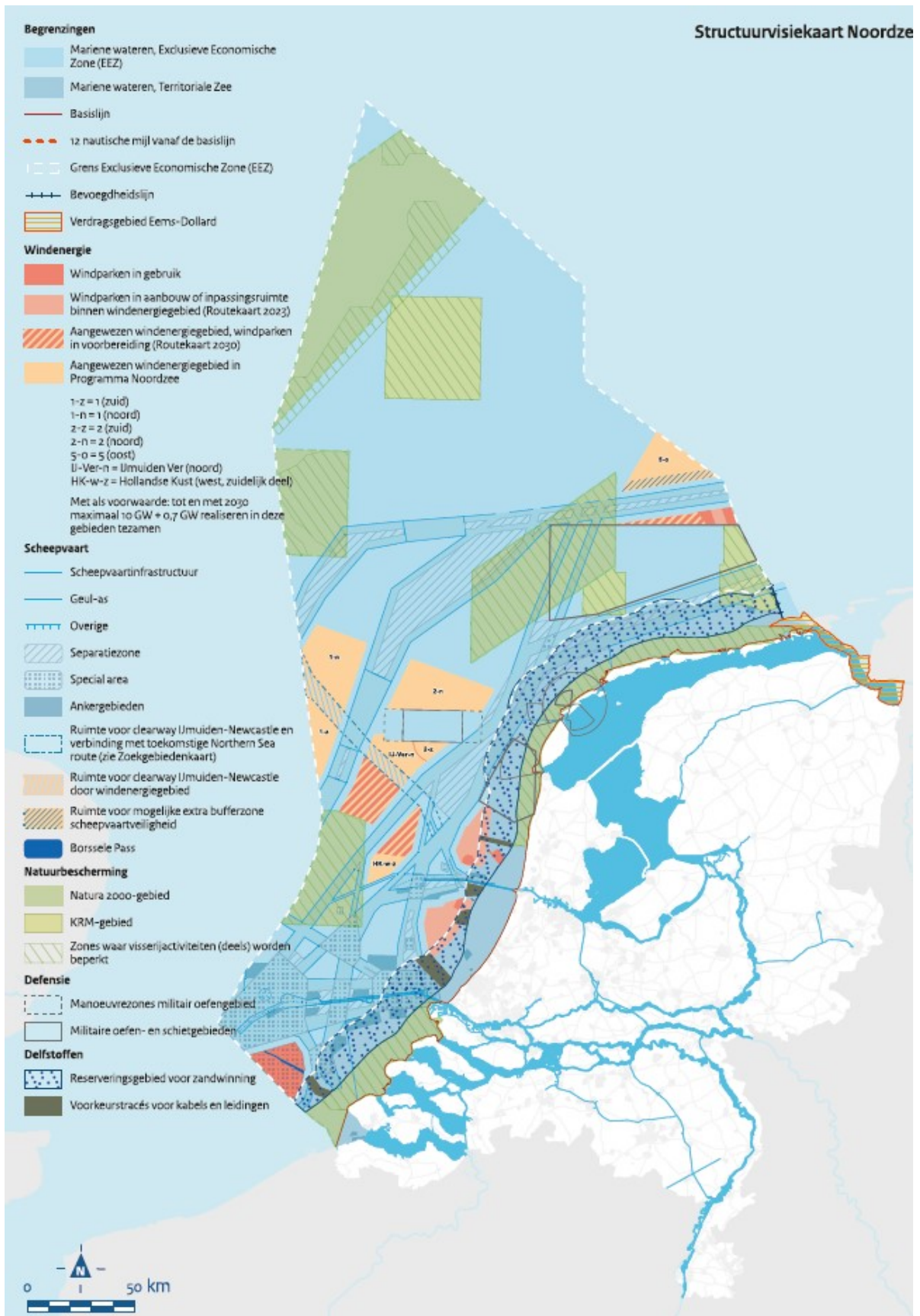


Figure A.2: Structuurvisiekaart Noordzee 2022-2027. From Ministerie van Infrastructuur en Waterstaat (2022).

B

Calculation reflection standing wave

In this appendix, a short overview is given of the formulas and channel characteristics used to make a first calculation of the response factor of the tidal wave within the estuary created by the construction of the DTP dam following the reference layout created in Chapter 4.

This appendix only gives the formulas used for the calculation. For a derivation and an explanation of the method is referred to Battjes and Labeur (2017).

The response factor of the channel is calculated with the following equation:

$$r = \frac{\hat{\zeta}(l)}{\hat{\zeta}(0)} = \frac{1}{\sqrt{\sinh^2(\mu l) + \cos^2(kl)}} \quad (\text{B.1})$$

The equations used for calculating the different variables in the equation are shown below.

$$\mu = k \tan(\delta) \quad (\text{B.2}) \quad k = \frac{k_0}{\sqrt{1 - \tan^2(\delta)}} \quad (\text{B.3})$$

$$k_0 = \frac{\omega}{c_0} \quad (\text{B.4}) \quad \delta = \frac{1}{2} \arctan(\sigma) \quad (\text{B.5})$$

$$\omega = \frac{2\pi}{T} \quad (\text{B.6}) \quad c_0 = \sqrt{gd} \quad (\text{B.7})$$

$$\sigma = \frac{8}{3\pi} c_f \frac{\hat{U}}{\omega R} \quad (\text{B.8}) \quad A_c = B_c * d \quad (\text{B.9})$$

For this calculation the input parameters are defined as:

- T has been defined as the wave period of the M_2 component of the tide, which is 12.42 hours.
- U is the peak tidal velocity, which is 1.25 m s^{-1}
- R is the hydraulic radius, which for shallow, wide cross sections is approximately equal to the averaged depth of the channel, d, which is 13 meters.
- C_f is the resistance factor of the channel. As this can not be calculated it is assumed to be 0.004, which Battjes and Labeur, 2017 state is a realistic value for the factor.
- Finally, l, the length of the channel is 57.5 km.

This results in a response factor $r = \frac{\hat{\zeta}(l)}{\hat{\zeta}(0)} = 1.13$, meaning that an amplification of the tidal wave is expected to occur in the estuary. As this calculation is based on a large number of assumptions and simplifications, this exact number does not have much value. However, based on this calculation the conclusion can be drawn that amplification of the tidal wave within the estuary is likely.



Model calibration and validation

In this appendix all results of the model validations are shown, the results of which have been summarised in sections 5.2.3 and 6.2.2.

C.1. Calibration of the coastal safety model

The coastal safety model has been calibrated for three different characteristics: the water level, the significant wave height and the peak period. The calibration of the water level has been performed for the same locations as in the model used for the energy output, shown in C.1. Measurement data for the significant wave height and the peak period is available for different locations. The locations at which the model has been calibrated for these characteristics are shown in Figure C.2. The graphs show results for four different models, as well as the measured data. The four models considered and their defining characteristics are summarised below.

- Model 1, with SWAN input GEN 3 ST6, based on Rogers et al. (2012) and with ERA5 wind input
- Model 2, with SWAN input GEN 3 ST6 and with CFSR wind input
- Model 3, with SWAN input GEN 3 Komen, with CFSR wind input
- Model 4, with SWAN input GEN 3 ST6, with CFSR wind input and with the breaking coefficient γ adjusted to 0.60.

The part of the SWAN input file that defines the physics of the model for the final three models is shown below. The SWAN input of Model 1 is identical to that of Model 2.

```
1 Model 2
2 GEN3 ST6 4.7E-7 6.6E-6 4.0 4.0 UP HWANG VECTAU U10PROXY 28.0 AGROW
3 FRIC JONSWAP 0.038
```

```
1 Model 3
2 GEN3          KOMEN
3 BREAK        CON      1.00      0.73
4 FRIC JON     0.038
5 LIM          10 1
```

```
1 Model 4
2 GEN3 ST6 4.7E-7 6.6E-6 4.0 4.0 UP HWANG VECTAU U10PROXY 28.0 AGROW
3 FRIC JONSWAP 0.038
4 BREAKING 1.0 0.60
```

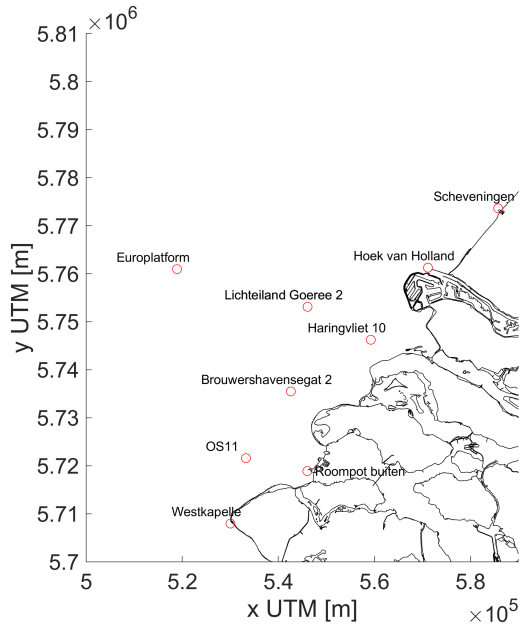


Figure C.1: Overview of locations at which the water level has been validated.

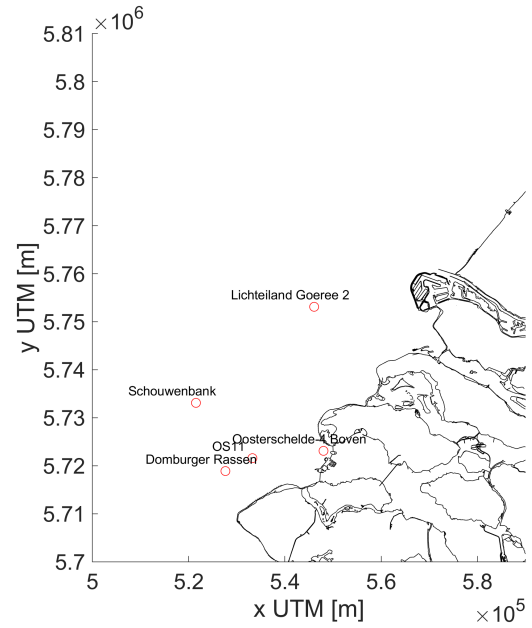


Figure C.2: Overview of the locations at which the SWAN model has been calibrated and validated.

C.1.1. Calibration Results Water Level

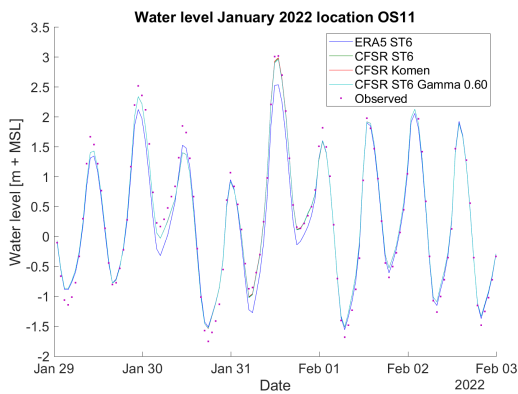


Figure C.3: Calibration of water level at location Europlatform

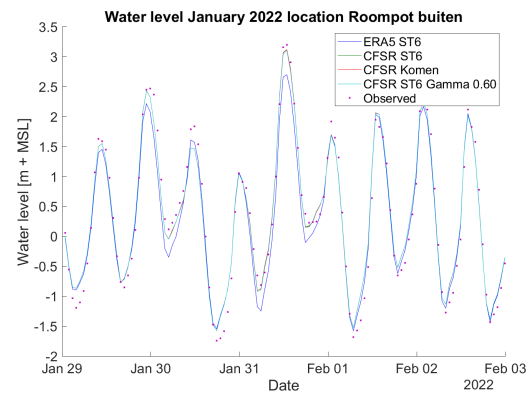


Figure C.4: Calibration of water level at location Roompot Buiten

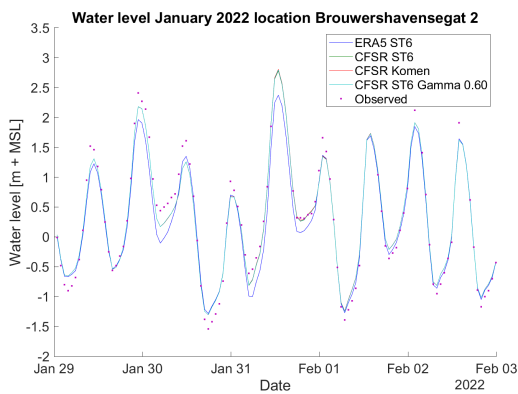


Figure C.5: Calibration of water level at location Brouwershavensegat 2

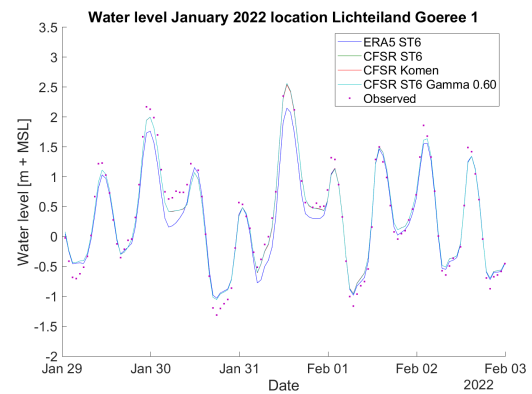


Figure C.6: Calibration of water level at location Lichteiland Goeree 1

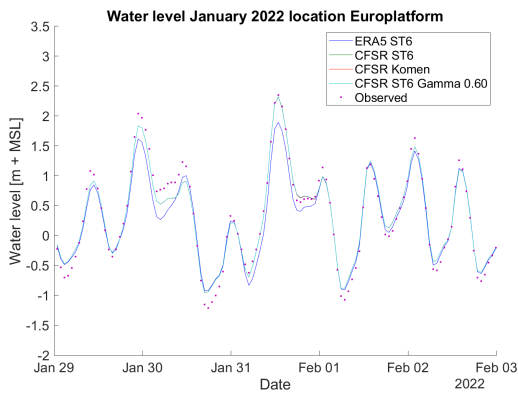


Figure C.7: Calibration of water level at location Europlatform

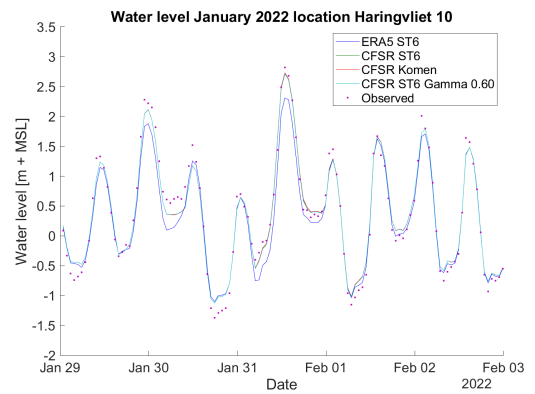


Figure C.8: Calibration of water level at location Haringvliet 10

C.1.2. Calibration Results Significant Wave Height

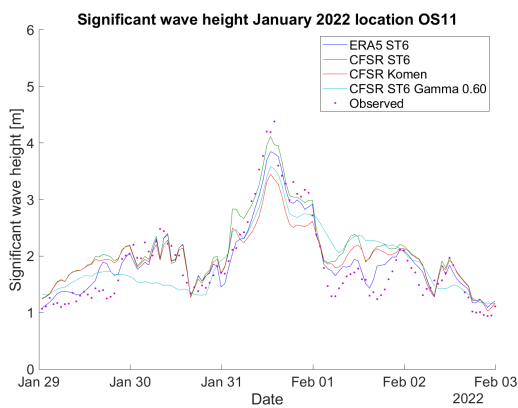


Figure C.9: Calibration of significant wave height at location OS11

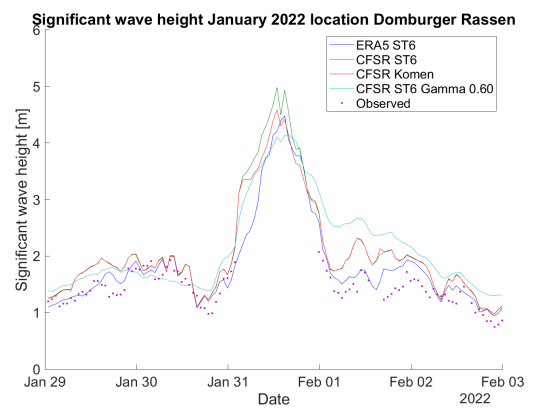


Figure C.10: Calibration of significant wave height at location Domburger Rassen.

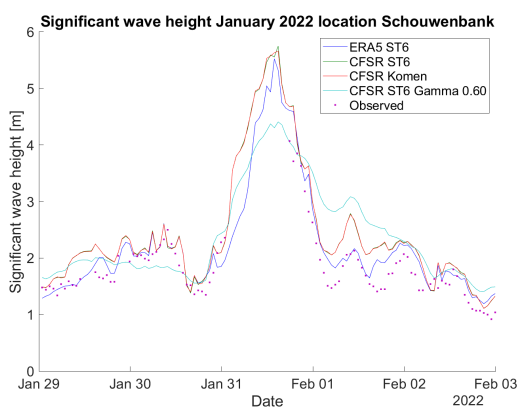


Figure C.11: Calibration of significant wave height at location Schouwenbank

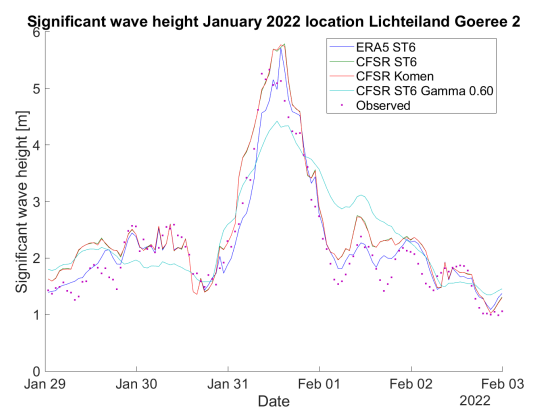


Figure C.12: Calibration of significant wave height at location Lichteiland Goeree 2.

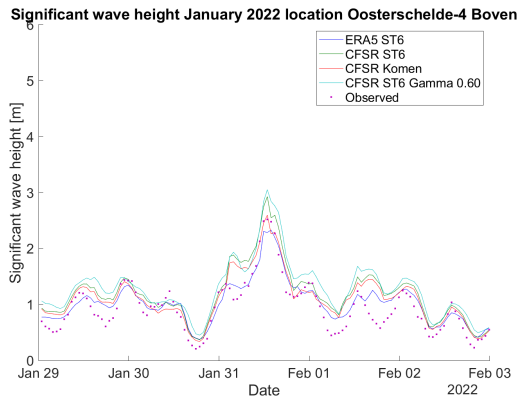


Figure C.13: Calibration of significant wave height at location Oosterschelde-4 boven

C.1.3. Calibration Results Peak Period

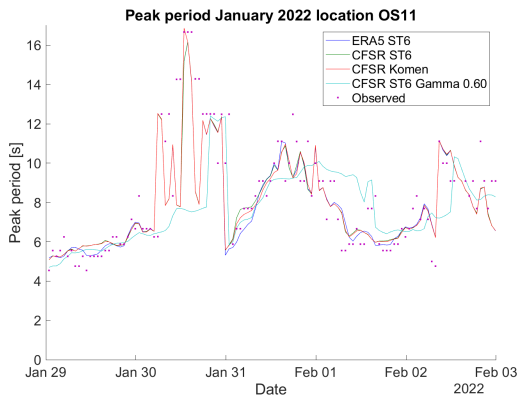


Figure C.14: Calibration of peak wave period at location OS11

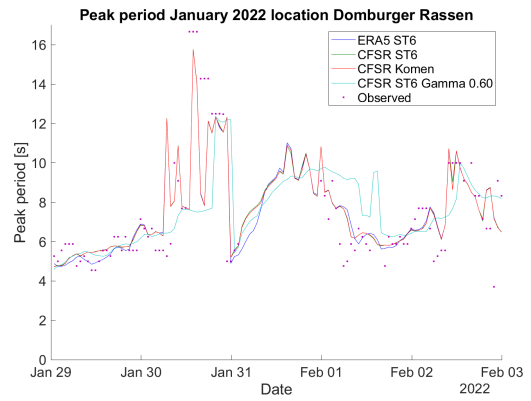


Figure C.15: Calibration of peak wave period at location Domburger Rassen.

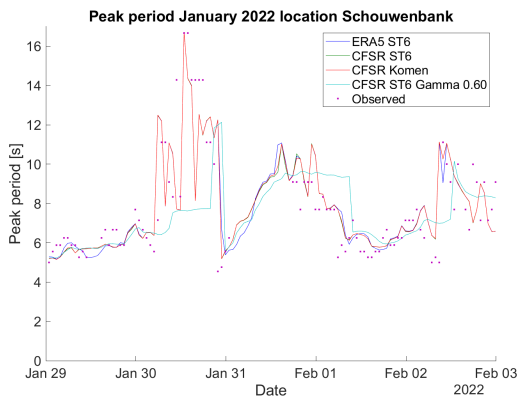


Figure C.16: Calibration of peak wave period at location Schouwenbank

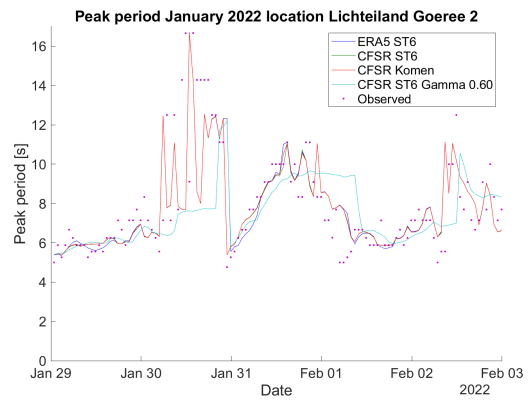


Figure C.17: Calibration of peak wave period at location Lichteiland Goeree 2.

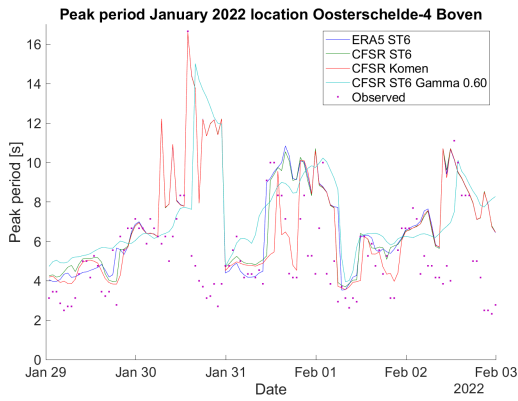


Figure C.18: Calibration of peak wave period at location Oosterschelde-4 boven

C.2. Validation of the combined FINEL-SWAN model

C.2.1. Validation Results Water Level

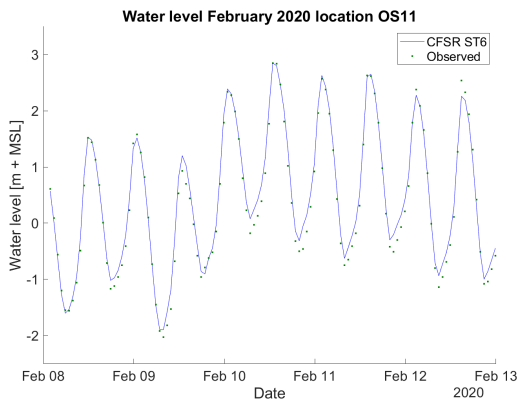


Figure C.19: Validation of water level at location OS11

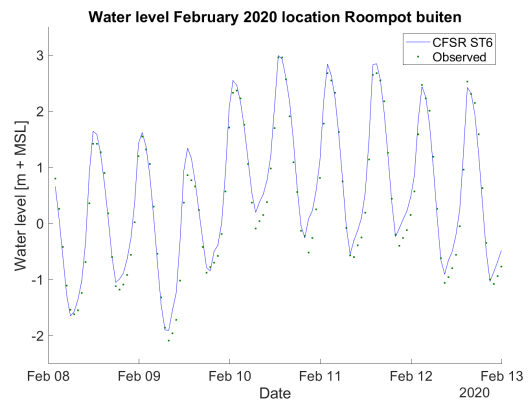


Figure C.20: Validation of water level at location Roompot Buiten

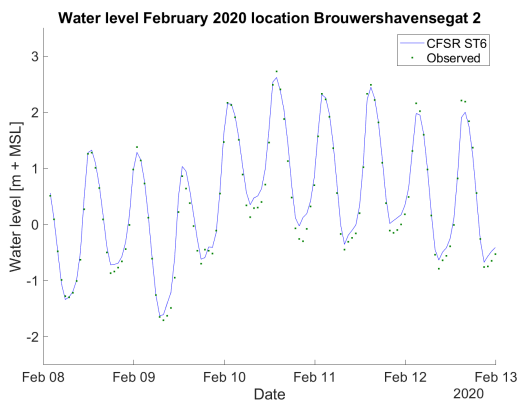


Figure C.21: Validation of water level at location Brouwershavensegat 2

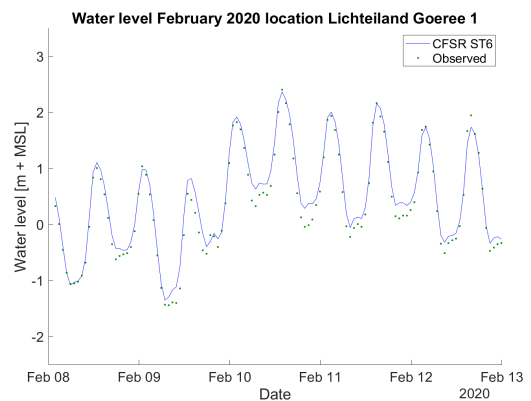


Figure C.22: Validation of water level at location Lichteiland Goeree 1

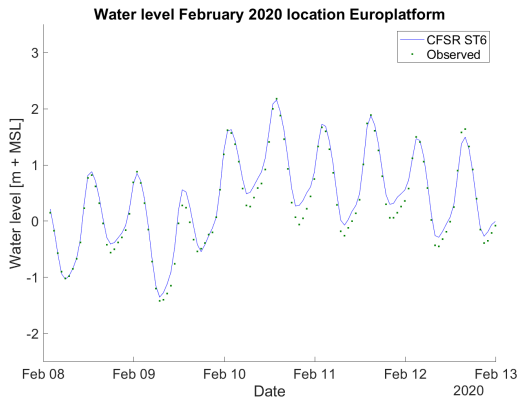


Figure C.23: Validation of water level at location Europlatform

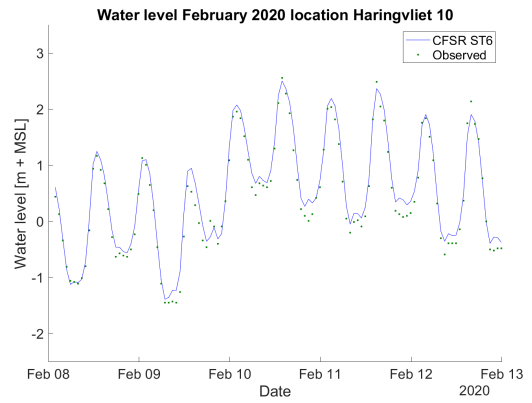


Figure C.24: Validation of water level at location Haringvliet 10

C.2.2. Validation Results Significant Wave Height

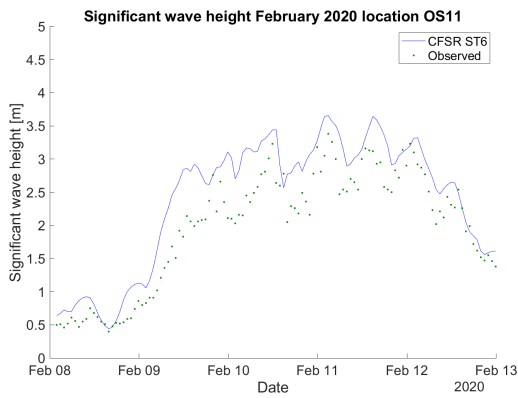


Figure C.25: Validation of significant wave height at location OS11

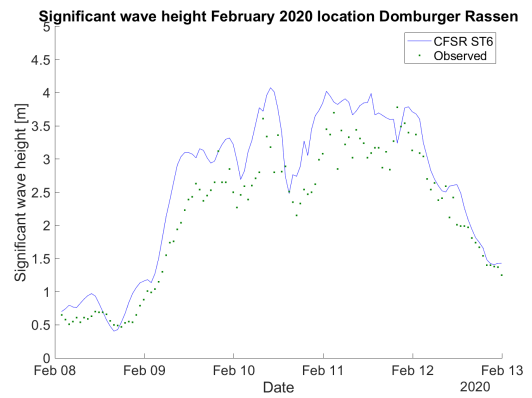


Figure C.26: Validation of significant wave height at location Domburger Rassen.

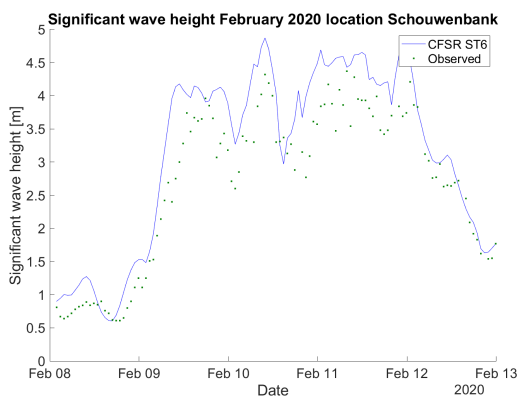


Figure C.27: Validation of significant wave height at location Schouwenbank

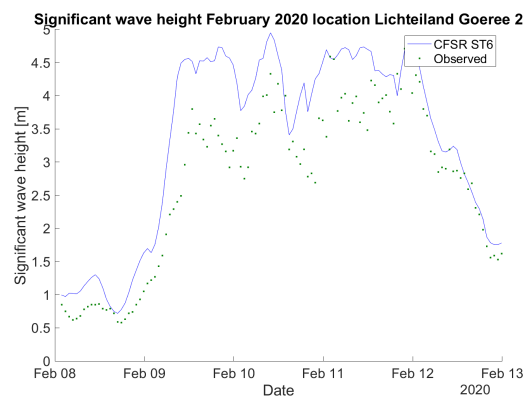


Figure C.28: Validation of significant wave height at location Lichteiland Goeree 2.

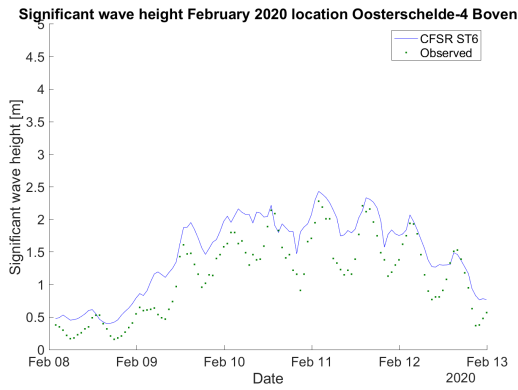


Figure C.29: Validation of significant wave height at location Oosterschelde-4 boven

C.2.3. Validation Results Peak Period

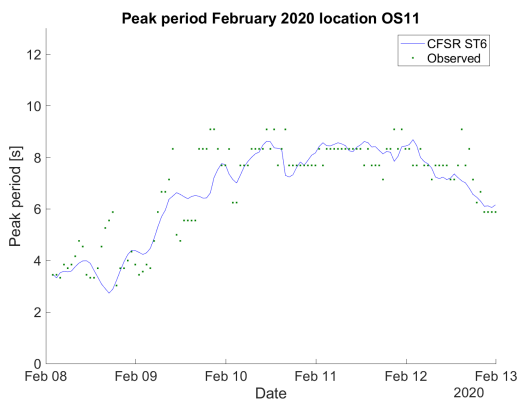


Figure C.30: Validation of peak wave period at location OS11

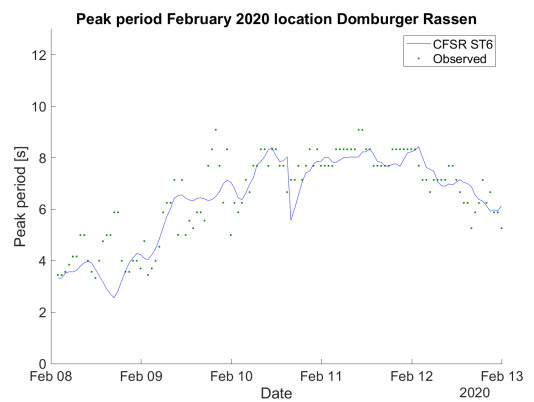


Figure C.31: Validation of peak wave period at location Domburger Rassen.

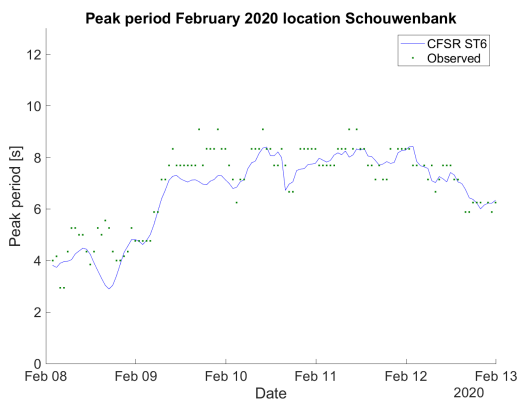


Figure C.32: Validation of peak wave period at location Schouwenbank

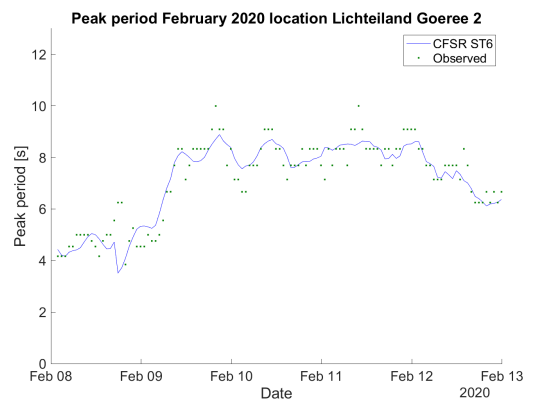


Figure C.33: Validation of peak wave period at location Lichteiland Goeree 2.

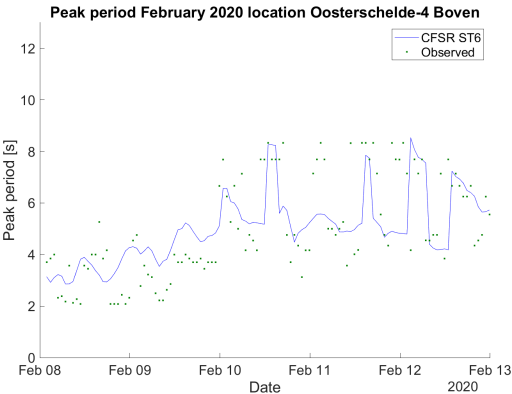


Figure C.34: Validation of peak wave period at location Oosterschelde-4 boven

C.3. Validation FINEL flow model

The locations can be seen in figure C.1. The figures show the water level measurements as well as the water level as has been modelled at the different locations for the entire period of December 2017 to January 2018. Next to that, a scatter plot comparing the results at every timestep is shown. The first section compares the measured data to the FINEL flow model results with ERA5 meteorological input applied, the second section shows the results of the FINEL flow model with CFSR meteorological input applied.

C.3.1. Validation FINEL model with ERA5 input

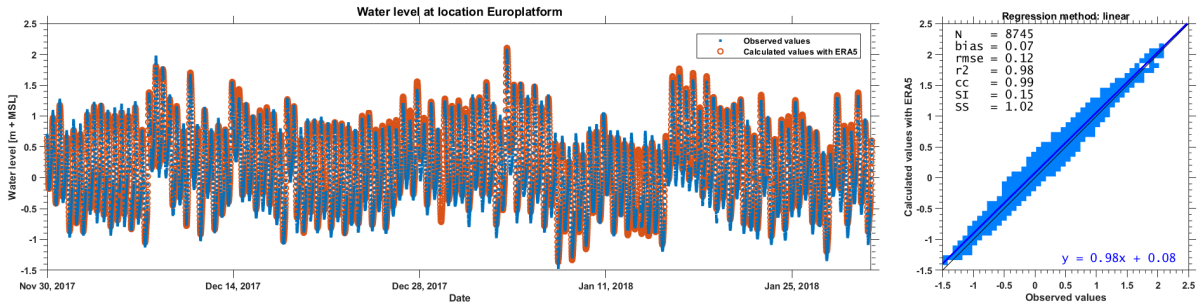


Figure C.35: Water level in the FINEL flow model with ERA5 data applied compared to measured data at location Europlatform.

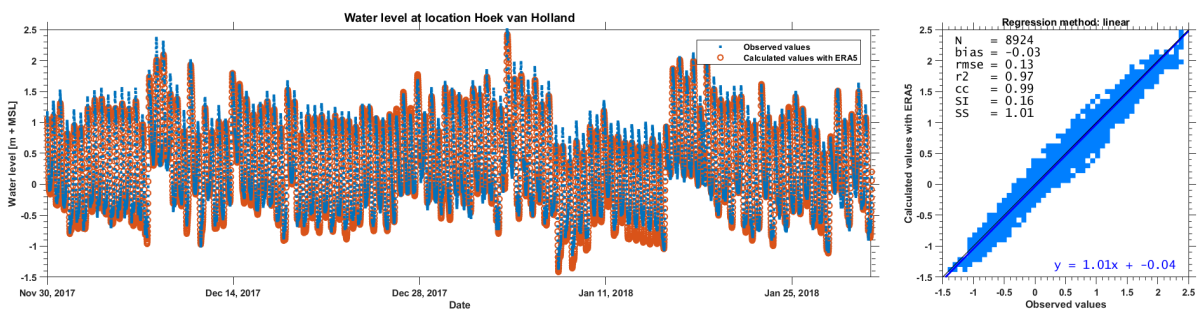


Figure C.36: Water level in the FINEL flow model with ERA5 data applied compared to measured data at location Hoek van Holland.

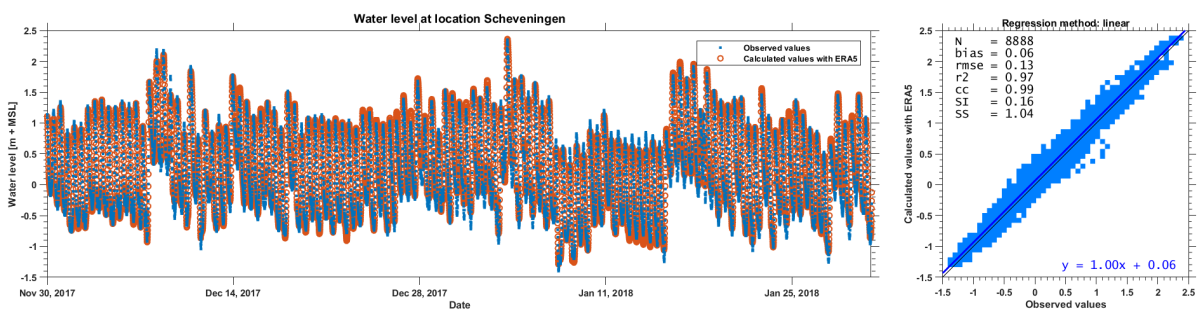


Figure C.37: Water level in the FINEL flow model with ERA5 data applied compared to measured data at location Scheveningen.

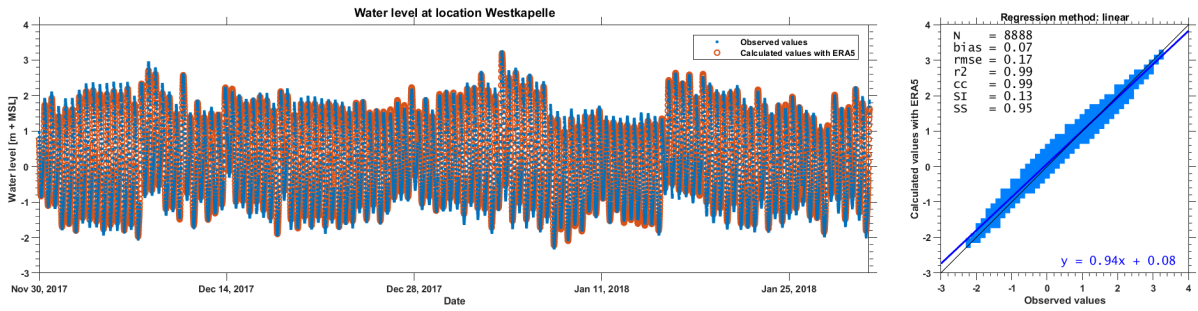


Figure C.38: Water level in the FINEL flow model with ERA5 data applied compared to measured data at location Westkapelle.

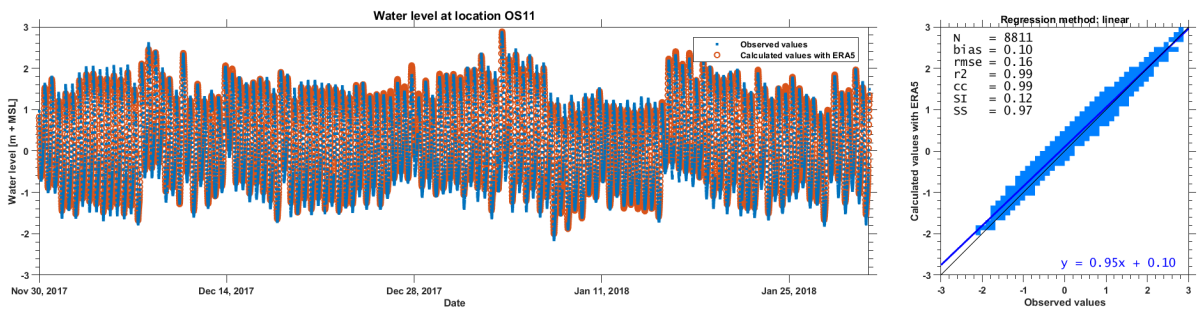


Figure C.39: Water level in the FINEL flow model with ERA5 data applied compared to measured data at location OS11.

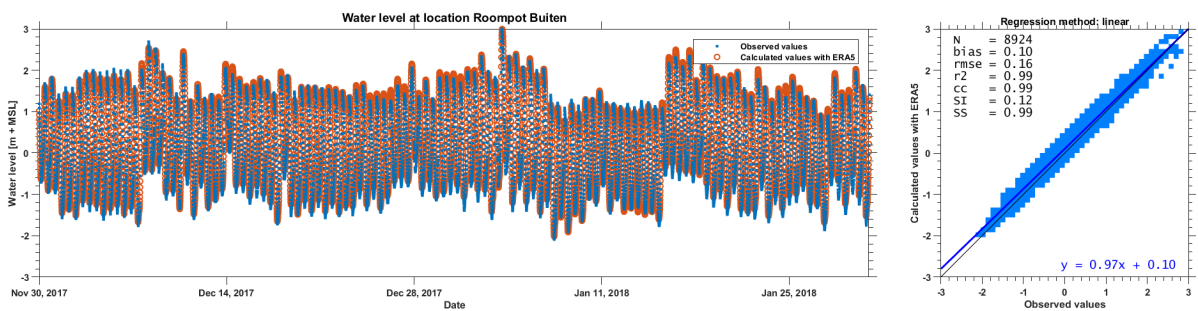


Figure C.40: Water level in the FINEL flow model with ERA5 data applied compared to measured data at location Roompot buiten.

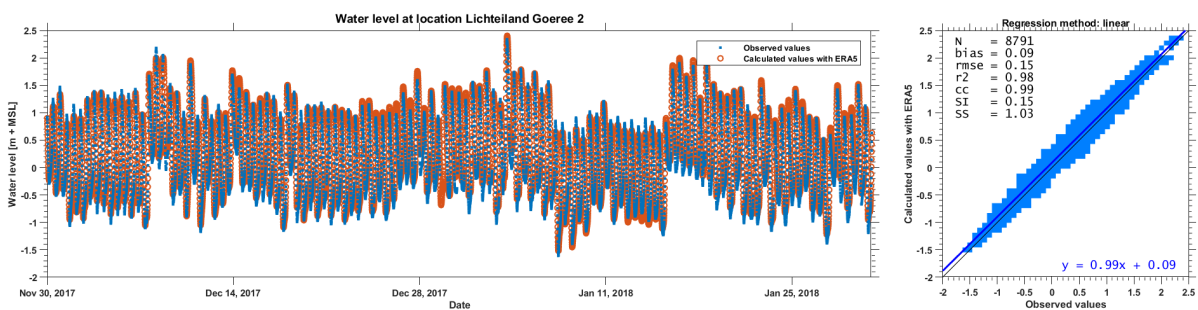


Figure C.41: Water level in the FINEL flow model with ERA5 data applied compared to measured data at location Lichteiland Goeree 2.

C.3.2. Validation FINEL model with CFSR input

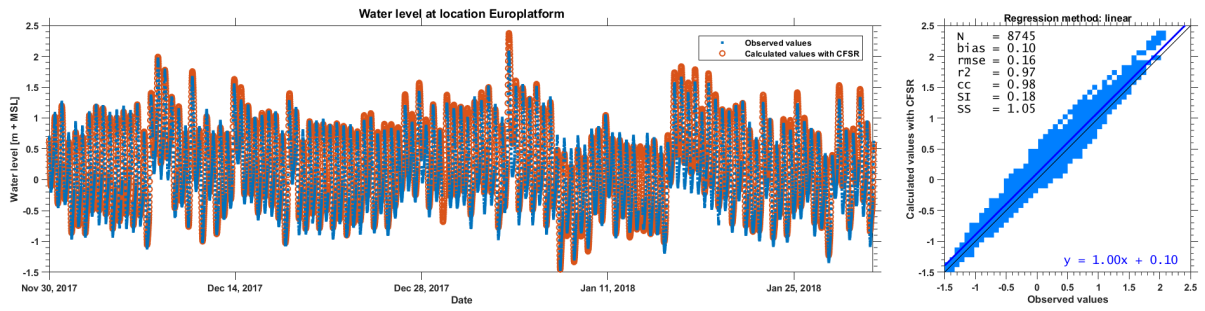


Figure C.42: Water level in the FINEL flow model with CFSR data applied compared to measured data at location Europlatform.

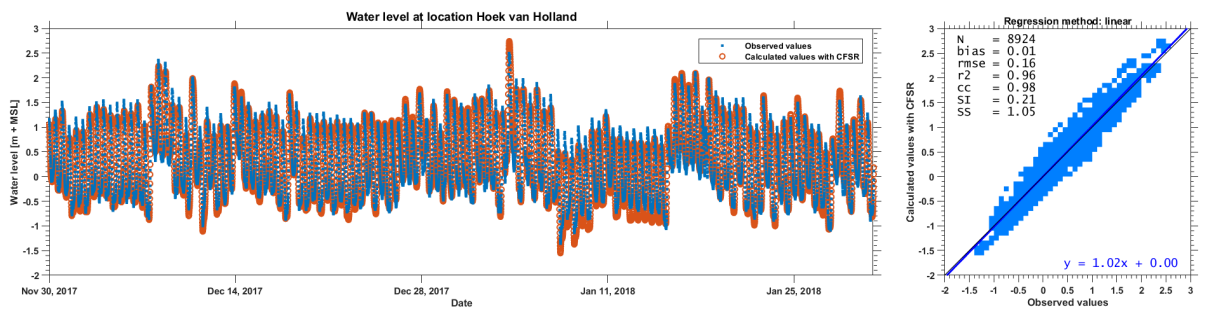


Figure C.43: Water level in the FINEL flow model with CFSR data applied compared to measured data at location Hoek van Holland.

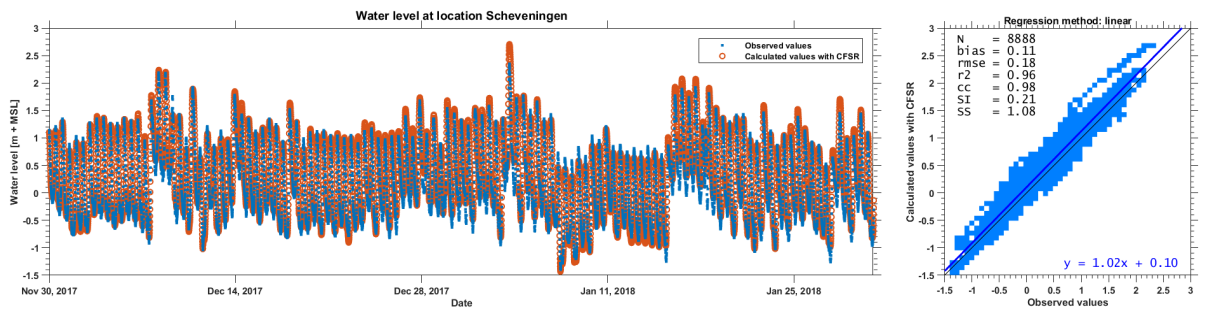


Figure C.44: Water level in the FINEL flow model with CFSR data applied compared to measured data at location Scheveningen.

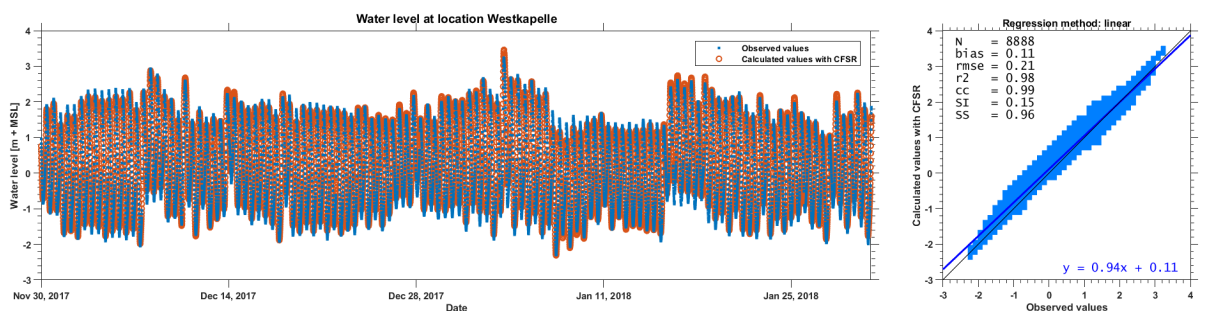


Figure C.45: Water level in the FINEL flow model with CFSR data applied compared to measured data at location Westkapelle.

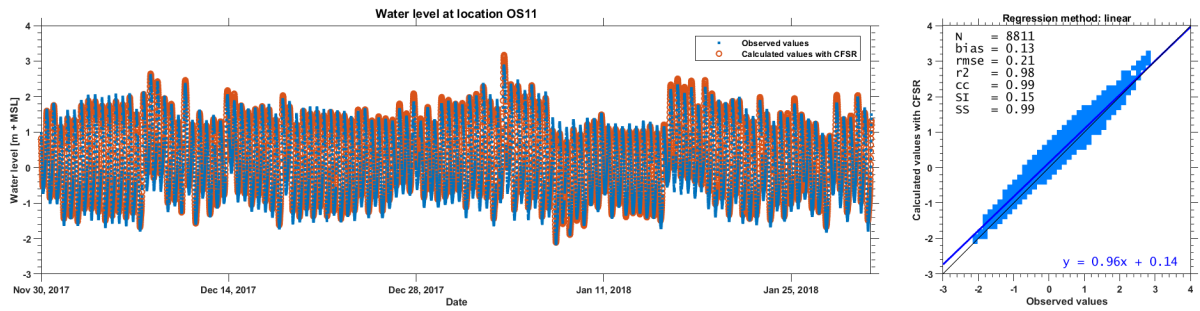


Figure C.46: Water level in the FINEL flow model with CFSR data applied compared to measured data at location OS11.

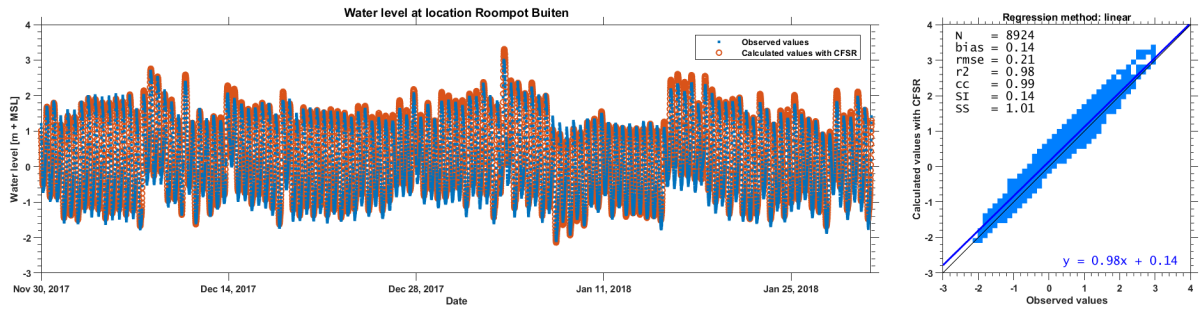


Figure C.47: Water level in the FINEL flow model with CFSR data applied compared to measured data at location Roompot buiten.

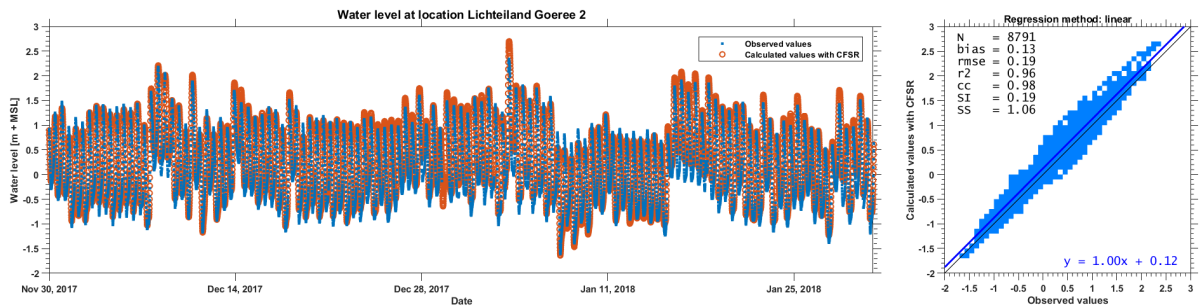


Figure C.48: Water level in the FINEL flow model with CFSR data applied compared to measured data at location Lichteiland Goeree 2.

D

SWAN input file

Given below is the SWAN input file which was used for every timestep. 'swan.bot', 'swan.lev', 'swan.cur' and 'swan.wnd' are output files made by FINEL for every timestep, representing the bathymetry, water level, currents and wind parameters respectively.

```
1 SET level=0 depmin = 0.05 maxerr=3 rho = 1020.00 NAUT
2 $
3 MODE NONSTAT
4 COORDINATES CARTesian
5 $
6 CGRID UNSTRUC CIRCLE 45 0.03 0.60
7 READGRID UNSTRUC TRIA 'DIRECTORY'
8
9 INPGRID BOTTOM UNSTRUC
10 READINP BOTTOM 1. 'swan.bot'
11
12 INPGRID WLEVEL UNSTRUC
13 READINP WLEVEL 1. 'swan.lev'
14
15 INPgrid CUR UNSTRUC
16 READinp CUR 1. 'swan.cur'
17
18 INPGRID WIND UNSTRUC NONSTAT %%VARINPUT1%% 60.0 MIN %%VARINPUT2%%
19 READINP WIND 1. 'swan.wnd'
20
21 BOUND SHAPE PEAK DSPR DEGREE
22 BOUNDspec SIDE 1 CON PAR %%VARINPUT5%% %%VARINPUT6%% %%VARINPUT7%% %%VARINPUT8%%
23
24 $ Physics
25 GEN3 ST6 4.7E-7 6.6E-6 4.0 4.0 UP HWANG VECTAU U10PROXY 28.0 AGROW
26 FRIC JONSWAP 0.038
27
28 $
29 %%VARINPUT4%% INIT HOTS MULTIPLE '../HOT/HOTFILE' UNFORMATTED
30 $
31 NUM STOPC 0.02 0.02 0.02 99 NONSTAT mxitns=20
32 $
33 $***** OUTPUT REQUEST *****
34 $
35 OUTPUT OPTIONS '%' TABLE 16 BLOCK 9 1000 SPEC 8
36
37 BLOCK 'COMPGRID' NOHEAD 'XP.mat' LAY-OUT 3 XP
38 BLOCK 'COMPGRID' NOHEAD 'YP.mat' LAY-OUT 3 YP
39 BLOCK 'COMPGRID' NOHEAD 'HS.mat' LAY-OUT 3 HSIGN
40 BLOCK 'COMPGRID' NOHEAD 'DIR.mat' LAY-OUT 3 DIR
41 BLOCK 'COMPGRID' NOHEAD 'UBOT.mat' LAY-OUT 3 UBOT
42 BLOCK 'COMPGRID' NOHEAD 'TPS.mat' LAY-OUT 3 TPS
43 BLOCK 'COMPGRID' NOHEAD 'FO.mat' LAY-OUT 3 FORCE
44
```

```
45 COMPUTE NONSTAT %%VARINPUT1%% 10.0 MIN %%VARINPUT2%%
46 HOTFile './HOT/HOTFILE' UNFORMATTED
47
48 STOP
```

The input parameters VARINPUT1 to VARINPUT 8 are boundary conditions of the SWAN model, which have been described in the FINEL input file. For every timestep of 10 minutes, the wave conditions at the boundary have been defined beforehand based on the measured wave conditions at Europlatform. An example of these boundary conditions is shown below.

```
1 wavecondition(1).varinput1 = 20200206.0000
2 wavecondition(1).varinput2 = 20200206.0100
3 wavecondition(1).varinput3 = 2020
4 wavecondition(1).varinput4 = '$'
5 wavecondition(1).varinput5 = 0.93
6 wavecondition(1).varinput6 = 7.69
7 wavecondition(1).varinput7 = 333.00
8 wavecondition(1).varinput8 = 48.00
9 wavecondition(1).tbeg = 0
10 wavecondition(1).tend = 3600
```

Varinputs one to three define the date and year for which the boundary conditions are representative. Varinput 4 is used to exempt the first timestep from loading a Hotfile. Varinputs 5 to 8 define the significant waveheight in metres, peak wave period in seconds, wave direction in degrees from North and wave spread in degrees respectively.

E

Results Coastal Safety

In this Appendix, all results of the combined SWAN and FINEL model used to generate the results as presented in Chapter 6 are shown. The results show the change in maximum modelled values after construction of the DTP dam for peak wave period, significant wave height and water level both in absolute values and in percentages of the original modelled maximum value. The figures shown in Chapter 6 are not repeated here.

Then, for several measurement locations the time series of the significant wave height, peak wave period and water level are shown for all eight models that have been run.

E.1. Change in Maximum Values

For all three scenarios of mean sea level rise, the change in the maximum value modelled is shown for the case with a northwestern storm, both the absolute values and as a percentage of the maximum value modelled at that location in the respective original model, without dam. The percentile changes of the scenario without MSLR are not shown, as these have been presented in Chapter 6. All graphs show results of the model described in Section 6.3.1, so all graphs show the results for a model with as input a design storm with a return period of 10000 years. For all graphs applies that red areas show an increase in the modelled value after construction of the dam compared to the situation without dam, while blue areas indicate a decrease. The same graphs are shown for the scenario with a southwestern storm, with no MSLR applied.

E.1.1. Scenario No MSLR

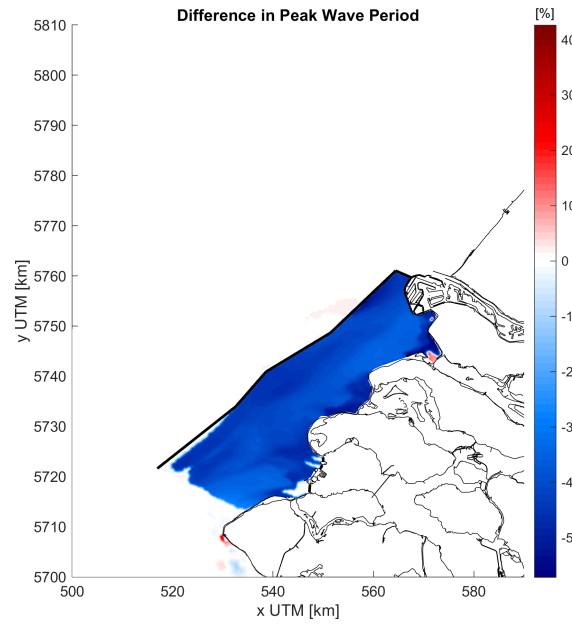
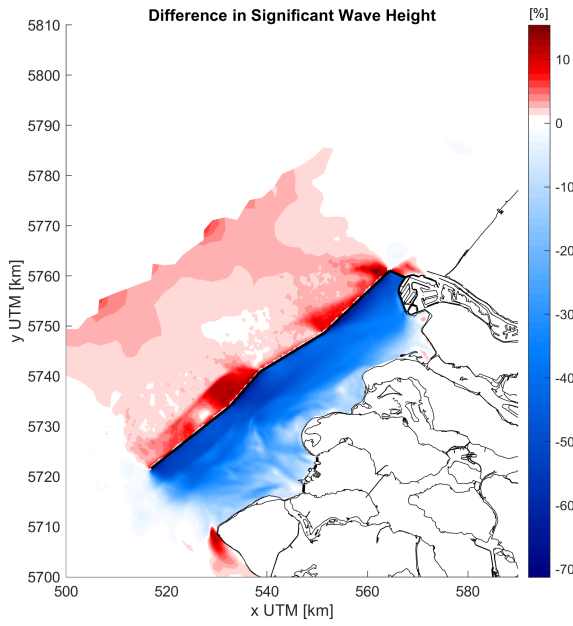


Figure E.1: Difference in maximum significant wave height as a percentage of the maximum value without dam, scenario without MSLR. **Figure E.2:** Absolute difference in maximum peak wave period modelled as a percentage of the maximum value without dam, scenario without MSLR.

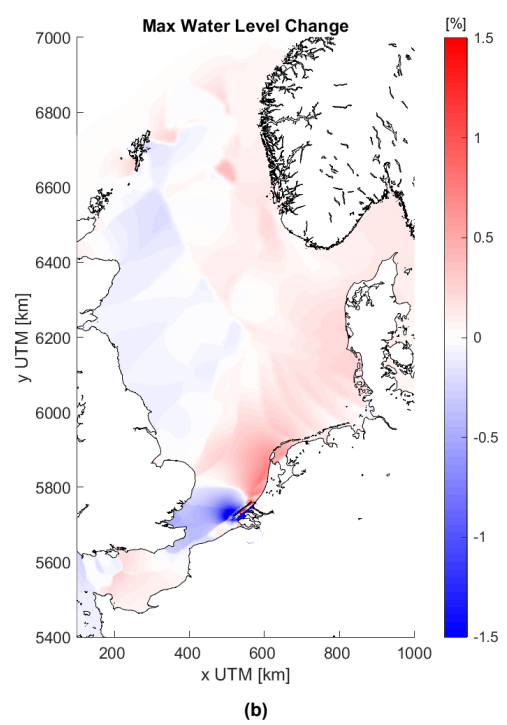
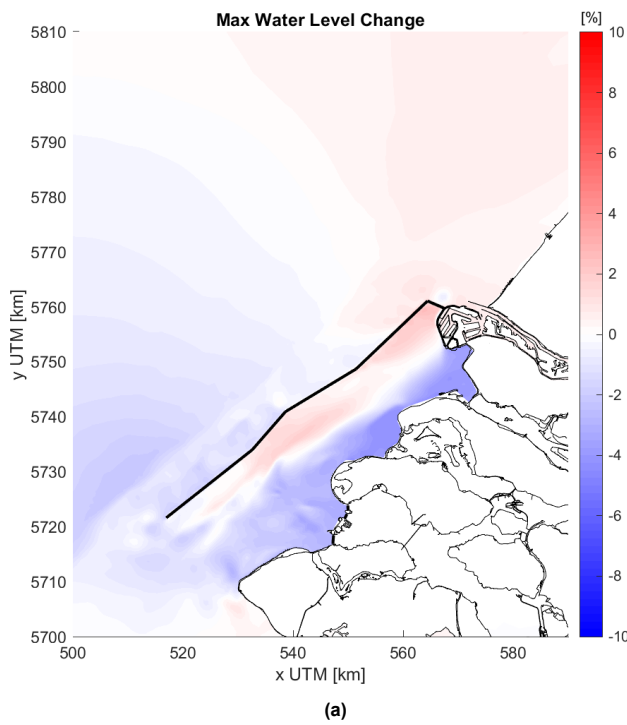


Figure E.3: Difference in maximum water level modelled as a percentage of the maximum value without dam, scenario without MSLR. Figure (a) shows the Voordelta, Figure (b) shows the entire North Sea.

E.1.2. Scenario 25 cm MSLR

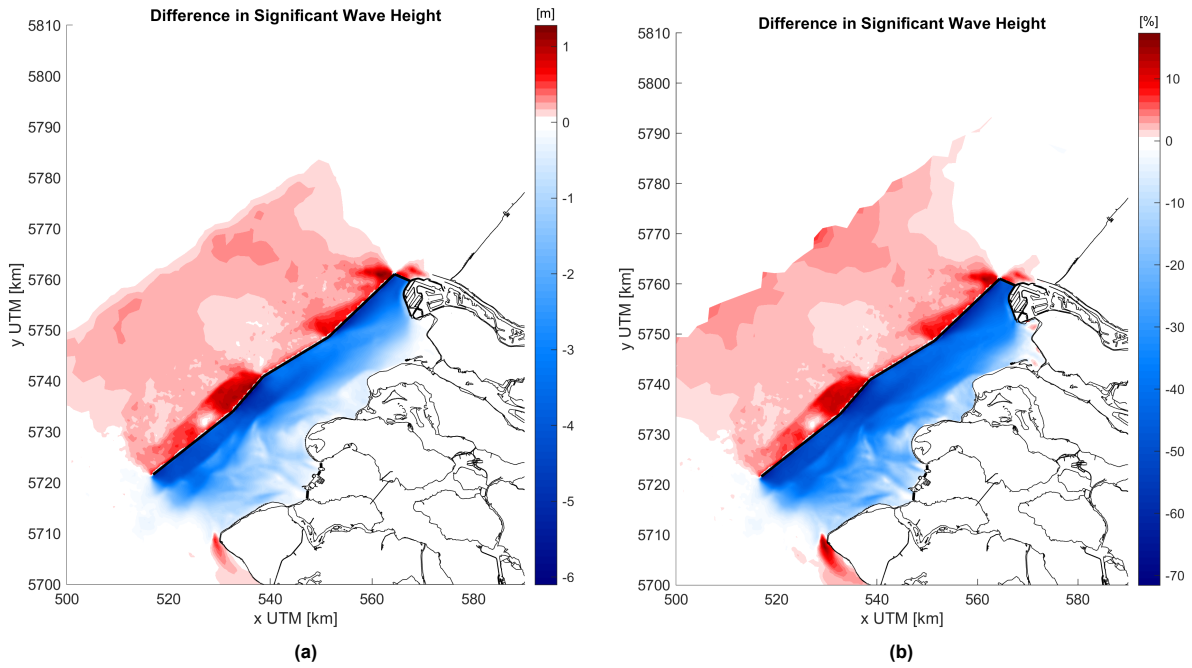


Figure E.4: Absolute (a) and percentile (b) difference in maximum water level modelled, scenario with 25 cm MSLR.

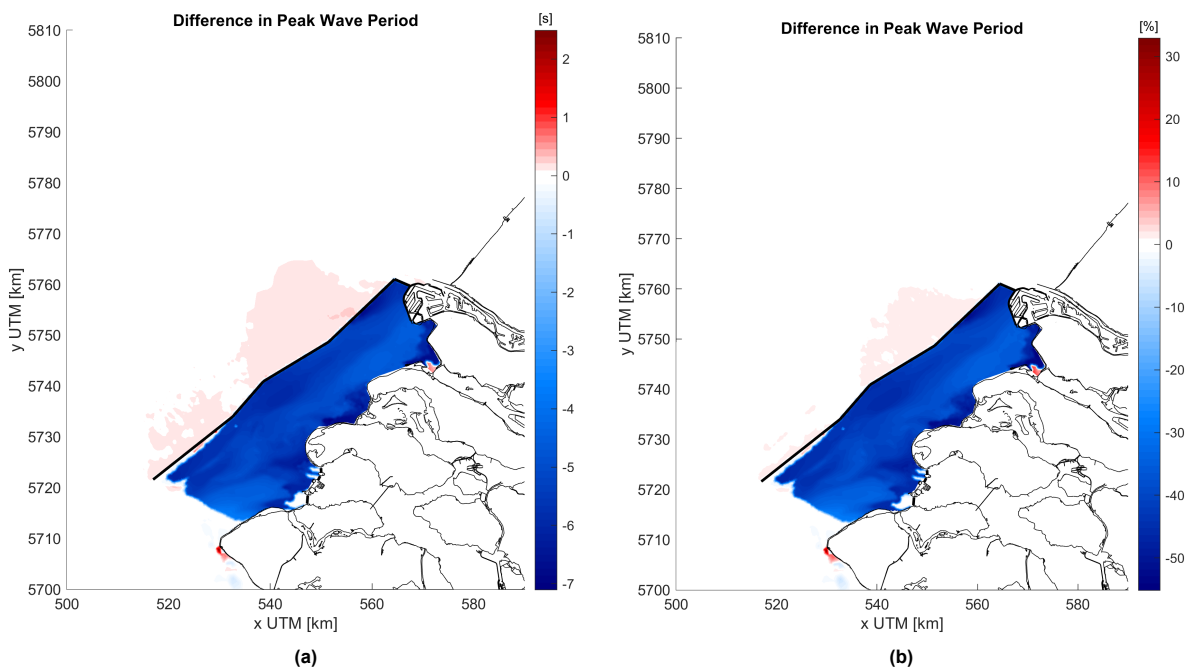


Figure E.5: Absolute (a) and percentile (b) difference in maximum peak wave period modelled, scenario with 25 cm MSLR.

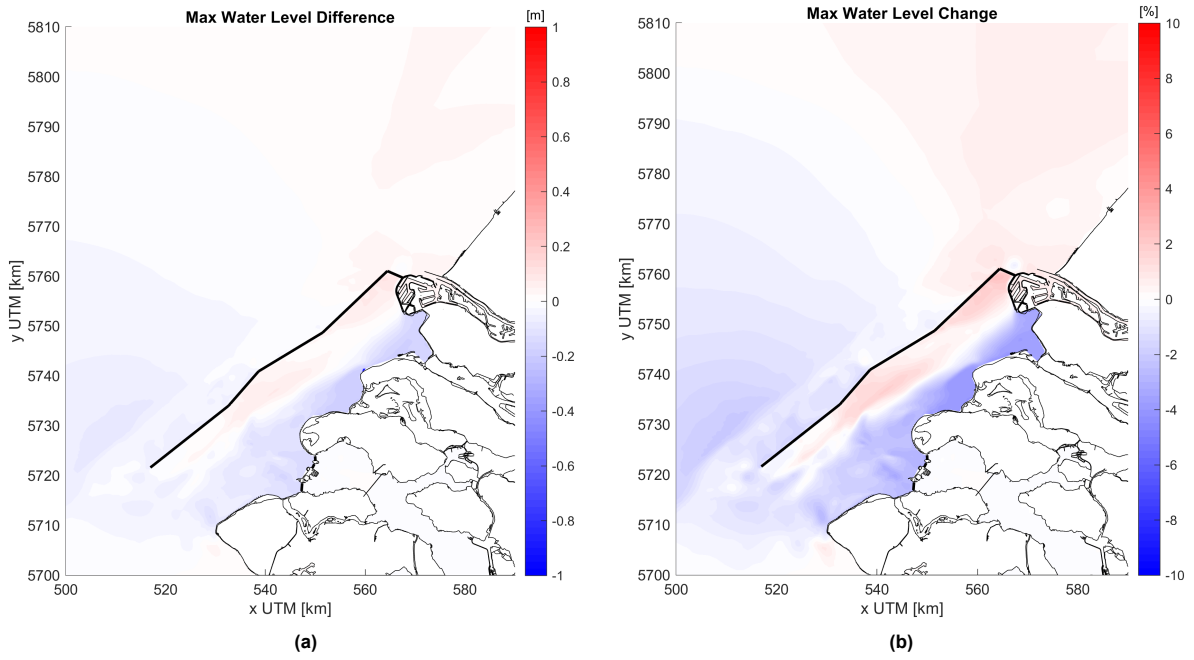


Figure E.6: Absolute (a) and percentile (b) difference in maximum water level modelled near the Voordelta, scenario with 25 cm MSLR.

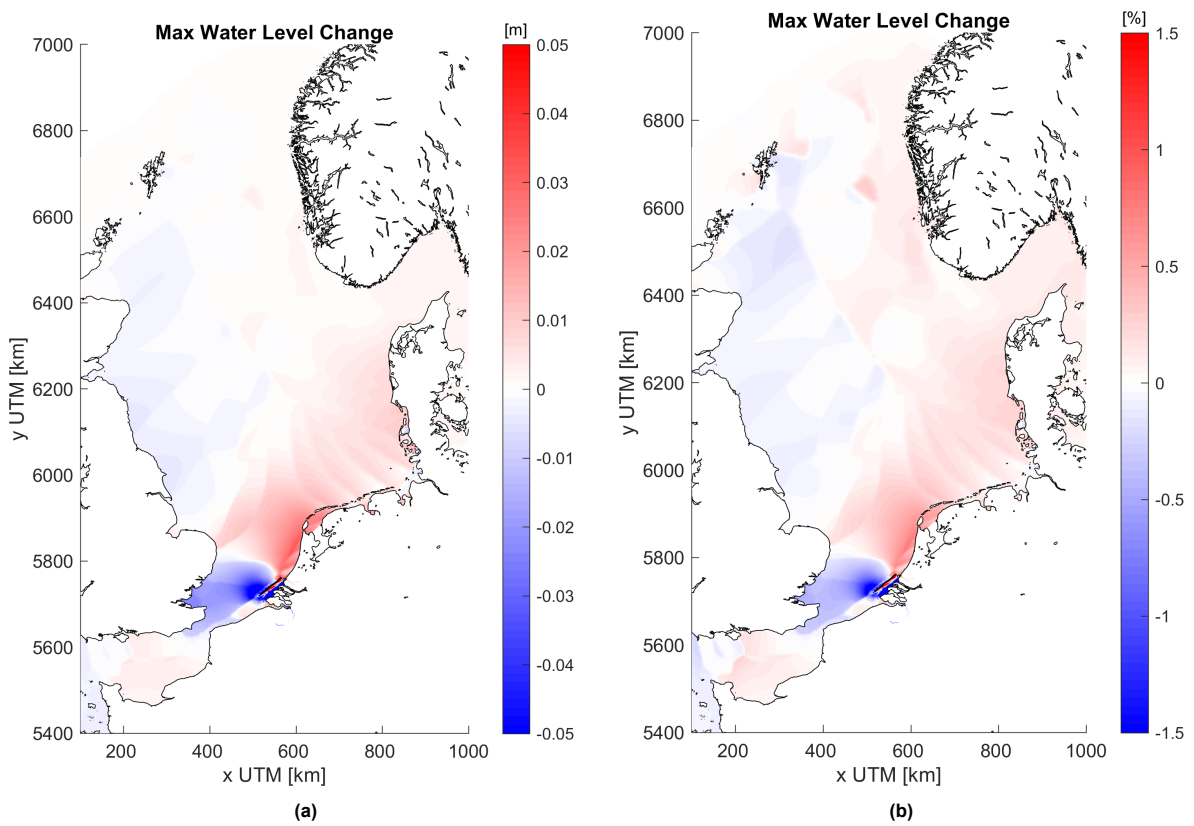


Figure E.7: Absolute (a) and percentile (b) difference in maximum water level modelled in the North Sea, scenario with 25 cm MSLR.

E.1.3. Scenario 80 cm MSLR

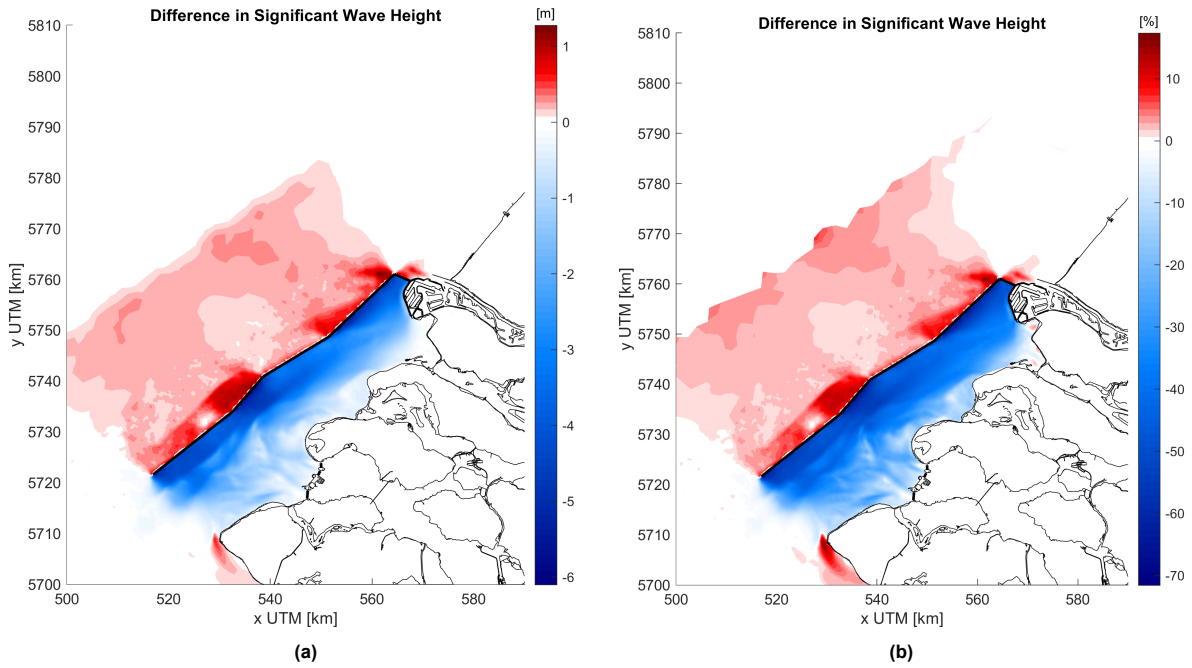


Figure E.8: Absolute (a) and percentile (b) difference in maximum water level modelled, scenario with 80 cm MSLR.

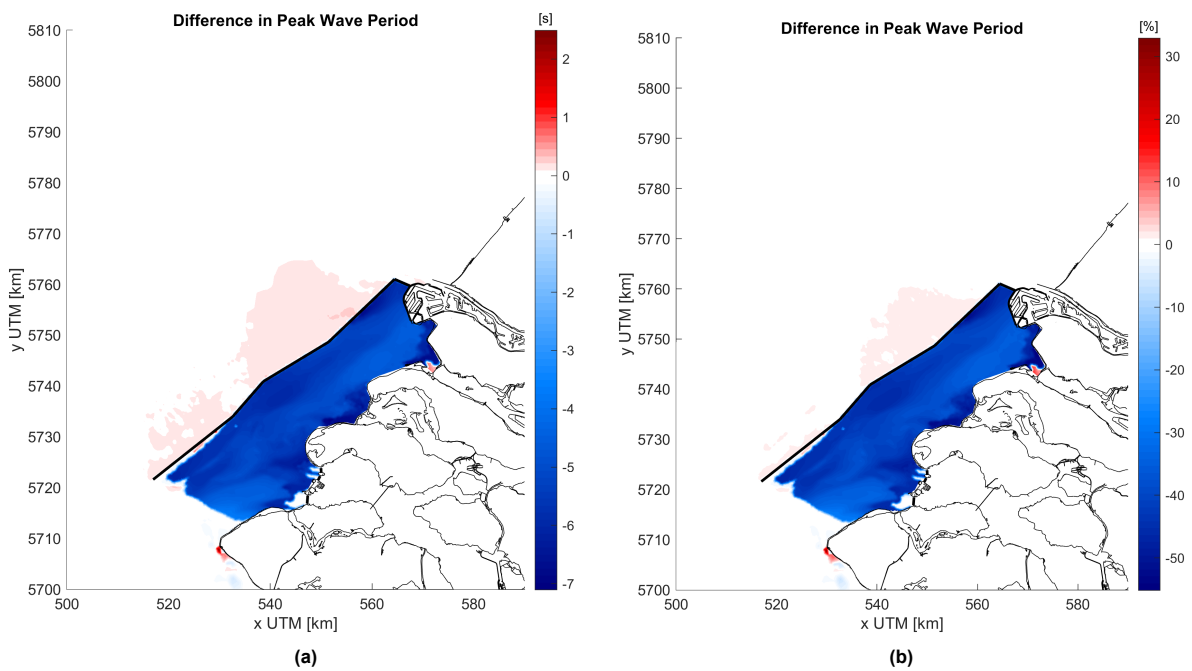


Figure E.9: Absolute (a) and percentile (b) difference in maximum peak wave period modelled, scenario with 80 cm MSLR.

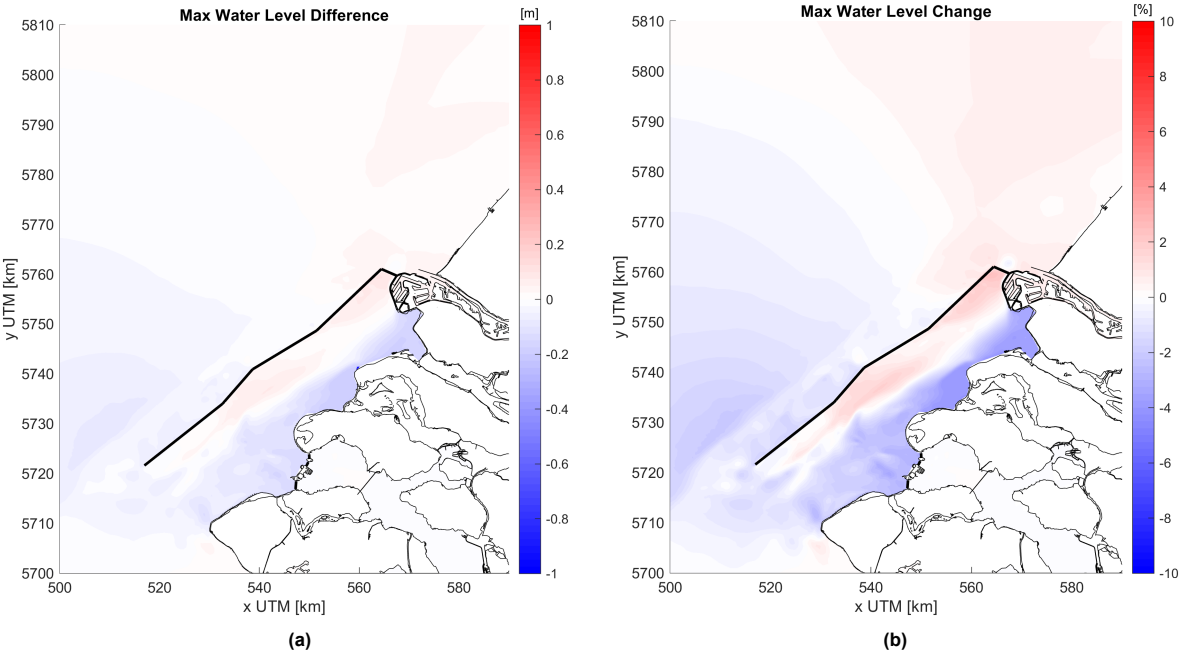


Figure E.10: Absolute (a) and percentile (b) difference in maximum water level modelled near the Voordelta, scenario with 80 cm MSLR.

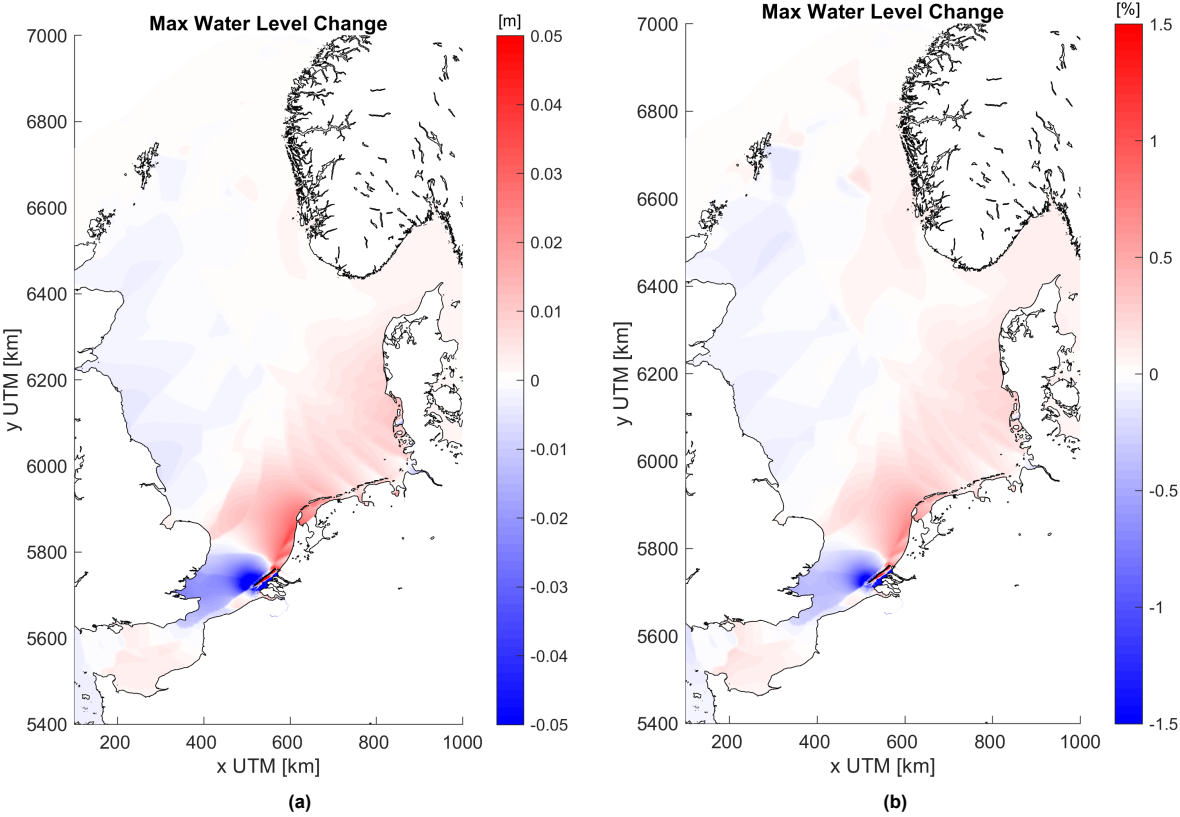


Figure E.11: Absolute (a) and percentile (b) difference in maximum water level modelled in the North Sea, scenario with 80 cm MSLR.

E.1.4. Southwestern Storm

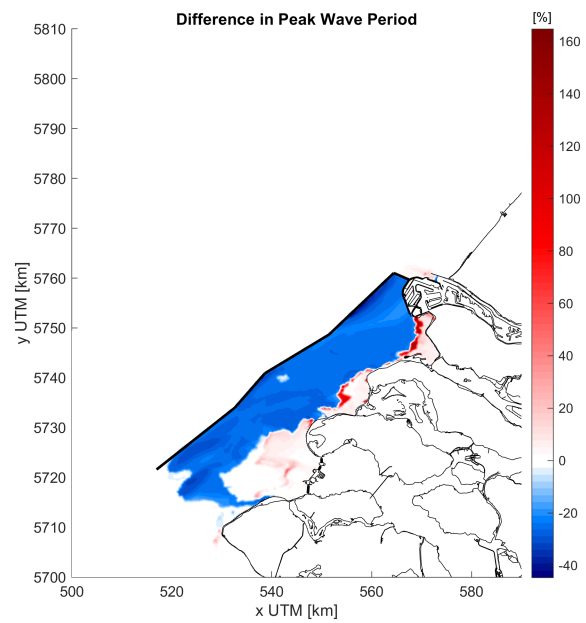
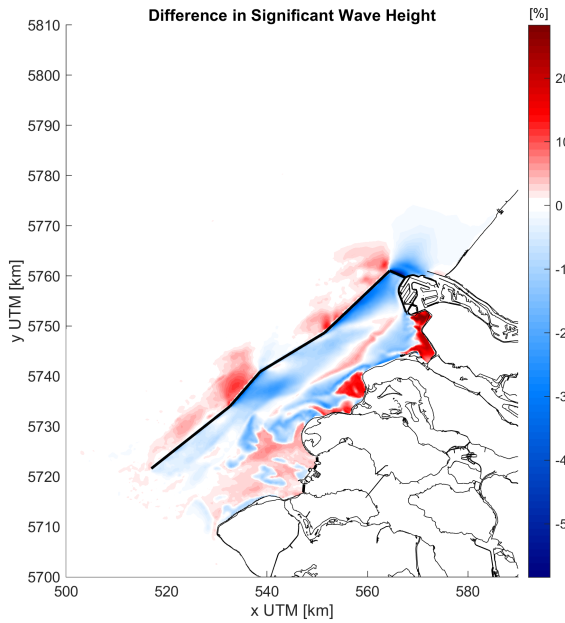


Figure E.12: Difference in maximum significant wave height as a percentage of the maximum value without dam, scenario without MSLR for a southwestern storm.

Figure E.13: Difference in maximum peak wave period modelled as a percentage of the maximum value without dam, scenario without MSLR for a southwestern storm.

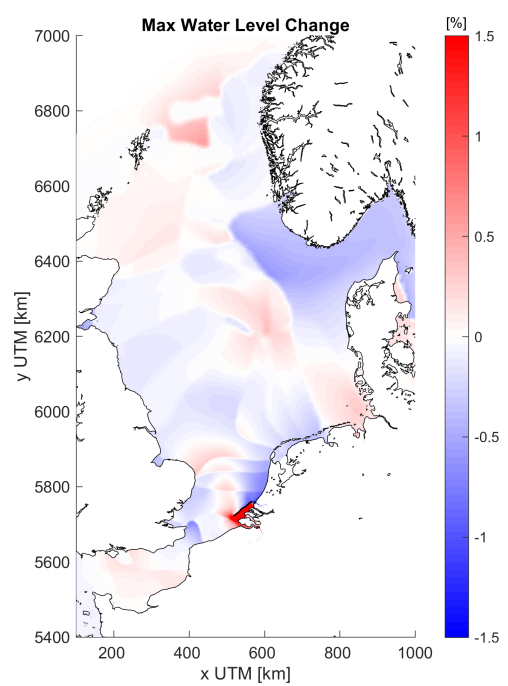
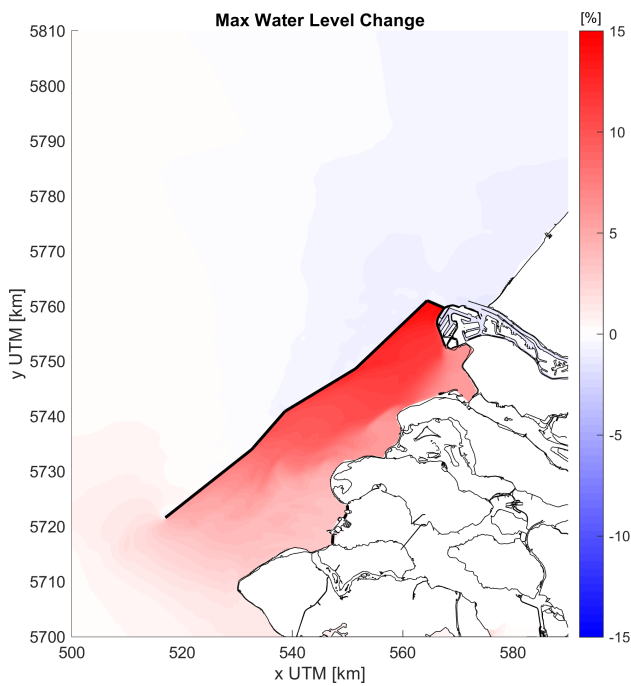


Figure E.14: Difference in maximum water level modelled as a percentage of the maximum value without dam, scenario without MSLR for a southwestern storm. Figure (a) shows the Voordelta, Figure (b) shows the entire North Sea.

E.2. Time Series

In this Section, the time series of the modelled significant wave height, peak wave period and water level are shown for several output locations. The graphs of the locations Brouwershavensegat 2 and Roompot Buiten are not shown, as these have been presented in Chapter 6. The exact locations of the output locations can be seen in Figure C.1. All graphs show the time series of the relevant characteristic for all eight models run.

E.2.1. Significant Wave Height

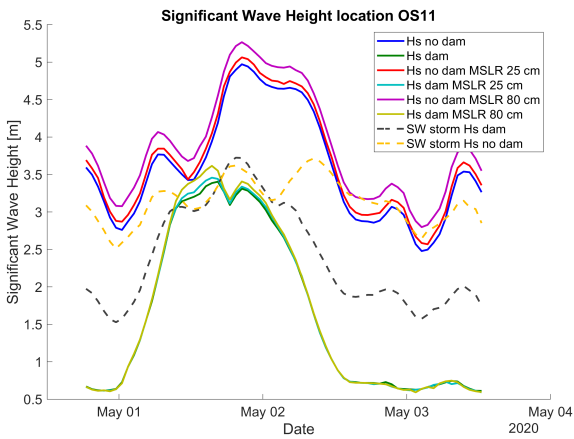


Figure E.15: Significant Wave Height modelled at location OS11.

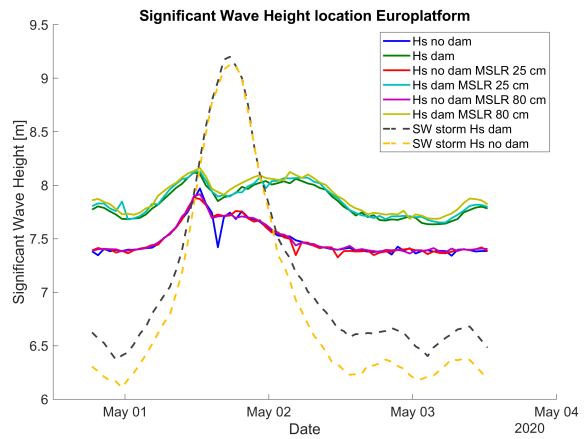


Figure E.16: Significant Wave Height modelled at location Europlatform.

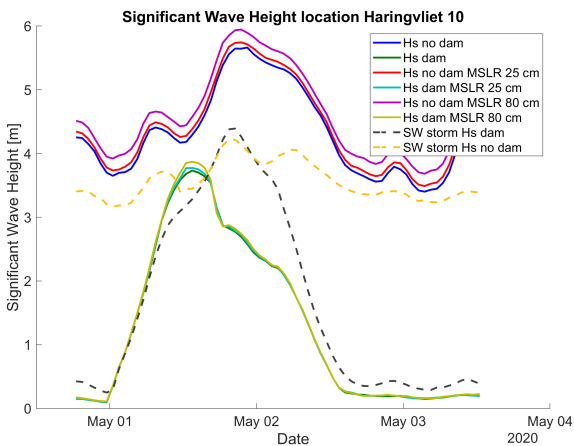


Figure E.17: Significant Wave Height modelled at location Haringvliet 10.

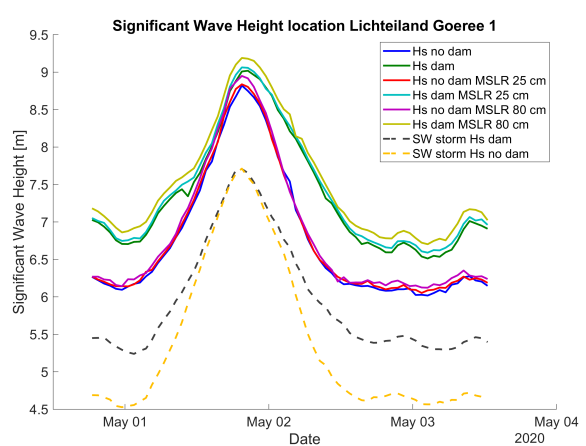


Figure E.18: Significant Wave Height modelled at location Lichteiland Goeree 1.

E.2.2. Peak Wave Period

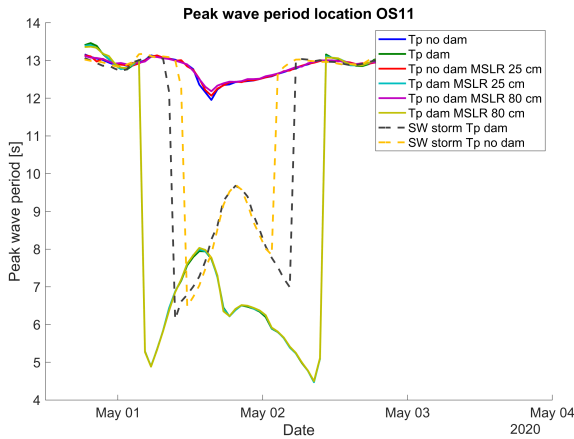


Figure E.19: Peak wave period modelled at location OS11.

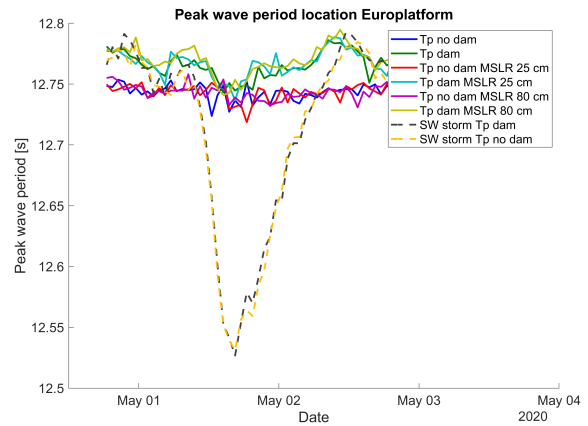


Figure E.20: Peak wave period modelled at location Europlatform.

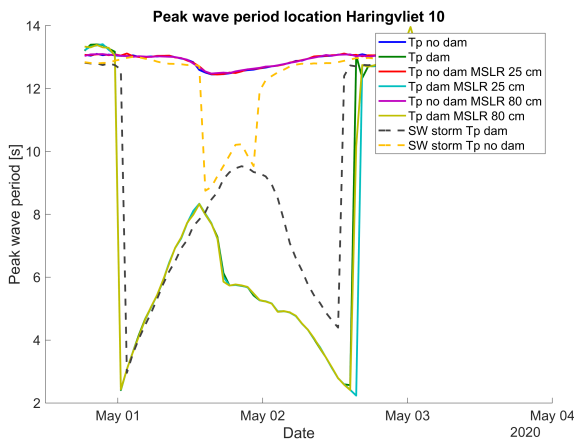


Figure E.21: Peak wave period modelled at location Haringvliet 10.

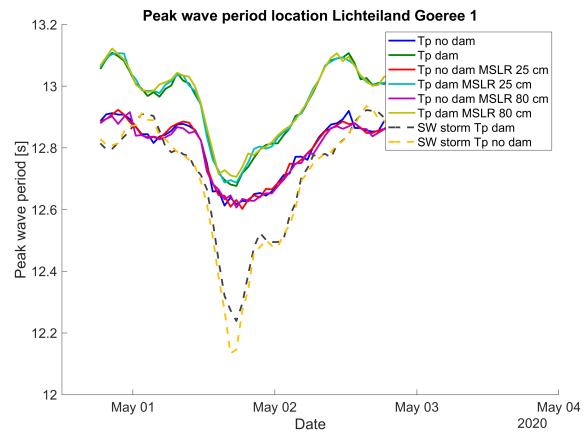


Figure E.22: Peak wave period modelled at location Lichteiland Goeree 1.

E.2.3. Maximum Water Level

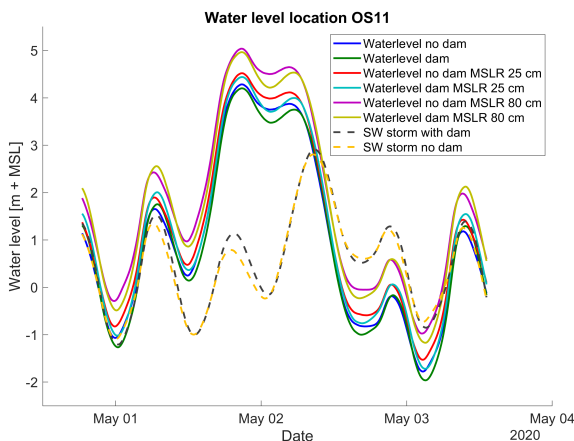


Figure E.23: Water level modelled at location OS11.

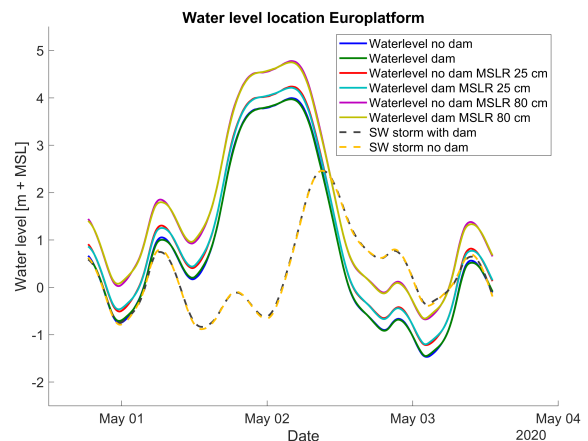


Figure E.24: Water level modelled at location Europlatform.

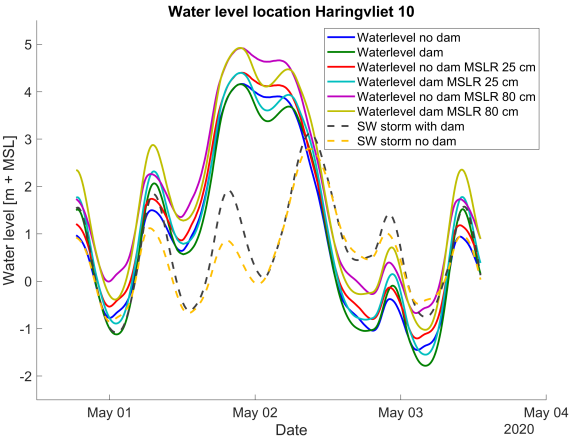


Figure E.25: Water level modelled at location Haringvliet 10.

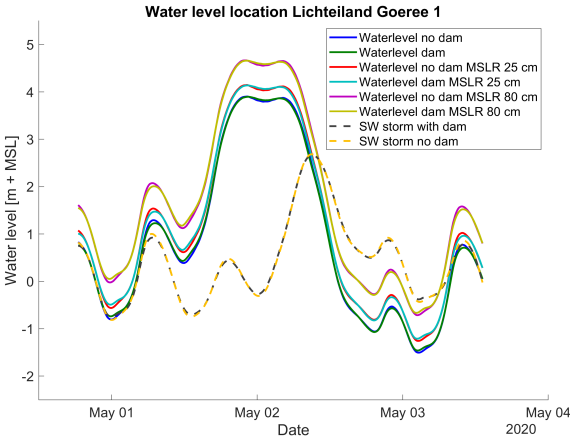


Figure E.26: Water level modelled at location Lichteiland Goeree 1.